ISSN 1307-8798

Official Publication of the Turkish Society of Anatomy and Clinical Anatomy

www.anatomy.org.tr

anatomy

An International Journal of Experimental and Clinical Anatomy

Volume 11 / Issue 2 / August 2017

Published three times a year

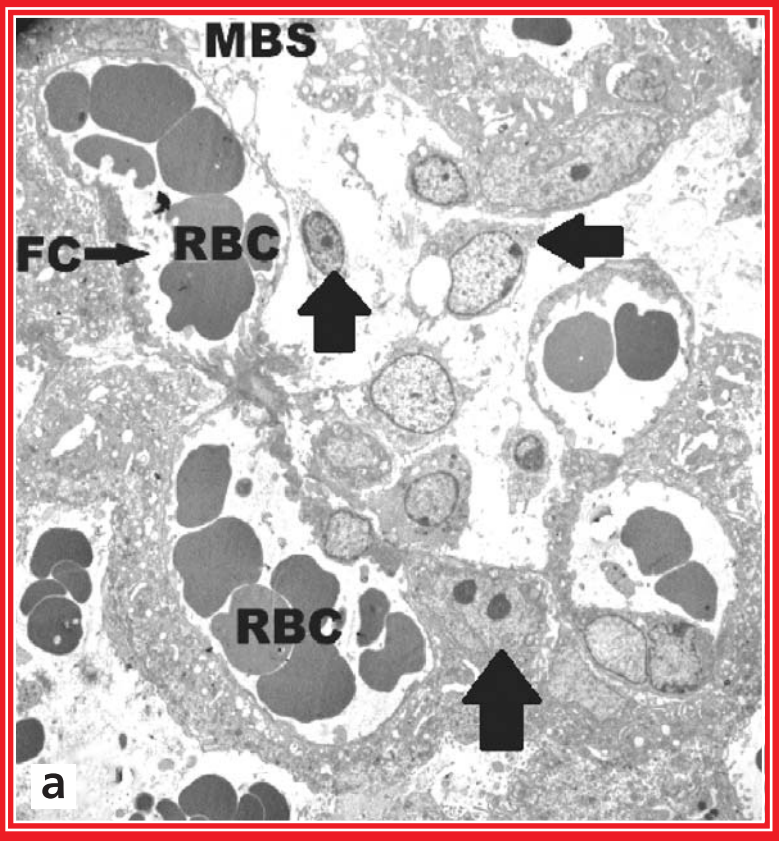

deomed®

www.anatomy.org.tr

anatomy

An International Journal of Experimental and Clinical Anatomy

Official Publication of the Turkish Society of Anatomy and Clinical Anatomy

Aim and Scope

Anatomy, an international journal of experimental and clinical anatomy, is a peer-reviewed journal published three times a year with an objective to publish manuscripts with high scientific quality from all areas of anatomy. The journal offers a forum for anatomical investigations involving gross, histologic, developmental, neurological, radiological and clinical anatomy, and anatomy teaching methods and techniques. The journal is open to original papers covering a link between gross anatomy and areas related with clinical anatomy such as experimental and functional anatomy, neuroanatomy, comparative anatomy, modern imaging techniques, molecular biology, cell biology, embryology, morphological studies of veterinary discipline, and teaching anatomy. The journal is currently indexing and abstracting in TUBITAK ULAKBIM Turkish Medical Index, Proquest, EBSCO Host, Index Copernicus and Google Scholar.

Publication Ethics

Anatomy is committed to upholding the highest standards of publication ethics and observes the principles of Journal's Publication Ethics and Malpractice Statement which is based on the recommendations and guidelines for journal editors developed by the Committee on Publication Ethics (COPE), Council of Science Editors (CSE), World Association of Medical Editors (WAME) and International Committee of Medical Journal Editors (ICMJE). Fore detailed information please visit the online version of the journal which is available at www.anatomy.org.tr

Authorship

All persons designated as authors should have participated sufficiently in the work to take public responsibility for the content of the manuscript. Authorship credit should be based on substantial contributions to (1) conception and design or analysis and interpretation of data, (2) drafting of the manuscript or revising it for important intellectual content and, (3) final approval of the version to be published. The Editor may require the authors to justify assignment of authorship. In the case of collective authorship, the key persons responsible for the article should be identified and others contributing to the work should be recognized with proper acknowledgment.

Copyright

Publication Information

Anatomy (p-ISSN 1307-8798; e-ISSN 1308-8459) is published by Deomed Publishing, Istanbul, for the Turkish Society of Anatomy and Clinical Anatomy, TSACA. Due the Press Law of Turkish Republic dated as June 26, 2004 and numbered as 5187, this publication is classified as a periodical in English language.

Ownership
On behalf of the Turkish Society of Anatomy and Clinical Anatomy,
Ahmet Kağan Karabulut, MD, PhD; Konya

Responsible Managing Editor
Nihal Apaydın, MD, PhD; Ankara

Administrative Office
Güven Mah. Güvenlik Cad. Onlar Ap. 129/2 Aşağı Ayrancı, Ankara
Phone: +90 312 447 55 52-53

Publisher
Deomed Publishing
Gür Sok. No:7/B Kadıköy, İstanbul, Turkey
Phone: +90 216 414 83 43 (Pbx) / Fax: +90 216 414 83 42
www.deomed.com / e-mail: medya@deomed.com

deomed®

Submission of Manuscripts

Contributions should be submitted for publication under the following categories to:

Gülgün Şengül, MD
Editor-in-Chief, *Anatomy*

Department of Anatomy,
Faculty of Medicine, Ege University,
35100, Bornova, Izmir, Turkey
Phone: 0090 232 390 39 84
Fax: 0090 232 342 21 42
e-mail: gulgun.sengul@gmail.com; gulgun.sengul@ege.edu.tr

Categories of Articles

- ***Original Articles*** describe substantial original research that falls within the scope of the Journal.
- ***Teaching Anatomy*** section contains regular or all formats of papers which are relevant to comparing teaching models or to introducing novel techniques, including especially the own experiences of the authors.
- ***Reviews*** section highlights current development in relevant areas of anatomy. The reviews are generally invited; other prospective authors should consult with the Editor-in-Chief.
- ***Case Reports*** include new, noteworthy or unusual cases which could be of help for basic notions and clinical practice.
- ***Technical Note*** articles cover technical innovations and developments with a specific technique or procedure or a modification of an existing technique. They should be sectioned like an original research article but not exceed 2000 words.
- ***Viewpoint*** articles give opinions on controversial topics or future projections, some of these are invited.
- ***Historical View*** category presents overview articles about historical sections from all areas of anatomy.
- ***Terminology Zone*** category is a platform for the articles which discuss some terminological controversies or opinions.

The categories above are peer-reviewed. They should include abstract and keywords. There are also categories including Letters to the Editor, Book Reviews, Abstracts, Obituary, News and Announcements which do not require a peer review process.

For detailed instructions concerning the submission of manuscripts, please refer to the Instructions to Authors.

Subscription

Please send your order to Deomed Publishing, Gür Sok. No: 7/B Kadıköy, Istanbul, Turkey. e-mail: alikoz@deomed.com

- ***Annual rates:*** Institutional 100 EUR, Individual 50 EUR (include postage and local VAT). Supplements are not included in the subscription rates.

Membership of the Turkish Society of Anatomy and Clinical Anatomy, TSACA includes a reduced subscription rate to this journal.

- ***Change of address:*** Please send to the publisher at least six weeks in advance, including both old and new addresses.
- ***Cancellations:*** Subscription cancellations will not be accepted after the first issue has been mailed.

The online version of this journal is available at www.anatomy.org.tr

Advertising and Reprint Requests

Please direct to publisher. e-mail: medya@deomed.com

Printing and Binding

Birmat Press, İstanbul, Turkey, Phone: +90 212 629 05 59-60
Printed in Turkey on acid-free paper (August 2017).

Editorial Board

www.anatomy.org.tr

anatomy
An International Journal of Experimental and Clinical Anatomy

anatomy
www.anatomy.org.tr
An International Journal of Experimental and Clinical Anatomy

Instructions to Authors

Anatomy, an international journal of experimental and clinical anatomy, is the official publication of the Turkish Society of Anatomy and Clinical Anatomy, TSACA. It is a peer-reviewed journal that publishes scientific articles in English. For a manuscript to be published in the journal, it should not be published previously in another journal or as full text in congress books and should be found relevant by the editorial board. Also, manuscripts submitted to Anatomy must not be under consideration by any other journal. Relevant manuscripts undergo conventional peer review procedure (at least three reviewers). For the publication of accepted manuscripts, author(s) should reveal to the Editor-in-Chief any conflict of interest and transfer the copyright to the Turkish Society of Anatomy and Clinical Anatomy, TSACA.

In the Materials and Methods section of the manuscripts where experimental studies on humans are presented, a statement that informed consent was obtained from each volunteer or patient after explanation of the procedures should be included. This section also should contain a statement that the investigation conforms with the principles outlined in the appropriate version of 1964 Declaration of Helsinki. For studies involving animals, all work must have been conducted according to applicable national and international guidelines. Prior approval must have been obtained for all protocols from the relevant author's institutional or other appropriate ethics committee, and the institution name and permit numbers must be provided at submission.

Anatomical terms used should comply with Terminologia Anatomica by FCAT (1998).

No publication cost is charged for the manuscripts but reprints and color printings are at authors' cost.

Preparation of manuscripts

During the preparation of the manuscripts, uniform requirements of the International Committee of Medical Journal Editors, a part of which is stated below, are valid (*see* ICMJE. Uniform requirements for manuscripts submitted to biomedical journals. Updated content is available at www.icmje.org). The manuscript should be typed double-spaced on one side of a 21x 29.7 cm (A4) blank sheet of paper. At the top, bottom and right and left sides of the pages a space of 2.5 cm should be left and all the pages should be numbered except for the title page.

Manuscripts should not exceed 15 pages (except for the title page). They must be accompanied by a cover letter signed by corresponding author and the Conflicts of Interest Disclosure Statement and Copyright Transfer Form signed by all authors. The contents of the manuscript (original articles and articles for Teaching Anatomy category) should include: 1- Title Page, 2- Abstract and Keywords, 3- Introduction, 4- Materials and Methods, 5- Results, 6- Discussion (Conclusion and/or Acknowledgement if necessary), 7- References

Title page

In all manuscripts the title of the manuscript should be written at the top and the full names and surnames and titles of the authors beneath. These should be followed with the affiliation of the author. Manuscripts with long titles are better accompanied underneath by a short version (maximum 80 characters) to be published as running head. In the title page the correspondence address and telephone, fax and e-mail should be written. At the bottom of this page, if present, funding sources supporting the work should be written with full names of all funding organizations and grant numbers. It should also be indicated in a separate line if the study has already been presented in a congress or likewise scientific meeting. Other information such as name and affiliation are not to be indicated in pages other than the title page.

Abstract

Abstract should be written after the title in 100–250 words. In original articles and articles prepared in IMRAD format for Teaching Anatomy category the abstract should be structured under sections Objectives, Methods, Results and Conclusion. Following the abstract at least 3 keywords should be added in alphabetical order separated by semicolumns.

References

Authors should provide direct references to original research sources. References should be numbered consecutively in square brackets, according to the order in which they are first mentioned in the manuscript. They should follow the standards detailed in the NLM's Citing Medicine, 2nd edition (Citing medicine: the NLM style guide for authors, editors, and publishers [Internet]. 2nd edition. Updated content is available at www.ncbi.nlm .nih.gov/books/NBK7256). The names of all contributing authors should be listed, and should be in the order they appear in the original reference. The author is responsible for the accuracy and completeness of references. When necessary, a copy of a referred article can be requested from the author. Journal names should be abbreviated as in *Index Medicus*. Examples of main reference types are shown below:

• **Journal articles:** Author's name(s), article title, journal title (abbreviated), year of publication, volume number, inclusive pages

– *Standard journal article:* Sargon MF, Celik HH, Aksit MD, Karaagaoglu E. Quantitative analysis of myelinated axons of corpus callosum in the human brain. Int J Neurosci 2007;117:749–55.

– *Journal article with indication article published electronically before print:* Sengul G, Fu Y, Yu Y, Paxinos G. Spinal cord projections to the cerebellum in the mouse. Brain Struct Funct Epub 2014 Jul 10. DOI 10.1007/s00429-014-0840-7.

• **Books:** Author's name(s), book title, place of publication, publisher, year of publication, total pages (entire book) or inclusive pages (contribution to a book or chapter in a book)

– *Entire book:*

- *Standard entire book:* Sengul G, Watson C, Tanaka I, Paxinos G. Atlas of the spinal cord of the rat, mouse, marmoset, rhesus and human. San Diego (CA): Academic Press Elsevier; 2013. 360 p.

- *Book with organization as author:* Federative Committee of Anatomical Terminology (FCAT). Terminologia anatomica. Stuttgart: Thieme; 1998. 292 p.

- *Citation to a book on the Internet:* Bergman RA, Afifi AK, Miyauchi R. Illustrated encyclopedia of human anatomic variation. Opus I: muscular system [Internet]. [Revised on March 24, 2015] Available from: http://www.anatomyatlases.org/AnatomicVariants/AnatomyHP.shtml

– *Contribution to a book:*

- *Standard reference to a contributed chapter:* Potten CS, Wilson JW. Development of epithelial stem cell concepts. In: Lanza R, Gearhart J, Blau H, Melton D, Moore M, Pedersen R, Thomson J, West M, editors. Handbook of stem cell. Vol. 2, Adult and fetal. Amsterdam: Elsevier; 2004. p. 1–11.

- *Contributed section with editors:* Johnson D, Ellis H, Collins P, editors. Pectoral girdle and upper limb. In: Standring S, editor. Gray's anatomy: the anatomical basis of clinical practice. 29th ed. Edinburgh (Scotland): Elsevier Churchill Livingstone; 2005. p. 799–942.

– *Chapter in a book:*

- *Standard chapter in a book:* Doyle JR, Botte MJ. Surgical anatomy of the hand and upper extremity. Philadelphia (PA): Lippincott Williams and Wilkins; 2003. Chapter 10, Hand, Part 1, Palmar hand; p. 532–641.

Illustrations and tables

Illustrations and tables should be numbered in different categories in the manuscript and Roman numbers should not to be used in numbering. Legends of the illustrations and tables should be added to the end of the manuscript as a separate page. Attention should be paid to the dimensions of the photographs to be proportional with 10x15 cm. Some abbreviations out of standards can be used in related illustrations and tables. In this case, abbreviation used should be explained in the legend. Figures and tables published previously can only be used when necessary for a comparison and only by giving reference after obtaining permission from the author(s) or the publisher (copyright holder).

Control list

- Length of the manuscript (max. 15 pages)
- Manuscript format (double space; one space before punctuation marks except for apostrophes)
- Title page (author names and affiliations; running head; correspondence)
- Abstract (100–250 words)
- Keywords (at least three)
- References (relevant to *Index Medicus)*
- Illustrations and tables (numbering; legends)
- Conflicts of Interest Disclosure Statement and Copyright Transfer Form
- Cover letter

Original Article

www.anatomy.org.tr
Received: July 17, 2017; Accepted: July 28, 2017
doi:10.2399/ana.17.024

anatomy
www.anatomy.org.tr
An International Journal of Experimental and Clinical Anatomy

Effect of streptozotocin-induced diabetes on the autonomic ganglia of albino rats

Muhamed Faizal, Aijaz Ahmed Khan

Department of Anatomy, Jawaharlal Nehru Medical College, Aligarh Muslim University, Aligarh, U.P, India

Abstract

Objectives: One of the common clinical observations regarding long-standing hyperglycemia is autonomic neuropathy, probably due to its unfavorable destructive effects on the neurons of the autonomic ganglia. Accordingly, the current study was aimed to analyze the effect of experimental hyperglycemia on parasympathetic pterygopalatine ganglion (PtG) and sympathetic coeliac ganglion (ClG) of albino rats.

Methods: Thirty-six albino rats were divided into six groups (n=6, each) and were designated as control, two weeks, one month, two months, four months and six months groups. Diabetes was induced with a single dose of streptozotocin (STZ, 60 mg/kg, i.p.). Body weight and blood sugar were monitored at biweekly intervals. At the end of each experimental period, animals were euthanized by deep ether anesthesia and blood samples were collected by direct puncture of heart for biochemical analysis. Animals were perfused with Karnovsky fixative. After 48 hours, tissue samples were collected and processed for light microscopy.

Results: Biochemical analysis of serum revealed increased serum creatinine and reduced serum total protein. Histopathology and histomorphometry of ganglia revealed that the progressively increasing duration of hyperglycemia was associated with decreased proportion of small-sized neurons, increased proportion of large-sized neurons, dark and dead neurons, and thickening of capsular and endoneurial collagen.

Conclusion: The association of the long-standing hyperglycemia with increased neuronal death, altered proportion of neurons and deposition of collagen fibers in autonomic ganglia appear to be important contributing factors likely to be responsible for diabetic autonomic neuropathy.

Keywords: autonomic ganglia; collagen; diabetes; neuropathy; streptozotocin induced

Anatomy 2017;11(2):51–60

Introduction

Diabetes mellitus is a group of common metabolic disorders that is characterized by hyperglycemia and insufficiency in production or action of insulin.[1] Hyperglycemia is believed to be associated with increased free radicals and cellular oxidative stress, which initiates cellular injury leading to diabetic complications including retinopathy, neuropathy, nephropathy and coronary artery diseases.[2] Hyperglycemia followed by high neuronal glucose levels leads to glucose neurotoxicity,[3] and prolonged high intracellular glucose in neurons leads to a variety of functional and structural disorders in various region of nervous system.[4] Due to high cytosolic oxidative stress, both sympathetic and parasympathetic neurons may be more susceptible to pathological changes of oxidative stress like those in diabetes.[5] Oxidative stress followed by mitochondrial dysfunction initiates neuronal apoptosis[6] and is a major mediator of neurodegeneration in diabetes.[7] Autonomic dysfunction affects normal functioning of the cardiovascular, respiratory, gastrointestinal, genitourinary, thermoregulatory, and neuroendocrine systems.[8]

Autonomic ganglia serve as the final output of discrete CNS structures that control the function of the periphery.[5] The pterygopalatine ganglion (PtG) is the largest parasympathetic ganglion located in the pterygopalatine fossa and is functionally attached to the facial nerve. Sensory fibers from the maxillary branch of trigeminal nerve and sympathetic fibers pass through ganglia, but do not synapse in them.[9] The coeliac ganglia (ClG) are a

well-defined prevertebral sympathetic ganglia located on the sides of the coeliac trunk having a varying number of neurons with extensive dendritic fields.[10] ClG receive convergent synaptic input from spinal preganglionic neurons and peripheral intestinofugal neurons projecting from the gut.[11] Related studies[12,13] found changes in neurons and alteration of myelinated and unmyelinated nerve fibers and collagen without using any special stain. Therefore, the present study aimed at demonstrating these and possibly other changes in the arrangement of collagen fibers and neuronal structure by using special stainings for collagen, picrosirius red (PSR) and cresyl violet (CV) stainings together with histopathological, histomorphological and biochemical parameters, in experimentally induced diabetic rats after two weeks to six months periods.

Materials and Methods

After approval from Institutional Animal Ethics Committee (No: 9025/2014), 36 albino rats of either sex weighing approximately 250 g were obtained from central animal house, Aligarh Muslim University, Aligarh were used for the present study. Prior to commencement of the experiments, all animals were placed to the new environmental condition for a period of one week. Animals were kept in a well-ventilated room and were supplied standard pellet diet and water *ad libitum* and maintained on a 12/12 h light/dark cycle.

Animals were divided into following six groups having six rats in each group: Group 1: non-diabetic healthy control, age-matched; diabetic experimental groups: Group 2: two week, Group 3: one month; Group 4: two months; Group 5: four months; Group 6: six months.

The experimental diabetic model was induced using streptozotocin (STZ) (60 mg/kg, aquous sol., I.P., only once; SRL-Sisco Research Laboratories, Mumbai, India) after 12 hours of fasting. Blood sugar level was monitored with a glucometer from the blood obtained from the lateral tail vein before and on the 2nd day of streptozotocin injection. Animals with blood sugar level 250 mg/dl and above were considered as diabetic. Both body weight and blood glucose levels of all animals in each group were monitored biweekly.[14]

After the designated period, all experimental and age-matched control rats were euthanized with overdose of ether general anesthesia, and the rats were perfusion-fixed with Karnovsky's fixative.

PtGs were carefully dissected out from the pterygopalatine fossa along with the maxillary branch of the trigeminal ganglion and the ClG from either sides of the celiac trunk were secured *en bloc*. Both tissues were processed for paraffin embedding. 5 µm thick sections were stained with Hematoxyline and Eosin (H&E), cresyl CV and PSR. Only H&E and CV stained sections were used for measuring the neuronal diameter. Random photomicrographs were recorded under ×400 magnification of trinocular microscope (Olympus, BX40, Tokyo, Japan) by digital camera (Sony 18.2 MP, Tokyo, Japan) and measurements were made by using software Motic Images Plus version 2.0 (Motic, Kowloon, Hong Kong)[14] Sufficient numbers of random images from both sides of PtG and ClG were taken in order to get 1000 neurons having a clear nucleus with one or more nucleoli to be used for the histomorphometry. Based on their diameter, neurons were divided into small (<20 µm), medium (20–30 µm) and large sized (>30 µm). Proportions of different size of neurons in randomly selected 1000 neurons were calculated in each group. The neurons were also identified as dark or light on the basis of their morphology and staining characteristics of cell body and nucleus with visible nucleolus.

Blood glucose levels were measured from the lateral tail vein blood at biweekly intervals with a glucometer. At the end of each study period, blood samples were obtained from direct puncture of heart and collected into sterilized plastic vials. Samples were allowed to clot, centrifuged at 2500 rpm for 30 minutes. The serum was separated and stored in sterile plastic vials and assayed for serum total protein content and serum creatinine level by using Avantor BeneSpheraTM Clinical Chemistry Analyzer C61 (Avantor Performance Materials, Inc., Center Valley, PA, USA).

The number of neurons, serum total protein and serum creatinine levels were statistically analyzed using one-way ANOVA followed by Tukey's test. All numerical values were expressed as Mean±SD and $p<005$ was considered as statistically significant.

Results

Consistent with the known effects of induced hyperglycemia, the STZ-treated rats displayed classical clinical symptoms of diabetes such as polydipsia, polyuria and polyphagia. The mean body weights of all diabetic groups were reduced compared to the control group during experimental period as reported earlier.[14] The changes observed between 2W diabetic and age-matched control group were statistically not significant (>0.05), but they were significantly ($p<0.05$) reduced at all stages of the induced diabetes compared to age-matched controls. Rise of blood sugar level was observed above 500 mg/dl after 48 hours of induction in diabetic groups which remained so throughout experimental period.

Table 1
Serum total protein and creatinine levels in diabetic groups compared to age-matched controls.

Parameter	Group	2W	1M	2M	4M	6M
Serum total protein (g/dl)	Control	5.97±0.04*	5.95±0.05*	5.99±0.03*	6.01±0.01*	5.98±0.05*
	Diabetic	5.23±0.01	5.12±0.03	5.00±0.07	4.05±0.03	3.96±0.04
Serum creatinine (mg/dl)	Control	0.43±0.02	0.42±0.06*	0.45±0.05*	0.44±0.07*	0.43±0.04*
	Diabetic	0.45±0.07	0.63±0.08	0.78±0.03	0.93±0.09	1.06±0.05

*p<0.05

After 2W, a significant difference ($p<0.01$) was observed when comparison was made between 2W, 1M, 2M, 4M, and 6M diabetic rats to age-matched controls and corresponding diabetic group rats, respectively (**Table 1**).

Microscopic observations

The PtG was located in the pterygopalatine fossa closely related with maxillary division of trigeminal nerve. Neurons in PtG were closely packed with homogenous distribution. Most neurons appeared round to oval in shape and almost all neurons were in the range of small to medium size with cell body diameter of 15 to 30 Ìm. Each neuron was surrounded by a thin capsule of small satellite cells with delicate connective tissue and unmyelinated nerve fibers between them. Fibrocytes and occasional intraganglionic blood capillaries were also noticed. Each ganglion had its own protective connective tissue capsule. Neuronal cell bodies were characterized by oval large euchromatic nuclei. In control, 2W and 1M diabetic groups, Nissl substance was coarser and sparse in the perikaryal area. However in 2M, 4M and 6M diabetic groups, most of the parasympathetic neurons had peripheral condensed rim of Nissl substance. Most of the literature suggest that nuclei of a sensory ganglion neurons are located centrally[14] and those in the autonomic ganglia are located eccentrically.[15] However, in the current study, we observed that the nucleus appeared to be located centrally in most of the PtG neurons. Similarly, the common text book description is that the autonomic ganglion neurons are multipolar,[15] but in the present study quite many of the neurons in both PtG and ClG had appearance very much similar to typical sensory ganglion neurons. Interestingly, all nuclei had a single and large densely stained eccentrically placed nucleolus. (**Figures 1** and **2**). Collagen fibers were observed in the perineuronal capsule. The unmyelinated nerve fibers and connective tissue fibers were also seen between the neurons. The control and 2W diabetic groups were associated with fewer collagen fibers around the neurons and along the nerve fibers, but in other groups progressively thickened collagen fibers in the periganglionic capsule, perineuronal capsule and also along the nerve bundles were noticed. Perineuronal spaces were commonly noticed in 1M, 2M, 4M, and 6M diabetic groups (**Figure 3**).

In cresyl violet-stained sections of the celiac ganglion, both control and diabetic groups showed the same basic cellular architecture, consisting of a moderately dense arrangement of sympathetic neurons separated by bundles of unmyelinated nerve fibers and surrounded by well-

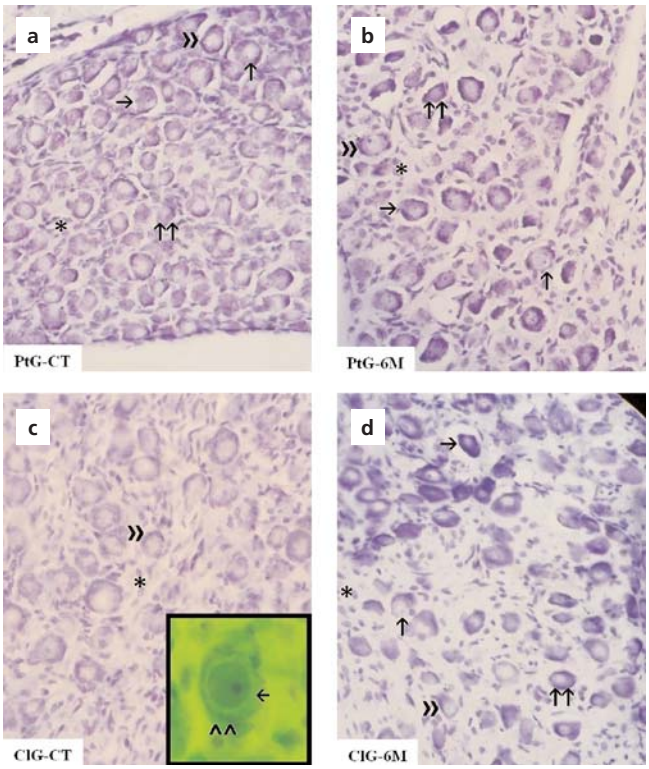

Figure 1. (**a**–**d**) Photomicrographs from rat autonomic ganglia showing neuron having peripheral ring (↑↑), eccentric nucleus (↑), eccentric nucleolus (»), dark neuron (→) and fibrocytes (*) (Cresyl violet stain, ×400). Inset showing moderate yellow fluorescence in perikarya occupied by fine Nissl granules (←) and no fluorescence in the peripheral rim (^^) (PSR stain, ×1000). [Color figure can be viewed in the online issue, which is available at www.anatomy.org.tr]

defined collagen fibers around the neurons and along the nerve fibers and ganglionic capsule. Most of the neuronal cell bodies inside the ClG had eccentrically placed, large, euchromatic nuclei having deeply stained nucleoli (**Figures 1–3**) which were also located eccentrically. Fine Nissl granules were distributed uniformly throughout the cytoplasm. Lipofuscin pigments were not obviously seen in both control and experimental groups. All ganglion neurons in the control group were covered by thin sheath of fewer sparsely located satellite glial cells. In prolonged diabetic groups, the satellite cells were less organized as compared to age-matched control groups (**Figures 1** and **2**). Though collagen fibers were present in variable amounts in the perineuronal capsules, nerve fascicles and periganglionic capsules. The overall amount of collagen and thickness of their fibers revealed direct correlation with the increasing duration of hyperglycemic state as compared to the age-matched controls. Perineuronal spaces were found in the 6M diabetic group. Intraganglionic blood capillaries were more often seen close to the neurons in diabetic groups (**Figure 4**). The 2W diabetic group revealed two medium sized neurons housed within the same perineuronal sheath as suggested by the absence of satellite cells and fibrous capsule between them (**Figure 4**).

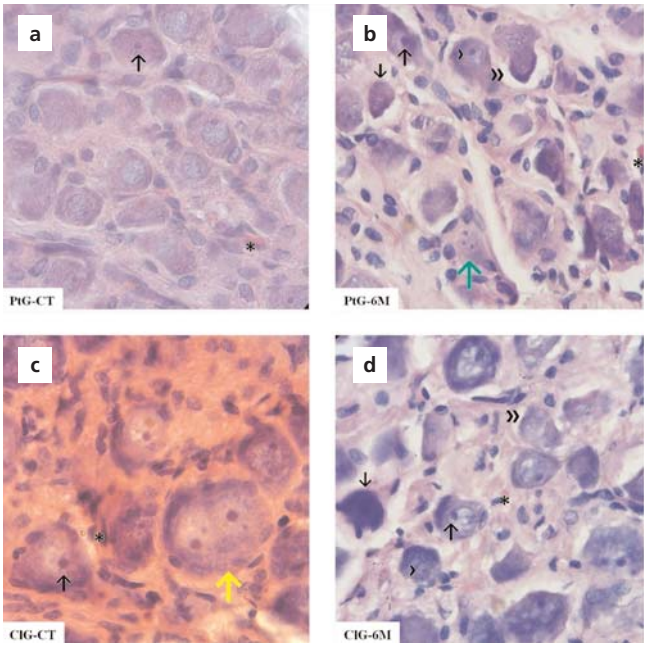

Figure 2. (**a**–**d**) Photomicrographs from rat autonomic ganglia showing eccentric nucleoli (↑) blood capillaries (*), dark neuron (»), dead neuron (↓) and perineuronal space (*). Yellow arrow showing organized two ClG neurons enclosed in common perineuronal sheath and glial satellite cells. Connective tissue sheath is not visible between two cells. Green colored arrow showing ClG neuronal nucleus having three nucleoli (H&E stain, ×1000). [Color figure can be viewed in the online issue, which is available at www.anatomy.org.tr]

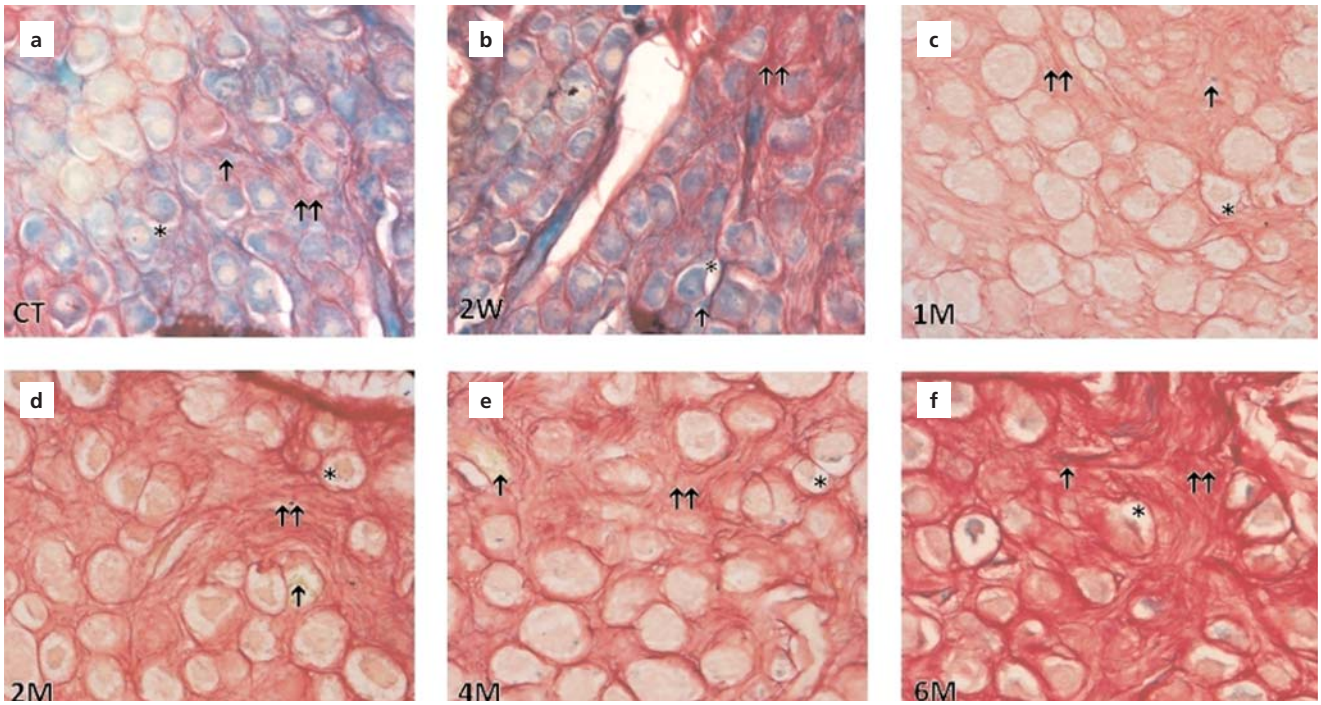

Figure 3. (**a**–**f**) Photomicrographs from rat PtG showing non-myelinated nerve fibers (↑↑), blood capillaries (↑), and perineuronal space (*). Note the prominence of collagen fibers (**red colour**) in 1M, 2M, 4M and 6M diabetic group (PSR with LFB stain, ×400). [Color figure can be viewed in the online issue, which is available at www.anatomy.org.tr]

Histomorphometry

In the PtG, the proportion of small sized neurons among 1000 neurons was significantly ($p<0.05$) decreased in 2M, 4M and 6M groups and the proportions of medium sized neurons were significantly ($p<0.05$) increased in 2M, 4M and 6M diabetic groups as compared to the age-matched control groups (**Figure 5**).

In 1000 neurons of the ClG of all diabetic groups, the proportion of small sized neurons were significantly ($p<0.05$) decreased. However, in the 2W diabetic group such decrement remained statistically non-significant as compared to the age-matched control group. In ClG of 1M, 2M, 4M and 6M diabetic groups, the proportion of medium and large sized neurons were significantly ($p<0.05$) increased as compared to the age-matched control group. In the 2W diabetic group, the proportions of the total number of medium and large sized neurons were less compared to the age-matched control group, but not at a statistically significant level (**Figure 6**).

Biochemical analysis

In all diabetic groups, the serum total protein levels were significantly ($p<0.05$) decreased compared to age-matched

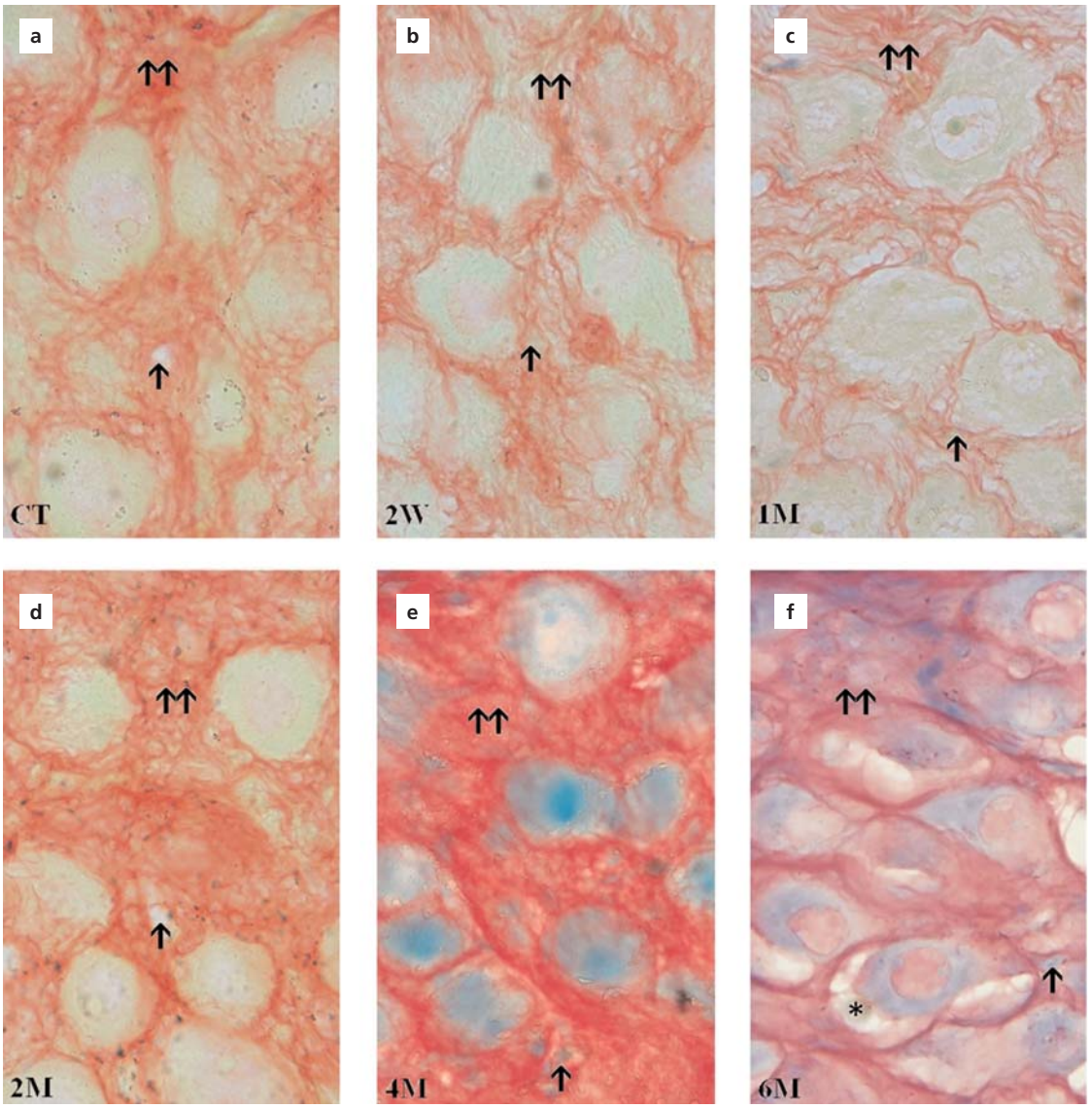

Figure 4. (**a**–**f**) Photomicrographs from rat ClG showing non-myelinated nerve fibers (↑↑), blood capillaries (↑), and perineuronal space (*). Note the prominence of collagen fibers (**red colour**) in 2M, 4M and 6M diabetic groups (PSR with LFB stain, x1000). [Color figure can be viewed in the online issue, which is available at www.anatomy.org.tr]

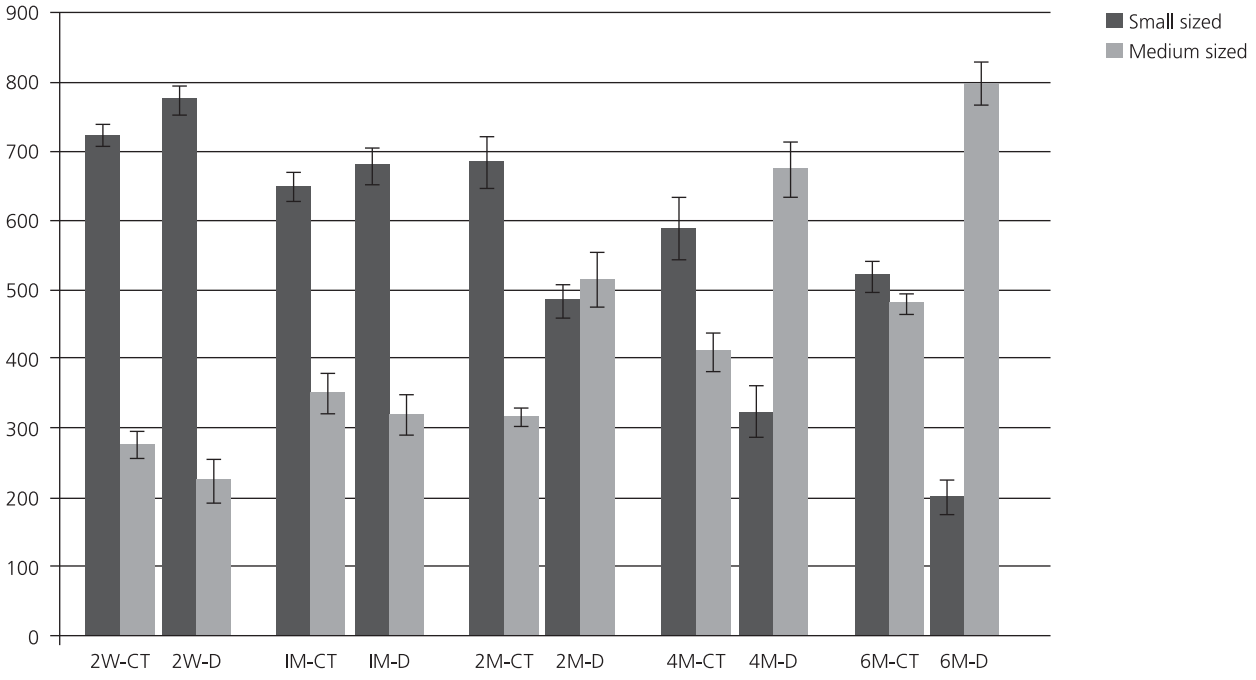

Figure 5. The proportion of small sized neurons was significantly ($p<0.05$) reduced in all diabetic groups, while that of medium sized neurons significantly ($p<0.05$) increased in all diabetic groups except 2W and 1M compared to age-matched control groups.

control groups, while serum creatinine levels were significantly ($p<0.05$) increased in all diabetic groups except 2W, as compared to age-matched control groups. In 2W diabetic group, the serum creatinine levels were less compared to the age-matched control group, but not at significant level ($p>0.05$) (**Table 1**).

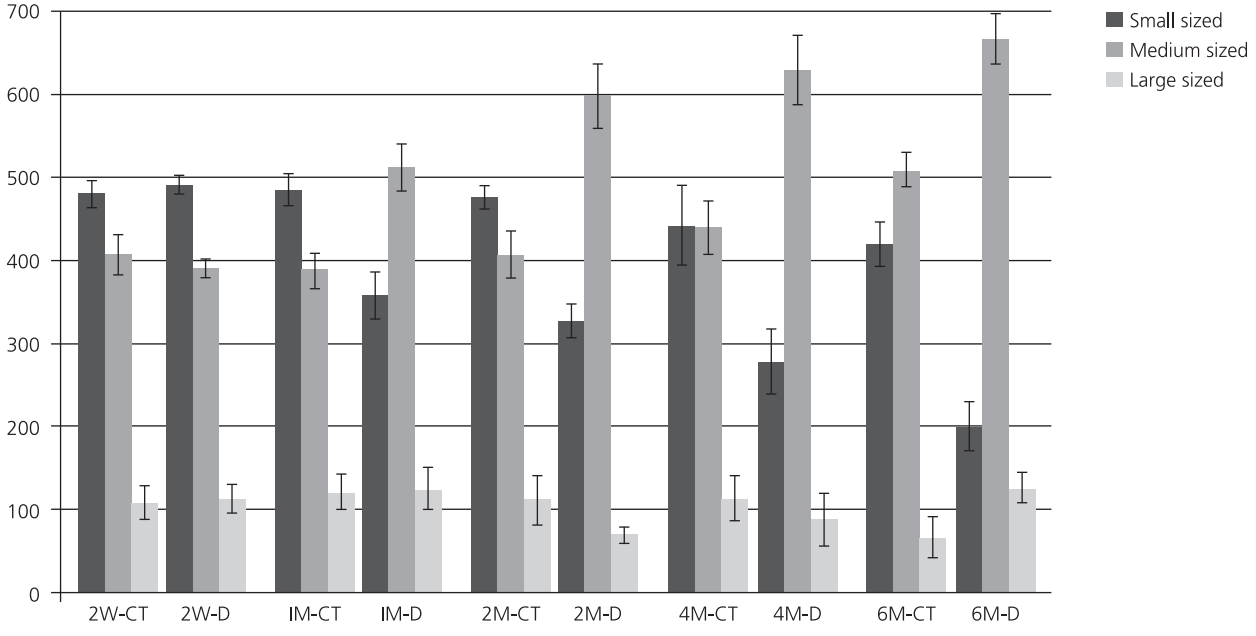

Figure 6. The proportion of small sized neurons in ClG was significantly ($p<0.05$) reduced in all diabetic groups except 2W group, while the total number of the medium and large sized neurons significantly ($p<0.05$) increased in all diabetic groups except 2W compared to age-matched control groups.

Discussion

Diabetes mellitus is a group of metabolic disorders of carbohydrate, fat and protein metabolism characterized by low grade inflammatory metabolic disorder[16,17] in which a person has high blood sugar, either characterized by insufficient amounts of insulin or because cells do not respond to the insulin that is produced, which leads to hyperglycemia.[18] Reduced anabolic insulin hormone in DM, promotes protein catabolism and releasing amino acids for gluconeogenesis[19] which leads to increased muscle wasting due to loss of tissue proteins and reduction of body weight.[20] In the current study, all diabetic groups maintained the hyperglycemic state throughout the experimental period and showed progressive reduction in body weight in the STZ-induced rats, reflecting an increase in protein catabolism and loss of tissue proteins. This result is in agreement with previous related studies.[21–23]

In this study, structure of both sympathetic and parasympathetic autonomic ganglia and orientation of nerve fibers in both control and experimental groups were, in general, found to be similar to those reported earlier.[10,24–26] Each neuron in ClG is anatomically and functionally independent. In the present study, a couple of neurons appeared to share a common sheath formed by satellite glial cells and the interneuronal sheath connective tissue was not visible. Significance of such intimate association between certain neurons remains unclear. On one hand, absence of the interneuronal sheath element makes its appearance very akin to a binucleate neuron; similar findings were observed in another study on the trigeminal ganglion.[27]

The present study demonstrates a concomitant increase in the thickness of collagen fibers located in the capsule of the ganglia, perineuronal capsule and interfascicular region of PtG and ClG. Previous studies showed progression of fibrosis in a diabetic heart by PKC-β, p38 mitogen activated protein kinase expression in redox reaction,[28] and AGE and RAGE interaction increased expression of TGF-β and contributed to the development of submesothelial fibrosis and neoangiogenesis.[29] In the current study, in PSR and CV stained sections, control and 2W diabetic groups of PtG, and control, 2W, and 1M diabetic groups of ClG revealed thin collagen fibers around the neurons and along the nerve bundles; however, in 1M and 2M diabetic groups of PtG and in the 2M diabetic group of ClG, the collagen fibers were of moderate thickness. However, in 4M and 6M diabetic groups, both PtG and ClG revealed a remarkable thickening of collagen in the capsule of the ClG ganglia, perineuronal capsule, interfascicular region, and endoneurium. Comparison of these with previous observations reported earlier[14,30] indicate that hyperglycemia seems to accelerate fibrosis in terms of the amount and thickness of collagen fibers. In earlier studies on sensory ganglia, the perineuronal spaces in some of the neurons were suggested to be due to either shrinkage or apoptosis of neurons with the progression of hyperglycemia.[14,30] In the present study, similar observations were found in 1M, 2M, 4M and 6M diabetic groups of PtG and 6M diabetic group of ClG.

The dark neurons are also considered as apoptotic type neurons or a type of cell degeneration with hyperelectron density properties and hyperbasophilia.[31–33] Many researchers consider neuronal cell death mainly due to apoptotic changes.[34] In the present study, it was observed that, on the progression of the duration of hyperglycemic state in both PtG and ClG, the number of dark neurons increased in agreement with earlier studies showing that hyperglycemia and increased free radical generation in diabetes accelerated the formation of dark neurons.[31] The number of neurons with a distinct peripheral rim of Nissl substance also seems to increase with the duration of hyperglycemia which may be secondary to chromatolytic changes.[35,36]

It is generally accepted that the PtG contains both vasomotor and secretomotor neurons[37] and that they are independent of each other.[38] In the present study, were observed both small and medium sized neurons in control and experimental groups. In another study on the otic ganglion of the cat, small and large sized neurons were described as vasomotor and secretomotor, mainly involved with blood vessel vasomotor activity and glandular secretion of the salivary gland.[39] In our study, there is evidence for a minor change in neuronal proportion in the parasympathetic ganglia of diabetic rats. The proportion of small sized neurons in PtG significantly ($p<0.05$) decreased in all diabetic groups. Therefore, these findings indicate that in diabetes the isolated asymptomatic progressive involvement of lacrimal secretion in progression of hyperglycemia. The impaired tear secretion in prolonged hyperglycemic state which is commonly believed to be due to age-dependent decline in glandular function and excessive fibrosis[40,41] may also be partly attributed to the loss of small sized neurons of PtG observed in the present study.

ClG is the part of sympathetic ganglia located near the celiac trunk, a complex relay and integrative center for projections from the parasympathetic, sensory, spinal cord-derived motor, and retrograde intestinofugal sources.[42] Most neurons are noradrenergic and supply the stomach, spleen, pancreas, small intestine and mesen-

teric blood vessels.[43] In the current study, we identified small, medium and large sized neurons. Such neuronal population has earlier been functionally divided into pilomotor, vasomotor and secretomotor neurons.[44] In our study, there is evidence for a minor change in neuronal proportion in the ClG. It was noticed that the proportion of small sized neurons in ClG were significantly ($p<0.05$) decreased, however medium and large sized neuron were significantly ($p<0.05$) increased in 1M, 2M, 4M and 6M diabetic groups. Therefore, these findings indicate that diabetes leads to progressive dysregulation of the sympathetic control of motility in the stomach and small intestine, and of fluid exchange in the small intestine with progression of hyperglycemia probably due to altered function and or loss different neurons along with age-dependent decline in glandular function and excessive fibrosis.[41,45]

In the present study, dead neurons were easily differentiated due to their dark staining characteristics as compared to normal neurons in the control group. In 4M and 6M diabetic groups, the neurons with dark nuclei appeared shrunken, nuclear membranes became less distinct and nucleoplasm no more remained open-faced as similar to described earlier.[46] However, with the progression of hyperglycemic state in diabetic groups, the number of dead neurons increased in agreement with an earlier study,[46] suggesting diabetes enhances neuronal death.

Lipofuscin pigment (senile pigment) is described to be one of the typical features of the sympathetic ganglia and can be shown described by H&E stain.[15] In our present study, lipofuscin pigment could neither be located in the control nor in any experimental groups after using with different stains. Certain literature suggest that lipofuscin pigment shows auto- fluorescent property with blue light.[47] Diabetes is said to accelerate accumulation of fluorescent granules in sensory[48] and sympathetic neurons[49] which could not be confirmed in the present study. However, the perikarya of ClG neurons showed a low-grade yellow fluorescence in the region occupied by fine Nissl substance (**Figure 1**).

In this study, it has been shown that, as shown earlier, abnormally high levels of serum creatinine are consistent with impaired kidney function[50] and the serum creatinine level increased in all diabetic groups parallel to the severity of hyperglycemia, but the serum total protein levels were reduced and altered in serum total protein relating the hyperglycemia to a low grade inflammatory process.[51] Similar findings have been shown in the other related studies.[52,53]

Conclusion

Based on histopathological, histomorphological and biochemical findings, it is concluded that prolonged hyperglycemic state leads to increased serum creatinine level, reduced serum total protein and proportion of small sized neurons, increase in dark and dead neurons and thickening of collagen fibers in autonomic ganglia. Therefore, it appears that one of the important contributory factors in development of autonomic neuropathy in chronic diabetes might be the hyperglycemia-induced neuronal cytotoxicity and altered perineuronal microenvironment in terms of increased fibrosis within the autonomic ganglia.

Acknowledgement

The authors would like to gratefully acknowledge all kinds of support and co-operation received from Department of Anatomy and Neuroanatomy Laboratory, Jawaharlal Nehru Medical College, Aligarh Muslim University, Aligarh, India.

References

1. Maritim AC, Sanders RA, Watkins JB. Diabetes, oxidative stress, and antioxidants: a review. J Biochem Mol Toxicol 2003;17:24–38.
2. Phillips M, Cataneo RN, Cheema T, Greenberg J. Increased breath biomarker of oxidative stress in diabetes mellitus. Clin Chim Acta 2004;344:189–94.
3. Tomlinson DR, Gardiner NJ. Glucose neurotoxicity. Nat Rev Neurosci 2008;9:36–45.
4. Guven A, Yavuz O, Cam M, Comunoglu C, Sevinc O. Central nervous system complications of diabetes in streptozotocin-induced diabetic rats: a histopathological and immunohistochemical examination. Int J Neurosci 2009;119:1155–69.
5. Rudchenko A, Akude E, Cooper E. Synapses on sympathetic neurons and parasympathetic neurons differ in their vulnerability to diabetes. J Neurosci 2014;34:8865–74.
6. Srinivasan S, Stevens M, Wiley JW. Diabetic peripheral neuropathy-evidence for apoptosis and associated mitochondrial dysfunction. Diabetes 2000;49:1932–8.
7. Fernyhough A, Chowdhury SKR, Schmidt RE. Mitochondrial stress and the pathogenesis of diabetic neuropathy. Expert Rev Endocrinol Metab 2010;5:39–49.
8. Vinik AI, Maser RE, Mitchell BD, Freeman R. Diabetic autonomic neuropathy. Diabetes Care 2003;26:1553–79.
9. Siessere S, Vitti M, de Sousa, LG, Semprini M, Iyomasa MM, Regalo SC. Anatomic variation of cranial parasympathetic ganglia. Braz Oral Res 2008;22:101–5.
10. Sisu AM, Petrescu CI, Cebzan CC, Motoc A, Bolintineanu S, vaida AM, Niculescu MC, Rusu MC. The adult coeliac ganglion: a morphologic study. Rom J Morphol Embryol 2008;49:491–4.
11. Sasahara TH, De souza RR, Machado MR, Da silva RA, Guidi WL, Ribeiro AA. Macro- and microstructural organization of the rabbit's celiac-mesenteric ganglion complex (Oryctolagus cuniculus). Ann Anat 2003;185:441–8.

12. Schmidt RE, Dorsey DA, Beaudet LN, Frederick KE, Parvin CA, Plurad SB, Levisetti MG. Non-obese diabetic mice rapidly develop dramatic sympathetic neuritic dystrophy a new experimental model of diabetic autonomic neuropathy. Am J Pathol 2003;163: 2077–91.
13. Olsson Y, Sourander P. Changes in the sympathetic nervous system in diabetes mellitus. J Neurovisc Relat 1968;81:86–95.
14. Faizal PAM, Khan AA, Elsy B. Effect of experimental hyperglycemia on the trigeminal ganglia of albino rats. Int J Health Sci Res 2017;7: 191–8.
15. Young B, O'Dowd G, Woodford P. Wheater's functional histology: a text and colour atlas. 6th edition. Philadelphia (PA): Churchill Livingstone, 2016. 139 p.
16. Ernst MC, Sinal CJ. Chemerin at the crossroads of inflammation and obesity. Trends Endocrinol Metab 2010;21:660–7.
17. King KD, Jones JD, Warthen J. Microvascular and macrovascular complications of diabetes mellitus. Am J Pharm Educ 2005;69:1–10.
18. Cheng D. Prevalence, predisposition and prevention of type II diabetes. Nutr Metab (Lond) 2005;18:2–29.
19. Air EL, Strowski MZ, Benoit SC, Conarello SL, Salituro GM, Guan XM, Liu K, Woods SC, Zhang BB. Small molecule insulin mimetics reduce food intake and body weight and prevent development of obesity. Nat Med 2002;8:179–83.
20. Jain D, Bansal MK, Dalvi R, Upganlawar A, Somani R. Protective effect of diosmin against diabetic neuropathy in experimental rats. J Integr Med 2014;12:35–41.
21. Cintra LTA, Samuel RO, Prieto AK, Sumida DH, Dezan-Junior E, Gomes-Filho JE. Oral health, diabetes, and body weight. Arch Oral Biol 2017;73:94–9.
22. Elsy B, Maheshwari V, Khan AA. Effects of d alpha-tocopherol on progression of reepithelialization, matrix remodeling and appearance of epidermal appendages in secondary skin wounds of diabetic rats. Journal of Dermatology and Clinical Research 2016;4:1081.
23. Doddigarla Z, Ahmad J, Parwez I. Effect of chromium picolinate and melatonin either in single or in a combination in high carbohydrate diet?fed male Wistar rats. Biofactors 2016;42:106–14.
24. Elfvin LG. The ultrastructure of the superior cervical sympathetic ganglion of the cat: I. The structure of the ganglion cell processes as studied by serial sections. J Ultrastruct Res 1963;8:403–40.
25. Jurgaitiene R, Pauziene N, Azelis V, Zurauskas E. Morphometric study of age-related changes in the human intracardiac ganglia. Medicina (Kaunas) 2004;40:574–81.
26. Szczurkowski A, Kuder T, Nowak E, Kuchinka J. Morphology, topography and cytoarchitectonics of the pterygopalatine ganglion in Egyptian spiny mouse (Acomys cahirinus, Desmarest). Folia Morphol (Warsz) 2002;61:107–10.
27. Dilkash MNA, Ahmed SS, Khan AA. Comparative light microscopic study of trigeminal ganglion neurons in mammals. Curr Neurobiol 2010;1:25–9.
28. Adebiyi OA, Adebiyi OO, Owira PM. Naringin reduces hyperglycemia-induced cardiac fibrosis by relieving oxidative stress. PloS One 2016;11:1–15.
29. De Vriese AS, Flyvbjerg A, Mortier S, Tilton RG, Lameire NH. Inhibition of the interaction of AGE-RAGE prevents hyperglycemia-induced fibrosis of the peritoneal membrane. J Am Soc Nephrol 2003;14:2109–18.
30. Malak HW, Saleh SI, Salah El Din RA, Abdul Hamid HF. Histological and immunohistochemical study on the consequences of acute glycemic level alteration on the dorsal root ganglia and sciatic nerve integrity in neonatal albino rats. Egyptian Journal of Histology 2015;38:332–45.
31. Ahmadpour SH, Haghir H. Diabetes mellitus type 1 induces dark neuron formation in the dentate gyrus: a study by Gallyas' method and transmission electron microscopy. Rom J Morphol Embryol 2011;52:575–9.
32. Zsombok A, Toth Z, Gallyas F. Basophilia, acidophilia and argyrophilia of 'dark' (compacted) neurons during their formation, recovery or death in an otherwise undamaged environment. J Neurosci Methods 2005;142:145–52.
33. Krysko DV, Vanden Berghe T, D'Herde K, Vandenabeele P. Apoptosis and necrosis: detection, discrimination and phagocytosis. Methods 2008;44:205–21.
34. Keane RW, Kraydieh S, Lotocki G, Alonso OF, Aldana P, Dietrich WD. Apoptotic and antiapoptotic mechanisms after traumatic brain injury. J Cereb Blood Flow Metab 2001;21:1189–98.
35. Sango, K, Horie H, Saito H, Ajiki K, Tokashiki A, Takeshita K, Ishigatsubo Y, Kawano H, Ishikawa Y. Diabetes is not a potent inducer of neuronal cell death in mouse sensory ganglia, but it enhances neurite regeneration in vitro. Life Sci 2002;71:2351–68.
36. Duchen LW, Scaravilli F. Quantitative and electron microscopic studies of sensory ganglion cells of the Sprawling mouse. J Neurocytol 1977;6:465–81.
37. Seylaz J, Hara H, Pinard E, Mraovitch S, MacKenzie ET, Edvinsson L. Effect of stimulation of the sphenopalatine ganglion on cortical blood flow in the rat. J Cereb Blood Flow Metab 1988;8:875–8.
38. Yasui T, Karita K, Izumi H, Tamai M. Correlation between vasodilatation and secretion in the lacrimal gland elicited by stimulation of the cornea and facial nerve root of the cat. Invest Ophthalmol Vis Sci 1997;38:2476–82.
39. Kaji A, Maeda T, Watanabe S. Parasympathetic innervation of cutaneous blood vessels examined by retrograde tracing in the rat lower lip. J Auton Nerv Syst 1991;32:153–8.
40. Yoon KC, Im SK, Seo MS. Changes of tear film and ocular surface in diabetes mellitus. Korean J Ophthalmol 2004;18:68–74.
41. Postorino M, Catalano C, Martorano C, Cutrupi S, Marino C, Cozzupoli P, Scudo P, Zoccali C. Salivary and lacrimal secretion is reduced in patients with ESRD. Am J Kidney Dis 2003;42:722–8.
42. Gibbins IL, Morris JL. Structure of peripheral synapses: autonomic ganglia. Cell Tissue Res 2006;326:205–26.
43. Hokfelt T, Elfvin LG, Elde R, Schultzberg M, Goldstein M, Luft R. Occurrence of somatostatin-like immunoreactivity in some peripheral sympathetic noradrenergic neurons. Proc Natl Acad Sci USA 1977;74:3587–91.
44. Gibbins IL. Vasomotor, pilomotor and secretomotor neurons distinguished by size and neuropeptide content in superior cervical ganglia of mice. J Auton Nerv Syst 1991;34:171–83.
45. Phillips LK, Rayner CK, Jones KL, Horowitz M. An update on autonomic neuropathy affecting the gastrointestinal tract. Curr Diab Rep 2006;6:417–23.
46. Ding C, He QP, Li PA. Diabetes increases expression of ICAM after a brief period of cerebral ischemia. J Neuroimmunol 2005;161:61–7.
47. Katz ML, Robison WG Jr. What is lipofuscin? Defining characteristics and differentiation from other autofluorescent lysosomal storage bodies. Arch Gerontol Geriatr 2002;34:169–84.

48. Sugaya A, Sugimioto H, Mogi N, Tsujigami H, Deguchi S. Experimental diabetes accelerates accumulation of fluorescent pigments in rat trigeminal neurons. Brain Res 2004;999:132–4.

49. Schmidt RE, Plurad SB, Parvin CA, Roth KA. Effect of diabetes and aging on human sympathetic autonomic ganglia. Am J Pathol 1993; 143:143–53.

50. Ronco C, Grammaticopoulos S, Rosner M, De Cal M, Soni S, Lentini P, Piccini P. Oliguria, creatinine and other biomarkers of acute kidney injury. Contrib Nephrol 2010;164:118–27.

51. Sjöholm A, Nyström T. Inflammation and the etiology of type 2 diabetes. Diabetes Metab Res Rev 2006;22:4–10.

52. Danielle AT de Almeida, Camila PB,. Ethel LBN, Ana Angelica HF. Evaluation of lipid profile and oxidative stress in STZ-induced rats treated with antioxidant vitamin. Brazilian Archieves of Biology and Technology 2012;55:527–36.

53. Upchurch GR Jr, Keagy BA, Johnson G Jr. An acute phase reaction in diabetic patients with foot ulcers. Cardiovasc Surg 1997;5: 32–6.

Online available at:
www.anatomy.org.tr
doi:10.2399/ana.17.024
QR code:

Correspondence to: Aijaz Ahmed Khan, MS, PhD
Department of Anatomy, Jawaharlal Nehru Medical College,
Aligarh Muslim University, Aligarh, U.P, India
Phone: +91 9897216343
e-mail: aijazahmedkhan7@live.com

Conflict of interest statement: No conflicts declared.

Original Article

www.anatomy.org.tr
Received: July 20, 2017; Accepted: August 4, 2017
doi:10.2399/ana.17.026

anatomy
An International Journal of Experimental and Clinical Anatomy

Evaluation of the groove for vertebral artery using CT angiography*

Ayşegül Fırat[1], Nurhan Erbil[2], Rahşan Göçmen[3]

[1]*Department of Anatomy, School of Medicine, Hacettepe University, Ankara, Turkey*
[2]*Department of Biophysics, School of Medicine, Hacettepe University, Ankara, Turkey*
[3]*Department of Radiology, School of Medicine, Hacettepe University, Ankara, Turkey*

Abstract

Objectives: Groove for vertebral artery (sulcus arteriae vertebralis) is located on the posterior arch of the first cervical vertebra (atlas) where the vertebral artery passes over to reach the foramen magnum. The bony process between the posterior arch and the superior articulating process of the atlas is a common variation usually detected by lateral radiographies. This bony bridge is most commonly named as the ponticulus posticus. The aim of this study was to evaluate the existence of the ponticulus posticus and morphological features of the groove for vertebral artery.

Methods: We performed a retrospective analysis of the groove for vertebral artery from 347 head and neck CT angiographies (694 bilaterally) at the Department of Radiology, Hacettepe University School of Medicine.

Results: Complete ponticulus posticus incidence was found to be 12.1%, and 27.38% of these were bilateral. Post-sulcus arterial dimensions were found to be narrower than the pre-sulcus dimensions of the vertebral artery if the ponticulus posticus was incomplete.

Conclusion: The groove for vertebral artery is a commonly studied variation among different nations and using different methods like lateral dental graphies, cadaveric studies and dry skulls. This study will be a guide for clinical problems like headache, vascular diseases and surgical interventions of the atlas in a very large patient population and using CT angiography, a sensitive method for visualizing this area.

Keywords: arcuate foramen; CT angiography; groove for vertebral artery; ponticulus posticus

Anatomy 2017;11(2):61–66

Introduction

The groove for vertebral atery (sulcus arteriae vertebralis) is located on the first cervical vertebra (atlas, C1) where the vertebral artery passes over the posterior arch of atlas to reach the foramen magnum. A bony bridge between the posterior of the superior articular process and the posterolateral of the posterior arch of the atlas is a common variation that can be detected by radiographic images. This bony process encircles the groove for vertebral artery and the first cervical nerve partially or completely. It is known by numerous names such as ponticulus posticus (little posterior bridge, PP), Kimmerle's anomaly and Kimmerle's variant (**Figure 1**); PP is the most commonly used terminology. If PP exists, the sulcus can become a foramen which is known as arcuate foramen, foramen arcuale atlantis, sagittal foramen, retroarticular canal, retroarticular vertebral ring, atlantal posterior foramen or the upper retroarticular foramen.[1-7] The causes of the PP remain debated, but it has been proposed to be linked to either an ossification of the posterior atlantooccipital ligament or a congenital anomaly. However, it is usually regarded as a simple variation of the atlas which is usually ignored by the physician.[8–11] We may observe the PP in patients who do not have any evidence of a symptom in the craniocervical region. However, recent studies have suggested otherwise. The compression of nervous and vascular structures pass-

**This study was presented at the 7th Global Neurologists Annual Meeting on Neurology and Neurosurgery, Vienna, Austria (22–24 August 2016).*

Table 1
Distribution of the patients according to the degree of the PP, gender, age and laterality.

	Left (mean)					Right (mean)				
	Female		Male			Female		Male		
Degree of PP	<40 y	>40 y	<40 y	>40 y	Total	<40 y	>40 y	<40 y	>40 y	Total
0	27 (33.75%)	34 (34.34%)	43 (54.43%)	21 (23.60%)	125 (36%)	26 (32.50%)	43 (43.43%)	38 (48.10%)	26 (29.21%)	133 (38.3%)
1	23 (28.75%)	33 (33.33%)	18 (22.78%)	31 (34.83%)	105 (30.3%)	22 (27.50%)	30 (30.30%)	17 (21.52%)	30 (33.71%)	99 (28.5%)
2	17 (21.25%)	12 (12.12%)	6 (7.59%)	16 (17.98%)	51 (14.7%)	17 (21.25%)	7 (7.07%)	7 (8.86%)	15 (16.85%)	46 (13.3%)
3	10 (12.50%)	7 (7.07%)	0 (0.00%)	4 (4.49%)	21 (6%)	9 (11.25%)	7 (7.07%)	8 (10.13%)	6 (6.74%)	30 (8.7%)
4	3 (3.75%)	13 (13.13%)	12 (15.19%)	17 (19.10%)	45 (13%)	6 (7.5%)	12 (12.12%)	9 (11.39%)	12 (13.48%)	39 (11.2%)

ing through the foramen may cause many symptoms like vertebrobasilar insufficiency, cervical migraine, neuro-sensory type hearing loss, vertigo and arm/shoulder pain. It may cause dissections of the neurovascular structures or could also be asymptomatic.[3,5,12–14] Nowadays, there has been an increase in the number of patients undergoing C1 lateral mass screw (C1LMS) operation.[1,3,5–7,10,13,15–18] If the patient suffers from PP, the placement of the screw could be difficult during these operations.[19] Due to this clinical condition, it's important to understand the anatomy of the craniocervical region. PP is a common variation of this region and its presence must be carefully evaluated especially before the surgeries. This study aims to determine and analyze the existence of PP and correlate the dimensions of the vertebral artery with its prevalence.

Materials and Methods

We conducted a retrospective study using head and neck CT angiographies of 347 patients (694 bilaterally) admitted to the Department of Radiology in Hacettepe University School of Medicine for stroke and vascular problems between January 2010 and December 2015. Radiological images used in research were with patient consent with records kept in the Radiology Department of Hacettepe University Hospital. Head and neck CT angiography imaging was performed using a 64-slice Dual Source CT Scanner (Siemens Medical Systems, Erlangen, Germany). We evaluated axial unprocessed and also sagittal and coronal reformatted images with 1 mm slice thickness. The images were evaluated for incidence, laterality, age and gender effect on the incidence of complete PP. The measurements for the dimensions of arcuate foramen and the vertebral artery were also conducted (**Figure 2**). For descriptive purposes, we divided the study groups into young (<40 years), old (>40 years), male and female. We also evaluated the groove for the vertebral artery according to the laterality (left-right and bilateral) and the degree of concavity of the groove for vertebral artery (scored between 0–4; 0: no PP; 1, 2, 3: incomplete PP presence; 4: complete PP presence) (**Tables 1** and **2**). The diameters of the vertebral artery were measured before the groove (defined as pre-sulcus), inside the groove (defined as in-sulcus) and after leaving the groove (defined as post-sulcus) (**Figure 2**). Image analysis and measurements were conducted using the PACS integrated 'centricity universal viewer-version 6' (GE Healthcare, Chicago, IL, USA). Once the measurements were completed, group comparisons were conducted using the paired samples t-test with Bonferroni correction. Correlations were statistically evaluated using the 'multivariate analysis of variance (MANOVA) test' using SPSS 15 (IBM Corporation, New York, NY, USA). Statistical significance was set at a p value less than 0.05.

Table 2
Diameters of the vertebral artery around the sulcus (mean±SD, mm).

	Left			Right		
Gender	Pre-sulcus	In-sulcus	Post-sulcus	Pre-sulcus	In-sulcus	Post-sulcus
Female (n=178)	0.25±0.07	0.27±0.07	0.25±0.08	0.25±0.07	0.26±0.07	0.26±0.08
Male (n=165)	0.31±0.08	0.29±0.08	0.29±0.08	0.31±0.07	0.28±0.08	0.29±0.08

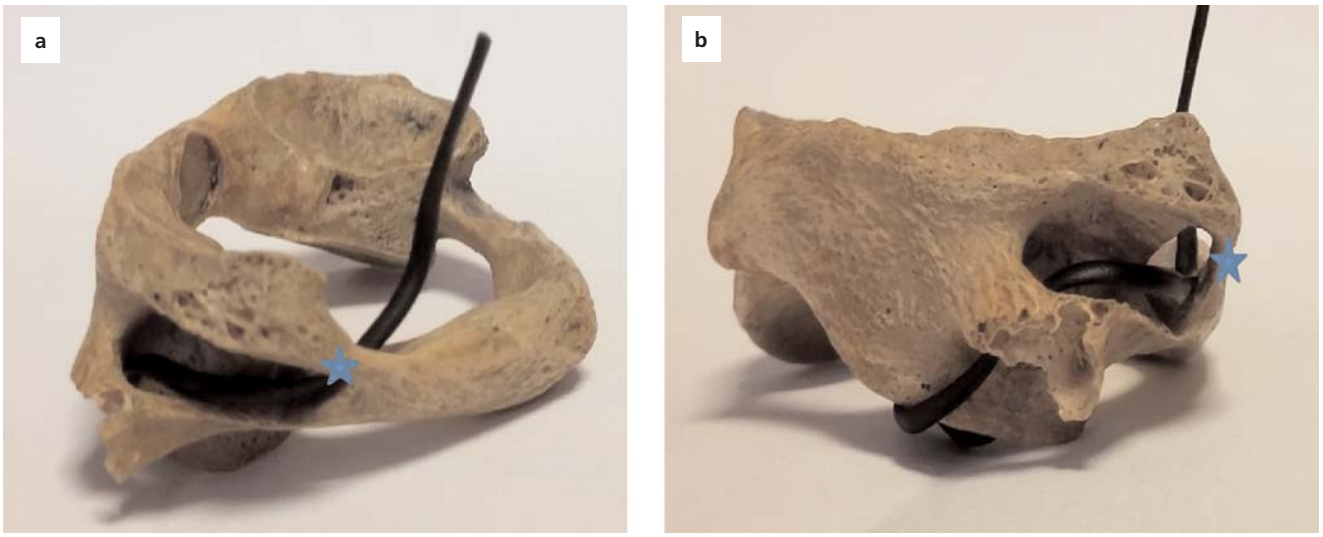

Figure 1. (**a**, **b**) Ponticulus posticus of atlas (*). [Color figure can be viewed in the online issue, which is available at www. anatomy.org.tr]

Results

The study group composed of 165 males and 178 females with a mean age of 49±19 (range: 14 to 87). We identified 84 patients with complete PP (Degree 4) which resulted in a prevalence of 12.1%. Of these, 6.3% were bilateral; which constituted 27.38% of the complete PPs. The analysis of the left side of the PP revealed that 13% were complete (Degree 4) and 51% were incomplete (Degree 1, 2, 3). As shown in **Table 1**, evaluations of patients' right side resulted with 11.2% with a complete PP and 50.5% with an incomplete PP. Furthermore, our results suggested that the amount of complete PP did not substantially vary based on gender ($p<0.383$) or laterality ($p<0.846$).

The mean area of the arcuate foramen was 8.5 mm^2 on the left side and 7 mm^2 on the right side. We measured the diameter of the vertebral artery prior to entry into the groove, within the groove, and immediately after leaving the groove (**Figure 2**). **Table 2** depicts the mean values and standart deviations. Our results indicated a significant difference of diameters of the vertebral artery in terms of laterality and gender (**Table 2**). The analysis of the vessel diameter for men and women indicated that the vessel diameter was significantly higher in

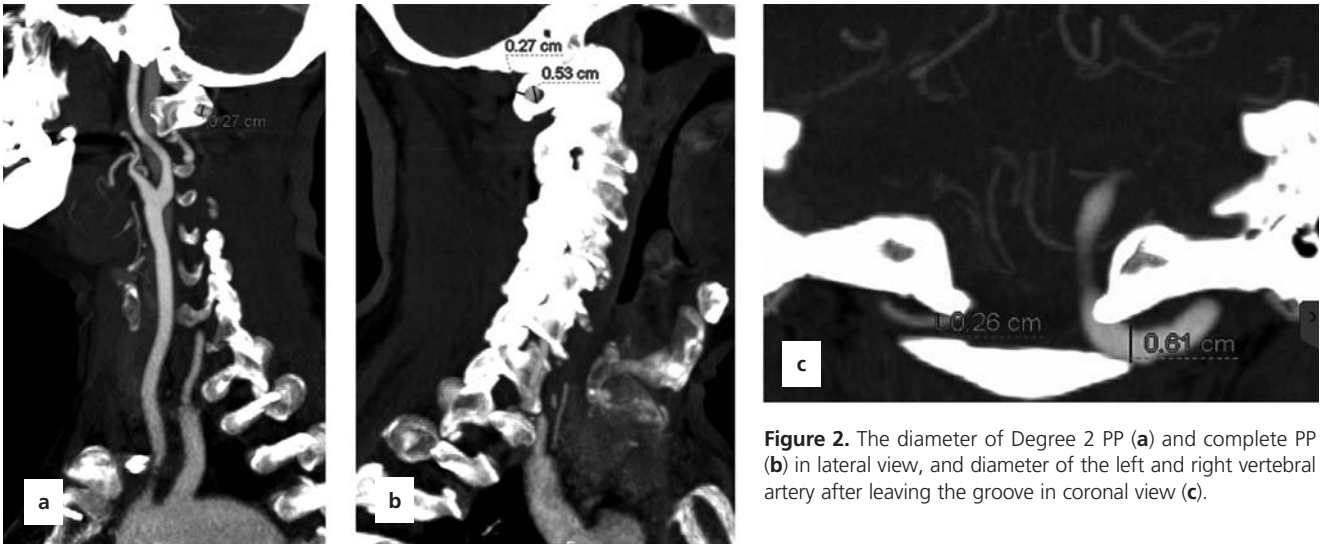

Figure 2. The diameter of Degree 2 PP (**a**) and complete PP (**b**) in lateral view, and diameter of the left and right vertebral artery after leaving the groove in coronal view (**c**).

Table 3
Comparison of diameters of the vertebral artery according to gender and laterality using ANOVA.

Side	Parameter	Comparison	Sum of squares	Mean square	F	p*
Left	Pre-sulcus vs. gender	Between groups	0.345	0.345	62.07	0
		Within groups	1.897	0.006		
		Total	2.242			
	In-sulcus vs. gender	Between groups	0.075	0.075	14.48	0
		Within groups	1.768	0.005		
		Total	1.843			
	Post-sulcus vs. gender	Between groups	0.186	0.186	31.37	0
		Within groups	2.018	0.006		
		Total	2.204			
Right	Pre-sulcus vs. gender	Between groups	0.303	0.186	61.39	0
		Within groups	1.684	0.005		
		Total	1.988			
	In-sulcus vs. gender	Between groups	0.038	0.038	7.61	0.006
		Within groups	1.715	0.005		
		Total	1.753			
	Post-sulcus vs. gender	Between groups	0.066	0.066	11.14	0.001
		Within groups	2.016	0.006		
		Total	2.082			

*p=0.05

men on both sides (p<0 on the left side and p<0.006 on the right side (**Table 3**).

This difference can be attributed to the higher values of the vessel diameter for men (**Table 2**). In Degree 1, 2 and 3 groups, the vessel diameter significantly decreased after leaving the sulcus on both sides (p<0.028 for the right side, p<0.001 for the left side (**Table 4**). We did not find a statistically significant difference between the degree of the PP and vessel diameter in terms of laterality. The mean diameter of the arcuate foramen was 0.33 cm on the left side and 0.30 cm on the right side. The mean thickness of the PP was 0.2 cm on the left side and 0.22 cm on the right side. Substantial variations were not evident for the thickness and diameter of the PP.

Discussion

A literature review revealed that multiple studies e produced different results in regard to the incidence of the PP (1.14–37%) (**Table 5**). Elliot and Tanweer[7] substantially contributed to the understanding of radiologists, anatomists and neurosurgeons by reviewing and analyzing radiographic, cadaveric and surgical databases. This examination reported the prevalence of complete PP as 44% from an on-line database of 21,789 cases, which has included 15,542 patients and 6247 body and cadaver samples. They found the the prevalence of complete PP as 9.3%, while incomplete PP had a prevalence of 8.7%. In 5.4% of their cases, the PP was bilateral. Furthermore, this examination did not confirm a statistical correlation to gender. Bayrakdar et al.[2] conducted another study that analyzed 730 cone beam computed tomography (CBCT) images, which found PP in 127 patients (17%). Males had a prevalence of 19.5% (54 of 277 patients) and females a prevalence of 16.1% (73 of 453 patients).

Sharma et al.[17] investigated lateral cephalometric radiographs of 858 Indian orthodontic patients for the presence of PP. In this study, complete PP prevalence was 4.3% with a male predominance of 5.33%. In lateral cephalometric radiographies of 353 Caucasion patients,

Table 4
Comparison of diameters of the vertebral artery according to the degree of the PP and laterality.

		n	Mean±SD (cm)	p
Degrees 1, 2, 3	Left	296	0.278±0.083	0.001
		296	0.268±0.081	
	Right	296	0.282±0.077	0.028
		296	0.276±0.076	
Degree 4	Left	86	0.277±0.069	0.254
		86	0.273±0.075	
	Right	86	0.27±0.078	0.405
		86	0.268±0.089	

Kendrick and Biggs[10] demonstrated a 15.8% prevalence of PP with no difference between men and women.

The majority of previous studies used lateral radiographies to identify PP, but this technique is not suitable for determining the laterality of the PP. Therefore, head and neck CT angiographies should be considered for evaluating the cervical region. Our study is one of the first examinations to evaluate the presence of PP and its relation with the arterial dimensions in the Turkish population using the CT angiography technique. We evaluated 347 head and neck CT angiographies which demonstrated a prevalence of complete PPs of 12.1% with no variation due to gender or laterality. This result should be considered extremely beneficial for daily clinical practice. Therefore, this region should be carefully examined especially before screw placement operations in order to avoid injury to the vertebral artery. The examination of PP is also important for neck pain, headaches, visual disturbances, speech and swallowing problems, vertigo and vascular problems. Considering these clinical problems, we examined the correlation of the vessel morphometry to the occurence of PP. This was the first detailed examination of the vertebral artery around the sulcus. Our results showed that the mean vessel diameter was higher in men for both sides. We did not statistically confirm the difference between the degree of PP and vessel diameter on both sides. In incomplete PP cases, the decrease in diameter of the vessel on both sides was been statistically confirmed. PP and arcuate foramen should not be considered as a simple anatomical variations. The change in the diameter of the vessel due to incomplete PP may cause many clinical problems such as vertebrobasilar insufficiency. Clinical coexistence of PP with headache, neck pain, and vascular problems should also be studied. Compression of the first cervical nerve may also result in clinical sypmtoms. Therefore, such morphological evaluations should be of interest to both anatomists and clinicians. Compression of the neurovascular structures passing through the foramen may result in a combination of symptoms.

A limitation of our study was that the patient group was selected from a symptomatic stroke and vascular diseases patients who applied to our third level university hospital. Further studies with asymptomatic subjects, cadavers and dry bones are recommended to declare the differences among populations and nations.

Split and Sawresevicz-Rybak[12] found that headache, neck, shoulder, and arm pains as well as vertigo was significantly higher in patients with complete PP than those with partial PP. A complete PP may be mistaken for a broad dorsal arch and the surgeon may accidentally insert the screw into the arcuate foramen which can result in damage to the vertebral artery and lead to stroke or death due to thrombosis, embolism, or arterial dissection.[19] Cushing et al.[5] observed arcuate foramen in eight of eleven patients with vertebral artery dissection and occlusion. The arterial injury was at the level of this anatomical variation in all cases. Since over 50% of head rotation occurs at the atlantoaxial joint, the vertebral artery is vulnerable to compression and stretching at this level and thus, additional compression/tethering due to an arcuate foramen can compound its predisposition to injury. During neck flexion, the vertebral artery glides superiorly and anteriorly relative to the posterior arch, which has a greater rate of occurence at the level of the lateral masses of the atlas compared to more caudal sites in the neck.[16]

Table 5
Incidence of complete PP in the literature and current study.[2,3,6–8,14,15,17,20–22]

Author	Material	Incidence of complete PP (%)
Lamberty and Zivanovic, 1973[14]	Dry bones	7.5
Lamberty and Zivanovic, 1973[14]	Radiography	15
Dhall et al., 1993[6]	Dry bones	37.83
Hasan et al., 2001[8]	Dry bones and cadaver	1.14
Cakmak et al., 2005[3]	Dry bones	11.7
Paraskevas et al., 2005[15]	Dry bones	10.23
Tubbs et al., 2007[21]	Cadaver	5
Kim et al., 2007[22]	CT	26
Kim et al., 2007[22]	Radiography	14
Sharma et al., 2010[17]	Radiography	4.3
Simsek et al, 2008[20]	Dry bones	3.8
Elliott and Tanweer, 2014[7]	Cadaver	18.8
Elliott and Tanweer, 2014[7]	CT	17.2
Elliott and Tanweer, 2014[7]	Radiography	16.6
Bayrakdar et al., 2014[2]	Cone beam CT	17.4
Fırat et al., 2017	CT angiography	12.1

The clinical significance of PP still remains unclear. Some scholars, such as Wight et al.,[13] identified correlations between PP and head pain and noted a significant overrepresentation of the ring in chiropractic patients with headaches without aura (i.e. visual or auditory disturbances). Surgical excision of the PP alleviates headache, vertigo, and basilar insufficiency.[18] Spinal manipulative therapy involving craniovertebral articulation also alleviates symptoms of vertigo, headaches, and nausea.[9,13] Chiropractic treatments significantly improve the treatment of migraines. In addition, the results of this study may also be relevant to manual therapists, such as chiropractors, physical therapists, or other health care providers. If PP is detected or suspected, it must be documented in the the health record of the patient and a specialist consultation must be sought.

Conclusion

Based on the findings in the present study, an incomplete arcuate foramen may compress the vertebral artery. The literature review reveals that the symptomatic compression of the vertebral artery at this location may be alleviated for some patients using decompressive procedures. Arcuate foramen is an anatomical variation that the neurosurgeons should consider when undertaking surgery near or on the posterior atlas. Our results confirm that the prevelance of PP is a common variation, although its prevalence in other groups remains to be investigated.

Acknowledgement

This study was funded by the Hacettepe University Scientific Research Unit with project number THD-2016-9170.

References

1. Ahmad FU, Wang MY. Lateral mass of C1 fixation and ponticulus-posticus. World Neurosurg 2014;82:E145–6.
2. Bayrakdar IS, Miloglu O, Altun O, Gumussoy I, Durna D, Yilmaz AB. Cone beam computed tomography imaging of ponticulus posticus: prevalence, characteristics, and a review of the literature. Oral Surg Oral Med Oral Pathol Oral Radiol 2014;118:E210–9.
3. Cakmak G, Gurdal E, Ekinci G, Yildiz E, Cavdar S. Arcuate foramen and its clinical significance. Saudi Med J 2005;26:1409–13.
4. Chen CH, Chen YK, Wang CK. Prevalence of ponticuli posticus among patients referred for dental examinations by cone-beam CT. Spine J 2015;15:1270–6.
5. Cushing KE, Ramesh V, Gardner-Medwin D, Todd NV, Gholkar A, Baxter P, Griffiths PD. Tethering of the vertebral artery in the congenital arcuate foramen of the atlas vertebra: a possible cause of vertebral artery dissection in children. Dev Med Child Neurol 2001;43:491–6.
6. Dhall U, Chhabra S, Dhall JC. Bilateral asymmetry in bridges and superior articular facets of atlas vertebra. J Anat Soc India 1993;42: 23–7.
7. Elliott RE, Tanweer O. The prevalence of the ponticulus posticus (arcuate foramen) and its importance in the goel-harms procedure: meta-analysis and review of the literature. World Neurosurg 2014;82:E335–43.
8. Hasan M, Shukla S, Siddiqui MS, Singh D. Posterolateral tunnels and ponticuli in human atlas vertebrae. J Anat 2001;199:339–43.
9. Kavakli A, Aydinlioglu A, Yesilyurt H, Kus I, Diyarbakirli S, Erdem S, Anlar O. Variants and deformities of atlas vertebrae in Eastern Anatolian people. Saudi Med J 2004;25:322–5.
10. Kendrick GS, Biggs NL. Incidence of ponticulus posticus of first cervical vertebra between ages 6 to 17. Anat Rec 1963;145:449–53.
11. Kim MS. Anatomical variant of atlas: arcuate foramen, occipitalization of atlas, and defect of posterior arch of atlas. J Korean Neurosurg Soc 2015;8:528–33.
12. Split W, Sawrasewicz-Rybak M. Character of headache in Kimmerle anomaly. Headache 2002;42:911–6.
13. Wight S, Osborne N, Breen AC. Incidence of ponticulus posterior of the atlas in migraine and cervicogenic headache. J Manipulative Physiol Ther 1999;22:15–20.
14. Lamberty BG, Zivanovic S. The retro-articular vertebral artery ring of the atlas and its significance. Acta Anat 1973;85:113–22.
15. Paraskevas G, Papaziogas B, Tsonidis C, Kapetanos G. Gross morphology of the bridges over the vertebral artery groove on the atlas. Surg Radiol Anat 2005;27:129–36.
16. Sekerci AE, Soylu E, Arikan MP, Ozcan G, Amuk M, Kocoglu F. Prevalence and morphologic characteristics of ponticulus posticus: analysis using cone-beam computed tomography. J Chiropr Med 2015;14:153–61.
17. Sharma V, Chaudhary D, Mitra R. Prevalence of ponticulus posticus in Indian orthodontic patients. Dentomaxillofac Radiol 2010;39:277–83.
18. Vernon H. Cervicogenic headache. In: Gatterman MI, editor. Foundations of the chiropractic subluxation. St Louis (MO): Mosby 1995;306–16.
19. Young JP, Young PH, Ackermann MJ, Anderson PA, Riew KD. The ponticulus posticus: implications for screw insertion into the first cervical lateral mass. J Bone Joint Surg Am 2005;87:2495–98.
20. Simsek S, Yigitkanli K, Comert A, Acar HI, Seckin H, Er U, Belen D, Tekdemir I, Elhan A. Posterior osseous bridging of C1. J Clin Neurosci 2008;15:686–8.
21. Tubbs RS, Johnson PC, Shoja MM, Loukas M, Oakes WJ. Foramen arcuale: anatomical study and review of the literature. J Neurosurg Spine 2007;6:31–4.
22. Kim KH, Park KW, Manh TH, Yeom JS, Chang BS, Lee CK. Prevalence and morphologic features of ponticulus posticus in Koreans: analysis of 312 radiographs and 225 three-dimensional CT scans. Asian Spine J 2007;1:27–31.

Online available at:
www.anatomy.org.tr
doi:10.2399/ana.17.026
QR code:

deomed.

Correspondence to: Ayşegül Fırat, MD
Department of Anatomy, School of Medicine,
Hacettepe University, Ankara, Turkey
Phone: +90 312 305 21 32
e-mail: aysfirat@hacettepe.edu.tr

Conflict of interest statement: No conflicts declared.

 Please cite this article as: Fırat A , Erbil N, Göçmen R. Evaluation of the groove for vertebral artery using CT angiography. Anatomy 2017;11(2):61–66.

Original Article

www.anatomy.org.tr
Received: July 5, 2017; Accepted: July 31, 2017
doi:10.2399/ana.17.022

anatomy
An International Journal of Experimental and Clinical Anatomy

Accessory renal artery associated with congenital kidney anomalies

Panneerselvam Sasikala, Sabita Singh

Department of Anatomy, Velammal Medical College, Madurai, Tamil Nadu, India

Abstract

Objectives: Common variations in the arterial supply of the kidney reflect the manner in which its vascularization changes during embryonic and early fetal life. The aim of the study was to determine the incidence of the accessory renal artery in association with congenital kidney anomalies.

Methods: The study was conducted on 37 dissected cadavers and 25 patients aged between 25–62 years who underwent renal CT angiography.

Results: Accessory renal artery associated with congenital kidney anomalies was observed in two cadavers: one had polycystic kidney disease with accessory renal artery in the right kidney, the second had malrotated kidney with accessory renal artery on the left kidney. Three cases in CT angiograms showed accessory renal artery with horseshoe kidney with three accessory renal arteries, pelvic kidney with accessory renal artery on the right side, and the third case had hypoplastic kidney with accessory renal artery on the right side.

Conclusion: Accessory renal artery can be due to the abnormal development of kidneys and variations in the positional anatomy of the kidney. This study supplements the presence of variations in renal arteries and its association with congenital kidney anomalies that are of clinical significance during diagnostic investigations and for avoiding complications during surgical approaches to the kidney.

Keywords: accessory renal artery; horseshoe kidney; malrotated kidney; polycystic kidney

Anatomy 2017;11(2):67–71

Introduction

Renal arteries are a pair of lateral branches from the abdominal aorta at the level of L1–L2, little below the origin of the superior mesenteric artery. Each renal artery divides into an anterior and a posterior division near the hilum of the kidney, which in turn divides into five segmental arteries supplying the different renal vascular segments.[1] Variations in the number, source and course of the renal arteries are common, most common variation being the accessory renal artery.[2] Variations in the kidney arterial supply reflect the manner in which the vascular supply continually changes during embryonic and early fetal life. Accessory renal arteries usually arise from the abdominal aorta above and below the main renal artery and follow it to the renal hilum. They are regarded as persistent embryonic lateral splanchnic arteries.[1] The frequency of accessory renal arteries varies from 9% to 76% with an average of 30%. In rare cases, accessory renal arteries may arise from the celiac trunk, superior mesenteric, inferior mesenteric, common iliac, middle sacral, or external iliac arteries.[3]

Accessory renal arteries arise as result of the complicated development of kidneys and variations in their positional anatomy.[4] They can be derived from the internal spermatic, superior mesenteric, common iliac, hypogastric or middle sacral arteries, and may be associated with ectopic or fused kidneys.[5] Accessory renal arteries are end arteries; therefore if they are damaged, the part of kidney supplied by it becomes ischemic.[6] The knowledge of the variation of renal arteries and associated congenital renal anomalies is very much essential for medical educators, surgeons and radiologists for proper diagnosis and management of the patient. Thus, this study aimed to widen

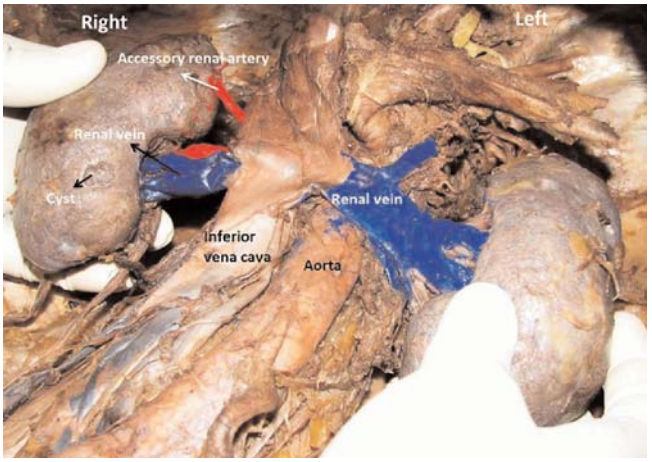

Figure 1. Polycystic kidney with accessory renal artery on the right side. [Color figure can be viewed in the online issue, which is available at www.anatomy.org.tr]

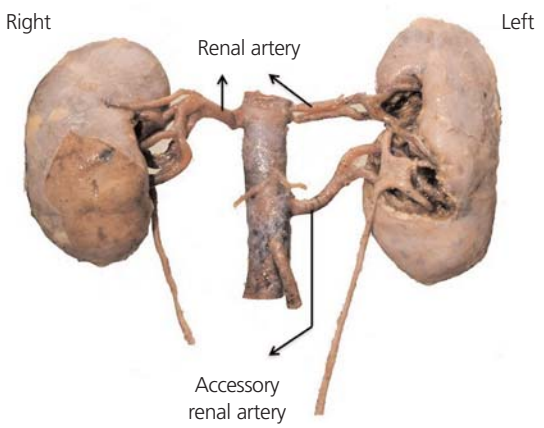

Figure 2. Malrotated kidney with accessory renal artery on the left side. [Color figure can be viewed in the online issue, which is available at www.anatomy.org.tr]

our knowledge about vascularization of the kidney, the incidence of accessory renal artery and its association with congenital anomalies of the kidney.

Materials and Methods

The present study was conducted on 37 dissected cadavers (31 males and 6 females) during routine dissection of the abdomen for medical undergraduate training in the Departments of Anatomy of Sri Ramachandra Medical College and Research Institute and the Chennai and Velammal Medical College, Madurai, India. This study also included 25 patients (16 males and 9 females) ranged between 25–62 years who underwent renal CT angiography in the Radiology and Imaging Sciences of Sri Ramachandra Medical College and Research Institute with due consent from the patients. The device used was a 64 Slice VCT xt high speed advantage scanner, Helical computed tomography (General Electric Medical Systems, Milwaukee, USA.)

Exposure of the kidney was done following the proper procedures in accordance with ethical standards of handling of cadavers for learning and teaching. Accessory renal arteries with associated congenital anomalies were examined in detail and photographed. The patients were informed about the angiographic procedures and probable complications were also explained to the patients. In this study, no additional interventions were performed on the patients. Ethics approval was received from the Institutional Ethics Committee of Sri Ramachandra University.

Results

Accessory renal artery associated with congenital anomalies was found in two cadavers and three CT angiograms. Of the two cadavers with accessory renal artery, one had polycystic kidney disease with accessory renal artery to the right kidney (**Figure 1**), and another had malrotated kidney with accessory renal artery on the left side (**Figure 2**). Three cases in CT angiograms showed accessory renal artery with various congenital anomalies. Horseshoe kidney (**Figure 3**) with three accessory renal arteries - one

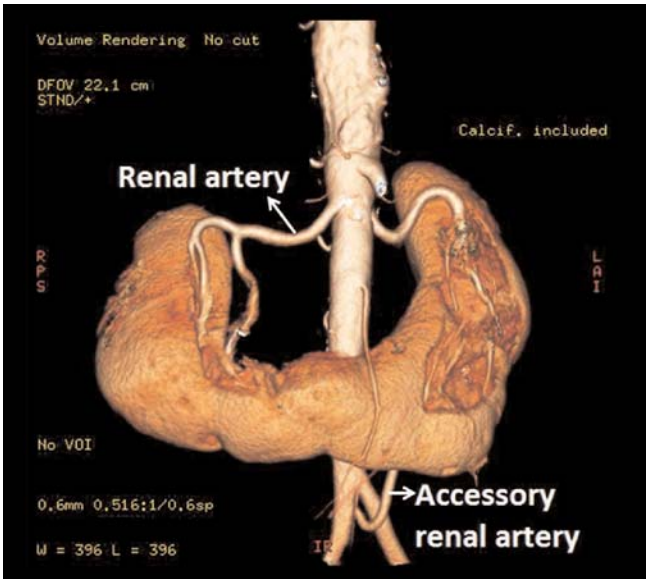

Figure 3. Horseshoe kidney with accessory renal artery on the left side. [Color figure can be viewed in the online issue, which is available at www.anatomy.org.tr]

from right common iliac artery and two from abdominal aorta - was found in the first case. The second case had pelvic kidney with accessory renal artery on the right side. The third case had hypoplastic kidney with accessory renal artery on the right side.

The incidence of the accessory renal artery and asscociated kidney anomalies in cadaver specimens and patients who underwent renal CT angiography are shown in **Table 1**.

Table 1
Incidence of the accessory renal artery and asscociated kidney anomalies in cadaver specimens and patients who underwent renal CT angiography.

Groups	Number of kidneys	Presence of associated kidney anomaly
Cadaver specimens	5/37 (13.5%)	2/37 (5.4%)
Renal CT angiography cases	8/25 (32%)	3/25 (12%)

Discussion

Knowledge of the variations of the renal artery and associated congenital anomalies is essential for exploring and managing renal trauma, renal transplantation, renovascular hypertension, renal artery embolization, angioplasty and vascular reconstruction for congenital and acquired lesions.[7] It is essential to know the embryology of the renal artery and structural development of the kidney to understand the multitude of anomalies that may occur. The complex development of the kidneys through pronephros, mesonephros and metanephros, and the ascent of the kidney from the pelvis to the lumbar region, its vertical rotation and simultaneous acquisition of a vascular supply explain the common variations in the blood supply of kidneys associated with congenital malformations.[6] The majority of renal artery variations are due to the changing position of the kidney, as a part of its normal development and ascent.[8] Kidneys develop from the intermediate mesoderm in the pelvic region. Later, they ascend to the adult position in the lumbar region. In the pelvic region, kidneys are supplied by branches of the internal iliac artery or the common iliac artery. The arterial supply shifts from the common iliac to the abdominal aorta with its ascent. In the ninth week of the intrauterine life, the kidneys come in contact with the suprarenal glands and the ascent ceases. This relative ascent results mainly from the growth of the embryo's body caudal to the kidneys. In effect, the caudal part of the embryo grows away from the kidneys so that they progressively occupy more cranial levels. The kidneys receive their most cranial branches from the abdominal aorta. These are the permanent renal arteries. Failure in degeneration of the initial branches leads to formation of accessory renal artery. Initially, the hilum of the kidney where vessels and nerves enter and leave faces ventrally; however, as the kidney relocates (ascends), it rotates medially by almost 90°. By the ninth week, the hilum is directed anteromedially.[9] Nino-Murcia et al., are of the opinion that renal rotation takes place before definitive vascularization. This process occurs between 38 and 49 days of development, during the ascent of the kidney. The developing metanephros rotates from the dorsomedial to a more lateral position, relative to the collecting system, resulting in the hilum of kidney eventually rotating from the anterior to the medial position. In nonrotation, the renal pelvis presents itself ventrally in relation to the kidney mass. In incomplete rotation, it presents itself ventromedially.[10]

The kidney may become ectopic in the pelvis, if it fails to ascend adequately. The horseshoe kidney may be developed if the lower pole is fused and becomes trapped by the inferior mesenteric artery, and thus the kidney cannot ascend to the lumbar region.[11]

According to Felix,[12] there are nine pairs of lateral mesonephric arteries arising from the dorsal aorta, arranged as cranial (1st and 2nd pair), middle (3rd and 4th pair) and caudal (6th to 9th pair) groups in 18 mm fetus. Renal artery develops from one pair of middle group. The persistence of more than one artery from the middle group results in formation of an accessory renal artery. Thus, the accessory renal arteries in our study are a result of persisting lateral mesonephric arteries from the middle group.

Varieties of congenital renal anomalies with accessory renal artery have been documented in literature so far. Accessory renal artery with unilateral congenital anomalies is more common than bilateral anomalies. Aberrant renal artery with unilateral anomaly was reported in 15% and bilateral anomaly in 5% specimens by Dhar and Lal.[13]

Accessory renal artery can delay the kidney migration that results in ectopic kidney or vice versa. The incidence of ectopic kidney with unilateral or bilateral accessary renal artery is about 1:500 to 1:110. The ectopic kidney can be unilateral or bilateral at various levels. Unilateral pelvic kidney was observed in 1:3000 and thoracic kidney in 1:13,000. Most of the cases of ectopic kidneys are asymptomatic.[14,15] The present study reported unilateral pelvic kidney with accessory renal artery in one out of 25 cases in CT angiograms.

Polycystic kidney disease is one of the life-threatening inherited disorders. For many years, it was thought that the cysts were the result of failure of the metanephric

diverticulum derivatives to join the tubules derived from the metanephrogenic blastema. It is now believed that the cystic structures are wide dilations of parts of the otherwise continuous nephrons, particularly the nephron loops (loops of Henle).[9] Polycystic kidney can be observed in association with accessory renal artery. Manpreet et al.[16] reported a case of left kidney with multiple cysts and accessory renal artery in right kidney. Both of these can cause renal failure, hypertension, hydronephrosis and even failure of renal transplants. We found multiple cysts in one out five cadavers who had accessory renal arteries.

Kidney rotates through 90° ventromedially during its normal development. However, according to Bauer,[17] the ureteral branching induces differentiation of the metanephric tissue, different degrees of unequal branching result in various forms of malrotation. Felix postulated that rotation is a result of unequal and different branching pattern of successive orders of ureteral tree. With excessive ventral branching more parenchyma develops ventrally and the renal pelvis seems to rotate medially.[12] There are various types of renal anomalies related to abnormal rotation like nonrotation, incomplete rotation, excessive rotation or reverse rotation. Renal pelvis position depends on the types of rotation of the kidney. In non-rotation, renal pelvis is present ventrally, in incomplete rotation ventromedially, whereas in reverse rotation ventrolaterally.[18] Our case is most probably unrotated kidney, since the pelvis is present ventrally .

Banerjee et al.[8] reported an incompletely rotated kidney with three accessory renal vessels, two renal arteries, and one renal vein at the lower pole in left kidney. Ramteerthankar et al.[19] found bilateral unrotation of the kidneys in a female cadaver without any associated variation. Atasever et al.[20] observedan unrotated left kidney with partly extrarenal calyces associated with an accessory renal artery in a male cadaver.

As the renal rudiments ascend from the pelvic region to the loin, they remain entirely separate. If they come in contact and adhere, usually at the lower poles, this results in horseshoe kidney.[21] The incidence of horseshoe kidney is less than 0.3%, in one out of 300 pyelographies.[22] Mohanty et al.,[23] in a case report, observed a horseshoe kidney in a female cadaver, with extrarenal calyces, with two small caliber renal arteries supplying the upper segment of the organ on either side and a single accessory renal artery originating from the aorta on the right side and branching to supply the right and left middle segments together with a well-developed connecting bridge. Vaniya et al.[24] noticed in a male cadaver, a horseshoe kidney with multiple renal arteries and extrarenal calyces. A horseshoe kidney may be problematic in abdominal aneurysm surgery, as the renal arteries arise normally only in 20% of these cases.[24] In the present study, we observed a horseshoe shaped kidney with three accessory renal arteries, but no extrarenal calyces.

The frequency of unilateral hypoplastic kidney was reported to be one in 500 autopsies. The cause of hypoplastic kidney can be congenital or as a result of pyelonephritic shrinkage or as a combination of both.[25] Guang-Qian Xiao et al.[26] reported a case of unilateral hypoplastic kidney in a 33 year old male patient. We found one hypoplastic kidney with accessory renal artery in the right kidney among eight cases with accessory artery in CT angiograms.

Advances in surgical and uroradiological techniques dictate a reappraisal and definition of renal artery variations. The present study revealed the percentage of accessory renal arteries and its association with congenital anomalies using cadaver dissection and CT angiography techniques. This study will supplement the knowledge of variation in renal arteries and its association with congenital anomalies for avoiding complications during diagnostic investigations or surgical approaches to the kidney. The renal arteries can not be evaluated properly only by axial images, because they usually have a tortuous and variable course. Therefore, there is a need for additional views by CT angiography.[8] Modification of CT protocol by generating thinner sections may improve the detection of accessory arteries. This information is exceedingly important to the surgeons in planning treatment strategies.

References

1. Bannister LH, Berus MM, Collins P, Dyson M, Dusek JE, Ferguson MWJ. Gray's anatomy. 40th ed. Edinburgh: Churchill Livingstone; 2008. p. 1225–33.
2. Bergman RA, Afifi AK, Miyauchi R. Illustrated encyclopedia of human anatomic variations: Opus II. Cardiovascular system: arteries: abdomen: renal arteries. http://www.anatomyatlases.org/AnatomicVariants/Cardiovascular/Text/Arteries/Renal.shtml [Retrieved April 7, 2010].
3. Hollinshead WH. Anatomy for surgeons. Volume 2. New York: Harper and Row; 1971. p. 533–46.
4. Bayramoglu A, Demiryurek D, Erbil KM. Bilateral additional renal arteries and an additional right renal vein associated with unrotated kidneys. Saudi Med J 2003;24:535–7.
5. Mcvay CB. Anson and Mcvay surgical anatomy. Volume 1. 6th ed. Philadelphia: W.B. Saunders; 1984. p. 739–43.
6. More Anju B, Hebbal GV, Rajesh S, Kunjumon PC. An unique asymmetrical bilateral variation of renal artery: right sided early division and left sided accessory/additional arteries. International Journal of Anatomy and Research 2014;2:583–8.
7. Cicekcibasi AE, Salbacak A, Seker M, Ziylan T, Buyukmumcu M, Tuncer I. An investigation of the origin, location, and variation of the renal arteries in human fetuses and their clinical relevance. Ann Anat 2005;187:421–7.

8. Banerjee SS, Paranjape, Arole V, Vatsalaswamy P. Variation of hilar anatomy in an incompletely rotated kidney associated with accessory renal vessels. Journal of Dr. D.Y. Patil University 2014;7:645–7.
9. Moore KL, Persaud TVN. Torchia MG. The developing human. Clinically oriented embryology. 9th ed. Philadelphia: Saunders; 2011. p. 249–50.
10. Nino-Murcia M, de Vries PA, Friedland GW. Congenital anomalies of the urinary tract. In: Pollack HM, McClennan BL, Dyer R, Kenny PJ, editors. Clinical urography. 2nd ed. Volume 1. Philadelphia: Saunders; 2000. p. 690-763.
11. Sadler TW. Langman's medical embryology. 12th ed. Philadelphia: Wolters Kluwer Health/Lippincott Williams and Wilkins; 2012. p. 238–40.
12. Felix W. Mesonephric arteries (aa. mesonephricae). In: Kiebel F, Mall FP, editors. Manual of human embryology. Vol. 2. Philadelphia: Lippincott; 1912. p. 820–5.
13. Dhar P, Lal K. Main and accessory renal arteries–a morphological study. Ital J Anat Embryol 2005;110:101–10.
14. Zagyapan R, Pelin C, Kürkçüoğlu A. A retrospective study on multiple renal arteries in Turkish population. Anatomy 2009;3:35–9.
15. Zahoi DE, Miclauş G, Alexa A, Sztika D, Pusztai AM, Farca Ureche M. Ectopic kidney with malrotation and bilateral multiple arteries diagnosed using CT angiography. Rom J Morphol Embryol 2010;51:589–92.
16. Manpreet K, Sangeeta W, Anupama M. Anomalies by birth in urogenital system: clinical aspect. International Journal of Basic Science and Pharmacy 2012;2:39–41.
17. Bauer SB. Anomalies of the kidney and ureteropelvic junction. In: Walsh PC, Retik AB, editors. Campbell's urology. 7th ed. Philadelphia: Saunders; 1998. p. 1728–30.
18. Braasch WF. Anomalous renal rotation and associated anomalies. J Urol 1931;25:9–21.
19. Ramteerthankar RN, Joshi DS, Joshi RA, Pote AJ. Bilateral unrotation of kidneys. Saudi J Kidney Dis Transpl 2011;22:1033–4.
20. Atasever A, Hamdi Celik H, Durgun B, Yilmaz E. Unrotated left kidney with an accessory renal artery. J Anat 1992;181:507–8.
21. McGregor AL, Decker GAG, Du Plessis DJ. Lee McGregor's synopsis of surgical anatomy. 12th ed. Bristol: John Wright; 1986. p. 298–9.
22. Dees JE. Clinical importance of congenital anomalies of the upper urinary tract. J Urol 1941;46:659–66.
23. Mohanty C, Ray B, Samaratunga U, Singh G. Horseshoe kidney with extrarenal calyces – a case report. Journal of the Anatomical Society of India 2002;51:57–8.
24. Vaniya VH. Horseshoe kidney with multiple renal arteries and extrarenal calyces: a case report. Journal of the Anatomical Society of India 2004;53:52–4.
25. Bengtsson C, Hood B. The unilateral small kidney with special reference to the hypoplastic kidney. Review of the literature and authors' points of view. Int Urol Nephrol 1971;3:337–51.
26. Xiao GQ, Jerome JG, Wu G. Unilateral hypoplastic kidney and ureter associated with diverse mesonephric remnant hyperplasia. Am J Clin Exp Urol 2015;3:107–11.

Online available at:
www.anatomy.org.tr
doi:10.2399/ana.17.022
QR code:

Correspondence to: Sabita Singh, M.B; B.S, M.D
Department of Anatomy, Velammal Medical College,
Madurai, 625009, Tamil Nadu, India
Phone: +917667908292
e-mail: drsabita1234@gmail.com

Conflict of interest statement: No conflicts declared.

anatomy
www.anatomy.org.tr
An International Journal of Experimental and Clinical Anatomy

Original Article

www.anatomy.org.tr
Received: May 6, 2017; Accepted: July 27, 2017
doi:10.2399/ana.17.013

Chronic anaemia causes degenerative changes in trophoblast cells of the rat placenta

Omer Awad, Shem J. Ochieng, Abdel Malek, Julius Ogeng'o

Department of Human Anatomy, University of Nairobi, Nairobi, Kenya

Abstract

Objectives: Iron deficiency anaemia causes adverse pregnancy outcome. There are few studies on effects of anaemia on the structure of trophoblastic cells which are important in placental function. These data are important for understanding the function and disorders of the placenta. The aim of this study was to investigate the ultrastructural cellular changes associated with iron deficiency anaemia in rat placenta.

Methods: Forty-nine female Sprague-Dawley rats were randomly separated into experimental and control groups. The experimental group was rendered anaemic by removing 1.5 ml of blood per bleed on five alternate days, and the placentas were collected on gestational days 17, 19 and 21. For light microscopy, five cubic millimeter segments were fixed in 10% buffered formaldehyde solution; dehydrated in ethanol and embedded in paraffin wax. Five micron thick sections were cut, deparaffinized and stained with Hematoxylin and Eosin. For transmission electron microscopy, 1 mm^3 sections were fixed in 2.5% phosphate buffered glutaraldehyde, post fixed in 2% osmium tetroxide, dehydrated in ethanol, cleared in propylene and embedded in epon resin. Ultrathin sections stained with uranyl acetate and lead citrate were examined with JEOL electron microscope.

Results: Cytotrophoblast, syncytiotrophoblast and giant trophoblastic cells of placentas of anaemic rats showed cytoplasmic and nuclear vacuolation with loss of cell margins. In addition, there was atrophy of microvilli on the cell surface, as well nuclear chromatolysis, nucleolar degeneration and appearance of dark bodies.

Conclusion: Chronic anaemia causes trophoblastic cell degeneration. This may undermine the functional integrity of the cells and constitute part of the mechanism for poor fetal outcome.

Keywords: anaemia; cytotrophoblast; degeneration; giant cells; placenta; syncytiotrophoblast

Anatomy 2017;11(2):72–78

Introduction

Trophoblastic cells of the placenta comprise cytotrophoblasts, syncytiotrophoblast cells in the labyrinthine zone, and spongiotrophoblasts, trophoblastic giant cells in the junctional zone.[1-4] The latter constitute the interhemal membrane or placental barrier. Anaemia causes adverse fetal outcome.[5-8] This poor outcome has been attributed to degenerative changes in the placenta which include reduction in size, placental infarcts, syncytial knots, decreased vascularity and fibrinoid necrosis.[2,9,10] Trophoblastic cells are important in the function of the placenta and are sensitive to placental insult.[11–13] Accordingly, knowledge of the effects of various insults is important in mitigating adverse fetal outcome. Studies on the anaemia induced ultrastructural changes in the placental trophoblastic cells are, however, scarce, but nonetheless important in elucidating the basis for poor fetal outcome. This study therefore investigated the effects of anaemia on the ultrastructure of placental trophoblastic cells.

Materials and Methods

This experimental study was carried out on forty-nine female Sprague-Dawley rats. The animals were derived from a generation of clones over a 19 year period and divided into control and experimental groups. The study was approved by the ethical committee in the University of Nairobi and implemented in accordance with international policies and directives governing the use of animals in experiments. These directives were formulated to secure best environment and care for animals. Basic principles in

Table 1
Effect of chronic anaemia on haemoglobin levels.

	Hb (g/dl): mean±SE		
Gestation day	**Control**	**Chronic**	**p-value**
Day 17	12.88±0.23	10.98±0.69	.039*
Day 19	12.98±0.16	10.67±0.5	.001*
Day 21	13.4±0.5	11.44±0.58	.013*

*p<0.05

animal care were applied in this study which included the following: using less invasive techniques, optimum living conditions and medical care, causing no pain or distress, not performing unnecessary tests, reducing the number of animals tested to the minimum. Rats were handled with care, without rushing to avoid frightening the animals.

Chronic anaemia was induced by withdrawing 1.5 ml of blood on five alternate days, through the retrobulbar plexus according to the protocol by Markovic et al. (2009).[14] Anaemia was diagnosed when the haemoglobin level dropped below 12 g/dl. The mean haemoglobin level for the control rats was 13.1 g/dl; ranging from 12.88 g/dl on day 17 to 13.4 g/dl on day 21. In anaemia on the other hand, haemoglobin was consistently below 12 g/dl range from 10.98 g/dl on day 17 to 11.44 on day 21. The difference was statistically significant on all gestational dates. Chronic anaemic rats had mean values of haemoglobin concentration that are significantly less than those of the control mean values in all studied groups (**Table 1**).

Rats were anaesthetised by ether inhalation, the abdomen was opened using a midline incision, the uterus was exposed and placentas were extracted on days 17, 19 and 21 (**Table 2**). All placentas were cut in two equal parts. Half was processed for light microscopy and the other processed for transmission electron microscopy.

For light microscopy, the placentas were cut into 5 mm^3 pieces, fixed in 10% buffered formaldehyde solution, dehydrated in alcohol, cleared in xylene and embedded in paraffin wax. Five micron sections were cut, deparaffinized, stained with Hematoxylin and Eosin and examined at various magnifications in control and anaemic rats using a Leica ICC 50 microscope (Leica Microsystems, Wetzlar Germany). Photographs were taken using a high resolution digital camera attached to a computer.

Table 2
Distribution on rats on different gestational days.

	Number of rats	
Day	**Control group**	**Experimental group**
17	6	5
19	5	8
21	13	12
Total	24	25

For transmission electron microscopy, 1 mm^3 tissue blocks of placenta were fixed in 2.5% phosphate buffered glutaraldehyde for two hours at 4°C. They were then washed in 0.1 M phosphate buffer 4×20 min and then for 24 hours again at 4°C. Secondary fixation was done in 2% osmium tetroxide in 0.1 M phosphate buffer, pH 7.4 for 1 hr at room temperature. This was then followed by washing in double distilled water 4×20 min at room temperature. Dehydration was done in ascending grades of ethanol, cleared in propylene oxide and embedded in epon resin. Semithin sections were cut at approximately 500–1000 nm thickness and stained with toluidine blue. Ultrathin sections were stained with uranyl acetate counter stained with lead citrate and then examined under JEOL transmission electron microscope at various magnifications using the protocols of Hunter[15] and Bozzola and Russel.[16] Images were taken by high resolution camera.

Results

The trophoblastic cells in the placenta of control animals showed clear margins, cytoplasm, nuclei with distinct chromatin and nucleoli. Microvilli on the cytotrophoblasts were definite, long and numerous. Those in placenta of anemic animals, on the other hand, showed features of degeneration. The nucleus of the trophoblastic cells in the interhemal membrane showed features of chromatolysis such that the chromatin material appeared to have disappeared from the nucleus, leaving a naked nucleolus. The cell margins became indistinct. This was in contrast to the controls in which cells appeared distinct with clear margins, nucleus and prominent chromatin and nucleoli (**Figures 1a** and **b**). The cells in the interhemal membrane displayed numerous dark bodies, vacuolation, disorganization, as well as degeneration of the endothelial lining with thickening of the basement membrane (BM) (**Figures 1c** and **d**).

The syncytiotrophoblasts showed chromatin and nucleolar degeneration, cytoplasmic and nuclear vacuolation (**Figures 2a** and **b**). Cytotrophoblasts developed marked nuclear vacuolation and dark bodies. The surfaces facing the MBS bore microvilli which were reduced in number and the cells had different orientations on the surface of the cytotrophoblast (**Figures 2c** and **d**).

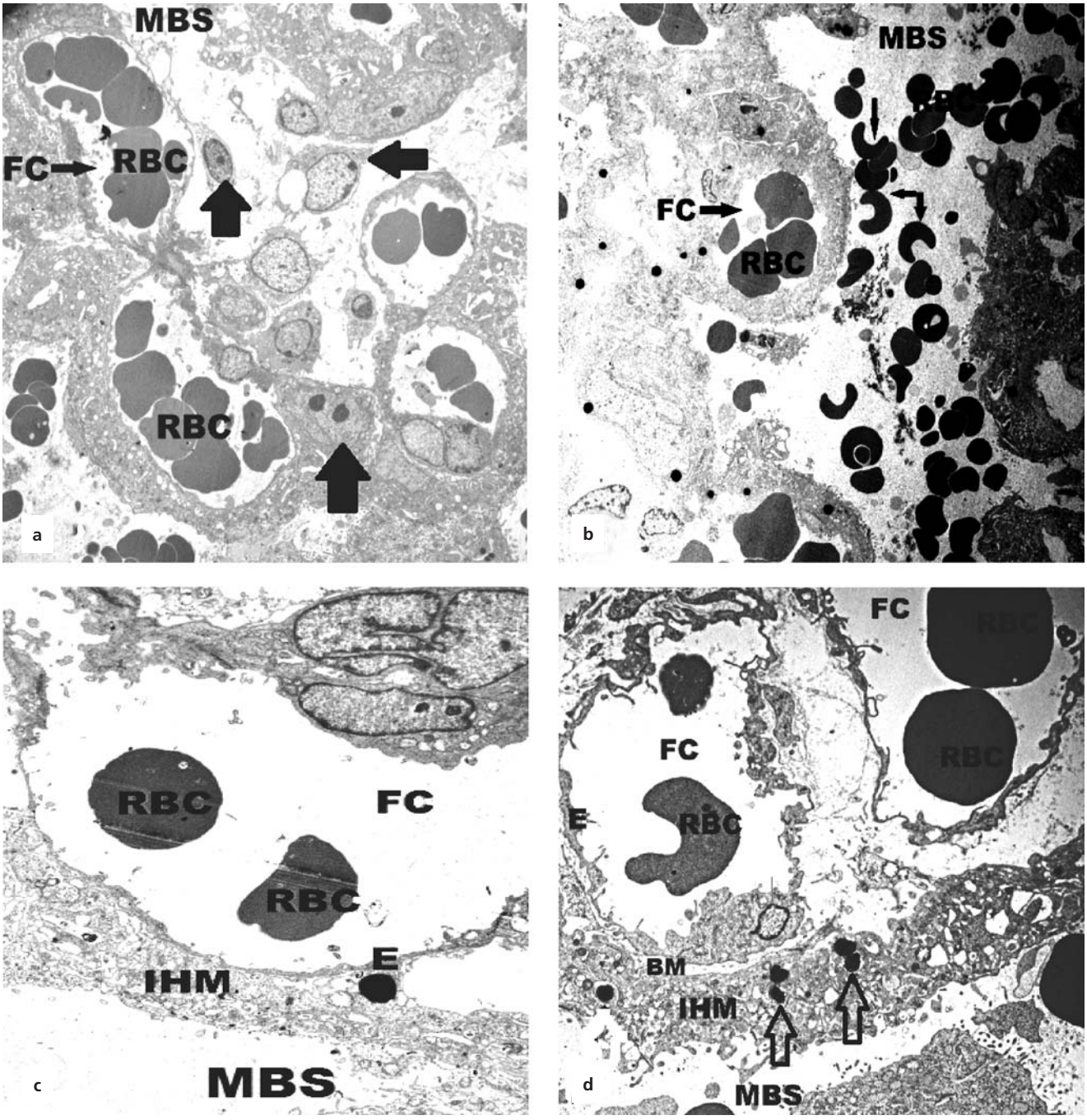

Figure 1. Electromicrographs of placental labyrinth in control and chronic anemic rat placenta at gestational day 21. (**a**) Electromicrograph of placental labyrinth in control rats showing normal maternal blood spaces (**MBS**), fetal capillaries (**FC**) with red blood cells (**RBCs**) and a number of giant cells with clear cell margins and prominent nucleoli (**arrows**) (×1200). (**b**) Electromicrograph of labyrinth in anaemic rats showing dilated **MBS**, fewer fetal capillary (**FC**), decreased numbers of giant cells and anisocytosis. Note the absence of clear cellular and nuclear margins of numerous dark bodies (×1200). (**c**) Electromicrograph of labyrinth of control animals showing **FC** with well-defined endothelial lining (**E**) and nuclei with 2 nucleoli. Note also the regular interhemal membrane (**IHM**) (×3000). (**d**) Electromicrograph of labyrinth in anaemic rats showing abnormal shape and size of RBCs in **FC**, disorganization of **E** of **FC** and disruption of its wall, more dark bodies (**arrows**) and disorganized **IHM** (×3000).

Giant trophoblastic cells in control animals showed clear margins, granular cytoplasm, and prominent homogeneous nucleus with prominent nucleolus. In anaemia on the other hand, the giant trophoblastic cells lost cell margins, the cytoplasm and nucleus developed vacuoles, as the nucleolus disappeared (**Figures 3** and **b**).

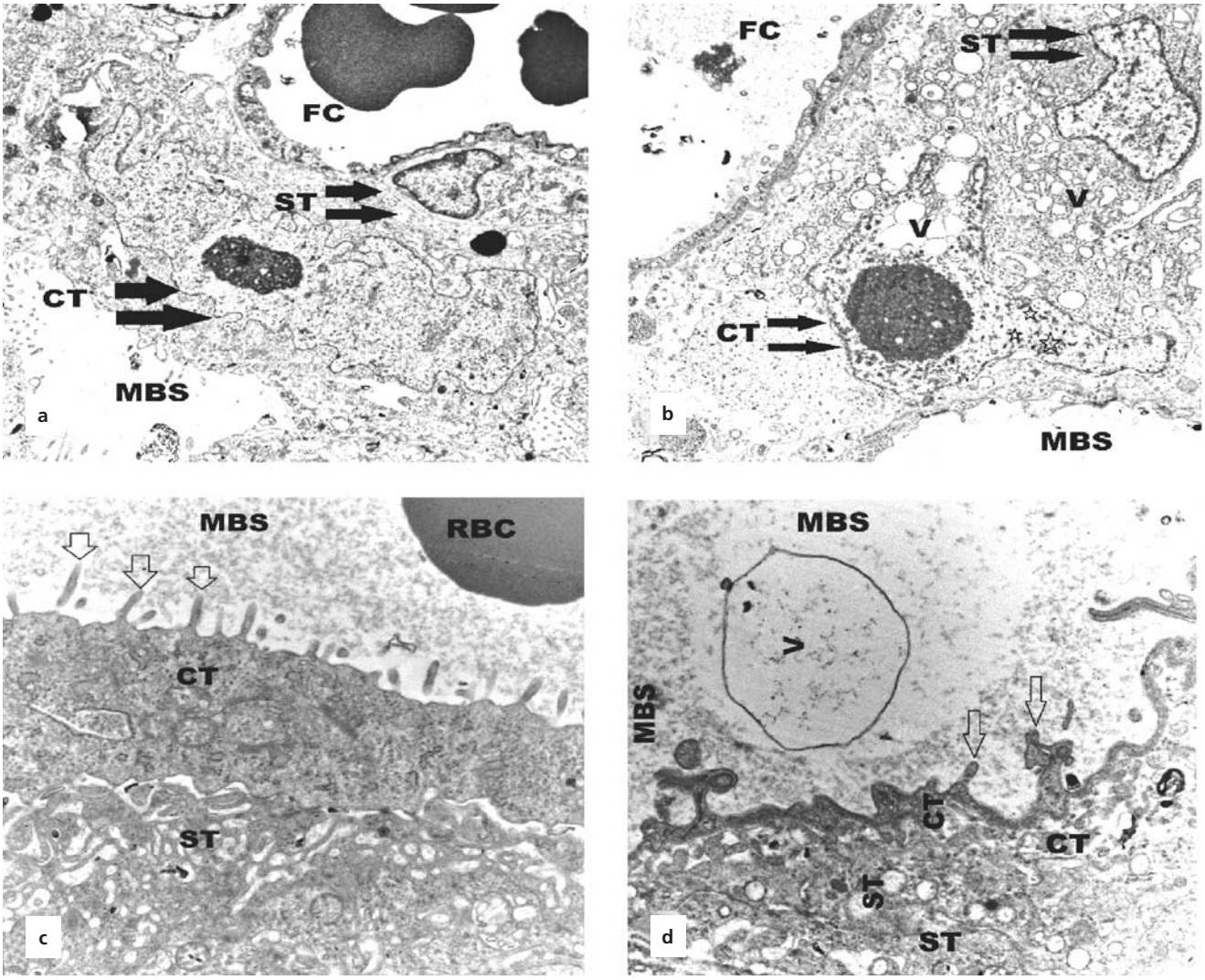

Figure 2. Electromicrographs of cytotrophoblasts and syncytiotrophoblasts of control and anemic rat placentae at gestational day 21. (**a**) Placenta of control rat with normal **CT** and **ST** lining the **MBS** and **FC**, respectively (×5000). (**b**) Anaemic placenta showing vacuolation (**V**), chromatin and nucleolar disappearance in **CT** and **ST** (×5000). (**c**) Placenta of control, showing prominent long microvilli on **CT** (**arrows**) projecting into the **MBS** (×10,000). (**d**) Anaemic placenta. Note the shorter and fewer microvilli (arrows) on **CT** cells (×10,000). **CT:** cytotrophoblast; **FC:** fetal capillaries; **MBS:** maternal blood spaces; **ST:** syncytiotrophoblast.

The number giant trophoblastic cells in the anaemic group was relatively less compared to the controls (**Figures 4a** and **b**).

Discussion

The cells most affected by anaemia were syncytiotrophoblasts, cytotrophoblasts and trophoblastic giant cells. Syncytiotrophoblasts and cytotrophoblasts showed changes characterized by nuclear and cytoplasmic vacuolation. Similar degenerative changes in these cells have been reported in hypoxia,[17,18] pre-eclampsia[19] and hypertensive disease of pregnancy.[20] The changes are concordant with reports that these cells are sensitive to factors which cause placental injury.[13,21,22] Many of them, especially those related to hypoxia occur due to placental apoptosis consequent to oxidative stress.[23] The syncytiotrophoblast is actively involved in the transport of metabolites to and from the embryo/fetus; production of hormones, growth factors and receptors which regulate maternal metabolism and placental development.[11,24] Accordingly, the changes observed are likely to adversely impact on placental function by decreasing transfer and synthetic activity[18] and hence contribute to poor fetal outcome. In addition, cytotrophoblastic cells

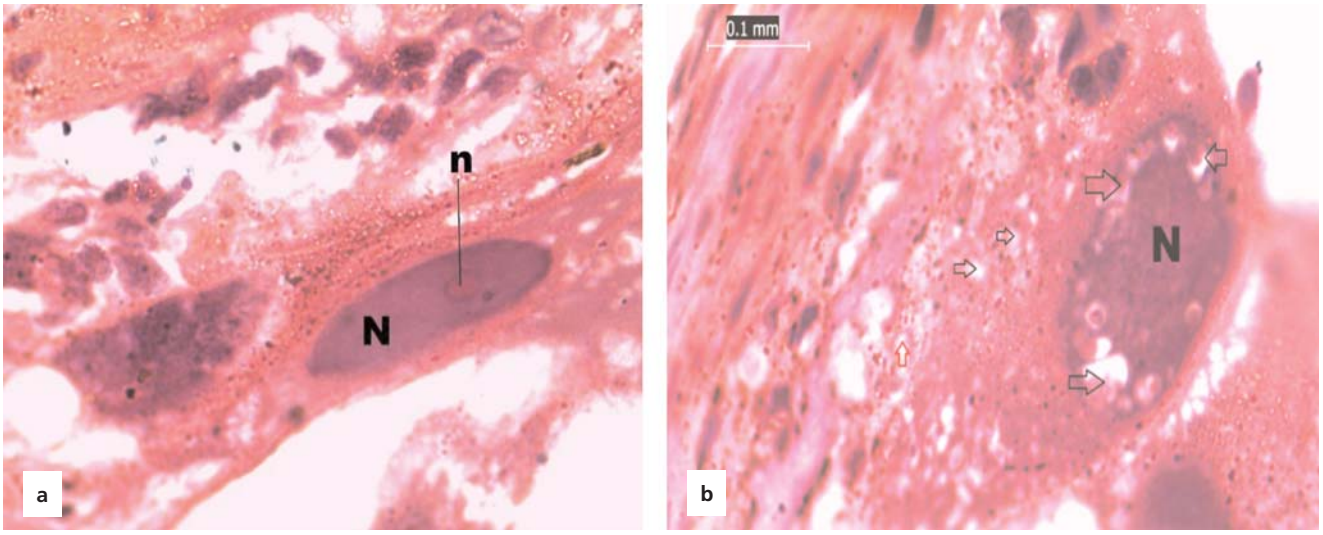

Figure 3. Photomicrographs of giant trophoblastic cells in rat placenta. (**a**) Giant cell in control at gestational day 17, showing normal homogeneous granular cytoplasm, uniform nucleus with prominent nucleolus. (**b**) Giant cell in anemia at gestational day 17 showing irregular cell margins, nuclear degeneration, cytoplasmic and nuclear vacuolation (**arrows**) (Hematoxylin and Eosin, ×1000). **N:** nucleus; **n:** nucleolus. [Color figure can be viewed in the online issue, which is available at www.anatomy.org.tr]

showed abnormal orientation, reduction in size and density of microvilli. The decreased microvillus density observed in the current study has also been reported in other complications such as IUGR placentae[25] and preeclampsia.[17] In the rat, cytotrophoblasts continuously differentiate into ST during villous formation and development and are important in invasion of blood vessels remodeling in early stages of implantation.[26] Their degeneration may undermine placenta function, and contribute to poor outcome.

The trophoblastic giant cells secrete steroid hormones and prolactin related cytokines, to work on preparation and adaptation of the maternal body systems to pregnancy to ensure that proper placentation occurs.[12,27,28] In the current study, these cells showed marked cytoplasmic and nuclear vacuolation. Similar degenerative changes have been reported in diabetes and hyperthermia,[29,30] and placental chemical toxicity,[31–33] and gestational protein restriction.[34] They are probably genetically programmed. Indeed it has been reported

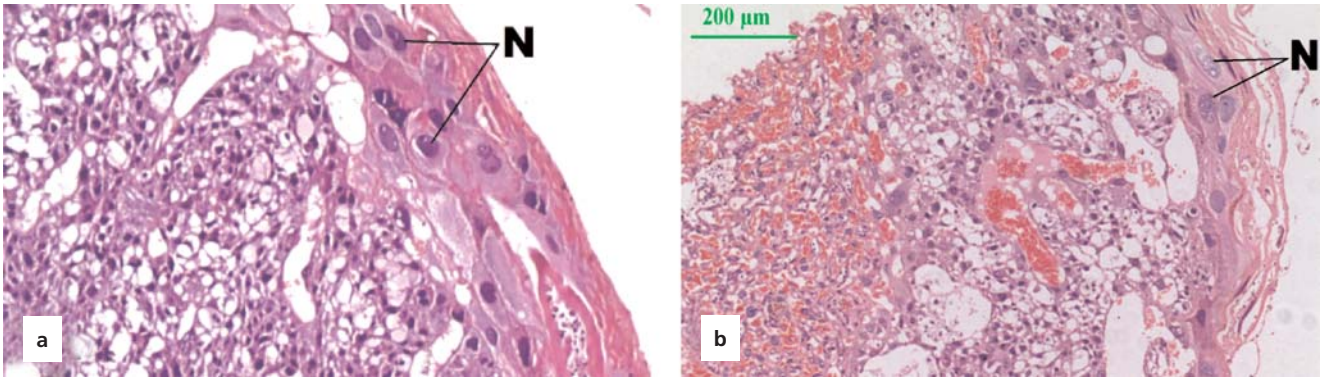

Figure 4. Photomicrograph of labyrinth and junctional zones in placenta of control rats at gestational day 19. (**a**) Giant trophoblastic cells in the control rat placenta showing normal distribution and appearance. Note the distinct dark nuclei (**N**) with definite nucleoli (**n**). (**b**) Giant cells in the anaemic group showing relative reduction in their number compared to the control. Note the nuclei (**N**) are lighter stained the nucleoli (**n**) are less distinct of giant cells. Hematoxylin and Eosin, ×100. [Color figure can be viewed in the online issue, which is available at www.anatomy.org.tr]

that O_2 levels regulate cell fate through hypoxia induced factor-1 (HIF-1) which activates genes involved in cellular response to O_2 deprivation.[32,35] These morphological changes may alter placental function and embryo nutrition, and contribute to the poor fetal outcome.

Conclusion

Chronic anaemia causes trophoblastic cell degeneration. This may undermine the functional integrity of the cells and constitute part of the mechanism for poor fetal outcome.

Acknowledgement

We are grateful to technical staff in the Departments of Biochemistry and Human Anatomy for technical support, Prof Oduor-Okello for expert advice and Antonina Odock-Opiko for typing the manuscript.

References

1. Mayhew TM. A stereological perspective on placental morphology in normal and complicated pregnancies. J Anat 2009;215:77–90.
2. Soni R, Nair S. Study of histological changes in placenta of anaemic mothers. IOSR Journal of Dental and Medical Sciences 2013;9:42–6.
3. Cline JM, Dixon D, Ernerudh J, Faas MM, Göhner C, Häger JD, Markert UR, Pfarrer C, Svensson-Arvelund J, Buse E. The placenta in toxicology. Paper III: Pathological assessment of the placenta. Toxicol Pathol 2014;42:339–44.
4. Furukawa S, Kuroda Y, Sugiyama A. A comparison of the histological structure of the placenta in experimental animals. J Toxicol Pathol 2014;27:11–8.
5. Allen L. Anemia and iron deficiency: effects on pregnancy outcome. Am J Clin Nutr 2000;71:1280S–4S.
6. Noronha JA, Bhaduri A, Vinod H, Kamath A. Maternal risk factors and anaemia in pregnancy: a prospective retrospective cohort study. Obstet Gynaecol 2010;30:132–6.
7. Kiran N, Zubair A, Khalid H, Zafar A. Morphometrical analysis of intervillous space and villous membrane thickness in maternal anaemia. J Ayub Med Coll Abbottabad 2014;26:207–11.
8. Sabina S, Iftequar S, Zaheer Z, Khan M, Khan S. An overview of anemia in pregnancy. Journal of Innovations in Pharmaceuticals and Biological Sciences 2015;2:144–51.
9. Agarwal KN, Gupta V, Agarwal S. Effect of maternal iron status on placenta, fetus and newborn. International Journal of Medicine and Medical Sciences 2013;5:391–5.
10. Biswas S, Meyur R, Adhikari A, Bose K, Kundu P. Placental changes associated with maternal anaemia. Eur J Anat 2014;18:165–9.
11. Crocker IP, Tansinda DM, Jones CJ, Baker PN. The influence of oxygen and tumor necrosis factor-α on the cellular kinetics on term placental villous explants in culture. J Histochem Cytochem 2004;52:749–57.
12. Hu D, Cross JC. Development and function of trophoblast giant cells in the rodent placenta. Int J Dev Biol 2010;54:341–54.
13. Hung TH, Skepper JN, Charnock-Jones DS, Burton GJ. Hypoxia-reoxygenation: a potent inducer of apoptotic changes in the human placenta and possible etiological factor in preeclampsia. Circ Res 2002;90:1274–81.
14. Markovic SD, Milosevic M, Dordevic N, Ognjanovic B, Stajn AS, Zorica S. Time course of hematological parameters in bleeding induced anemia. Archives of Biological Science Belgrade 2009;61: 165–70.
15. Hunter E. Practical electron microscopy: a beginner's illustrated guide. 2nd ed. Cambridge (NY): Cambridge University Press; 1993.
16. Bozzola JJ, Russell LD. Electron microscopy. 2nd ed. Sudbury (MA): Jones and Bartlett Publishers; 1999.
17. de Luca Brunori I, Battini L, Brunori E, Lenzi P, Paparelli A, Simonelli M, Valentino V, Genazzani AR. Placental barrier breakage in pre- eclampsia: ultrastructural evidence. Eur J Obstet Gynecol Reprod Biol 2005;118:182–9.
18. Salgado SS, Salgado MKR. Structural changes in pre-eclamptic and eclamptic placentas – an ultrastructural study. J Coll Physicians Surg Pak 2011;21:482–6.
19. Selim ME, Elshmry NG, Rashed EA. Electron scanning microscopic observations on the syncitiotrophoblast microvillous membrane contribution to preeclampsia in early placental rats. J Blood Disord Transfus 2013;4:137.
20. Judson JP, Fun LP, Nadarajah VD, Nalliah S, Chakravathi S, Thanikhacalam P, Santhanaraj L. Ultrastructural and immunofluorescence studies of placental tissue in hypertensive diseases of pregnancy. Research Journal of Biological Sciences 2010;5:155–63.
21. Crocker IP, Barratt S, Kaur M, Baker PN. The in-vitro characterization of induced apoptosis in placental cytotrophoblasts and syncytiotrophoblasts. Placenta 2001;22:822–30.
22. Serin IS, Ozçelik B, Basbug M, Kiliç H, Okur D, Erez R. Predictive value of tumor necrosis factor alpha (TNF-alpha) in preeclampsia. Eur J Obstet Gynecol Reprod Biol 2002;100:143–5.
23. Grill S, Rusterholz C, Zanetti-Dällenbach R, Tercanli S, Holzgreve W, Hahn S, Lapaire O. Potential markers of preeclampsia–a review. Reprod Biol Endocrinol 2009;7:70.
24. Linton EA. Human trophoblast syncytialization: a cornerstone of placental function. Endocrine Abstracts 2005;10:515.
25. Battistelli M, Burattini S, Pomini F, Scavo M, Caruso A, Falcieri E. Ultrastuctural study on human placenta from intrauterine growth cases. Microsc Res Tech 2004;65:150–8.
26. James JL, Stone PR, Chainley LW. Cytotrophoblast differentiation in the first trimester of pregnancy: evidence for separate progenitors of extravillous trophoblasts and syncytiotrophoblast. Reproduction 2005;130:95–103.
27. Ain R, Canham LN, Soares MJ. Gestation stage-dependent intrauterine trophoblast cell invasion in the rat and mouse: novel endocrine phenotype and regulation. Dev Biol 2003;260:176–90.
28. Soares MJ, Konno T, Alam SM. The prolactin family: effectors of pregnancy-dependent adaptations. Trends Endocrinol Metab 2007; 18:114–21.
29. Padmanabhan R, Shafiullah M. Intrauterine growth retardation in experimental diabetes: possible role of the placenta. Arch Physiol Biochem 2001;109:260–71.
30. Padmanabhan R, Al-Menhali NM, Ahmed I, Kataya HH, Ayoub MA. Histological, histochemical and electron microscopic changes of the placenta induced by exposure to hyperthermia in the rat. Int J Hyperthermia 2005;21:29–44.

31. Kosif R, Akta G, Öztekin A. Microscopic examination of placenta of rats prenatally exposed to aloe barbadensis: A preliminary study. Int J Morphol 2008;26:275–81.
32. Tait S, Tassinari R, Maranghi F, Mantovani A. Bisphenol A affects placental layers morphology and angiogenesis during early pregnancy phase in mice. J Appl Toxicol 2015;35:1278–91.
33. Omar AR, El-Din EYS, Abdelrahman HA. Implications arising from the use of cymbopogen proximus; proximal on placenta of pregnant albino rats. Brazilian Archives of Biology and Technology 2016;59: e16160165.
34. Rebelato HJ, Esquisatto MA, de Sousa Righi EF, Catisti R. Gestational protein restriction alters cell proliferation in rat placenta. J Mol Histol 2016;47:203–11.
35. Adelman DM, Gertsenstein M, Nagy A, Simon MC, Maltepe E. Placental cell fates are regulated in vivo by HIF-mediated hypoxia responses. Genes Dev 2000;14:3191–203.

Online available at:
www.anatomy.org.tr
doi:10.2399/ana.17.013
QR code:

Correspondence to: Omer Awad, MSc
Department of Human Anatomy, University of Nairobi,
P.O. Box: 30197 Nairobi, Kenya
Phone: +254 731 426117
e-mail: omarawad12@yahoo.com

Conflict of interest statement: No conflicts declared.

Original Article

www.anatomy.org.tr
Received: May 16, 2017; Accepted: July 28, 2017
doi:10.2399/ana.17.015

anatomy
An International Journal of Experimental and Clinical Anatomy

Lead induces inflammation and neurodegenerative changes in the rat medial prefrontal cortex

Adekomi Damilare Adedayo[1], Adewole Olarinde Stephen[2], Tijani Ahmad Adekilekun[3], Adeniyi Temidayo Daniel[4]

[1]*Department of Anatomy, Faculty of Basic Medical Sciences, College of Health Sciences, Osun State University, Osogbo, Osun State, Nigeria*
[2]*Department of Anatomy and Cell Biology, Obafemi Awolowo University, Ile-Ife, Osun State, Nigeria*
[3]*Department of Anatomy, Ekiti State University, Ado Ekiti, Ekiti State, Nigeria*
[4]*Department of Medical Laboratory Science, Kwara State University, Nigeria*

Abstract

Objectives: Lead (Pb) is a neurotoxicant heavy metal ubiquitously present in the eco-system. The precise mechanism by which Pb confers its deleterious effects on the cellular profile of the central nervous system remains unknown. The aim of this study was to investigate the effect of Pb on the medial prefrontal cortex (mPFC) using histological, immunohistological and morphological techniques.

Methods: Thirthy juvenile male Wistar rats were used in this study. The rats were randomly assigned into three groups. Group A served as the control group, Group B received 5 mg/kg Pb-nitrate ($PbNO_3$) orally for 21 days, and Group C received 5 mg/kg $PbNO_3$ and left for an additional 21 days to recover.

Results: There was a significant decrease in the number of normal neurons in the mPFC of the $PbNO_3$-treated rats. The number of degenerating neurons significantly increased in the $PbNO_3$-treated groups compared with the control group. A marked increase was observed in the number of astrocytic cell count in the $PbNO_3$-treated groups compared with the control. The neuronal cells in the cytoarchitectural profile of the mPFC of the rats receiving $PbNO_3$ showed marked neurodegenerative modification with features of distorted morphology, swollen and vacuolized cytoplasm, and features of either pyknotic or karyorrhectic nuclei. The cytoarchitecture of the mPFC of the rats in the control group preserved the normal histological outline suggestive of a normal and functional mPFC.

Conclusion: Exposure to Pb ingestion can result in significant inflammatory responses in the cytoarchitectural profile of the mPFC. Furthermore, 21 days of cessation of exposure to $PbNO_3$ did not halt or reverse the deleterious effects of Pb on the mPFC of the rats, suggesting that Pb persists in the central nervous system of the rats.

Keywords: astrogliosis; cell death; heavy metals; neurodegeneration; pathology

Anatomy 2017;11(2):79–86

Introduction

Lead (Pb) is a lustrous bluish-silver colored metal heavy metal naturally present in human environment.[1,2] According to Ahmed et al. (2013),[3] exposure to Pb is unavoidable, as it occurs through many routes including contaminated air, water, soil, food and consumer products. Other sources of Pb are gasoline and house paint, which has been extended to lead bullets, plumbing pipes, pewter pitchers, storage batteries, toys and faucets.[4] Pb is commercially important as it is used in the manufacture of Pb-acid storage electrical batteries, production of fusible metal alloys and foils, fabrication and synthesis of anti-friction metals and solder.[5]

Despite the enormous efforts put in place by the government and international health organizations in the developed and developing countries, exposure to PB persists as one of the major health challenge.[6]

Pb is known to be a neurotoxicant that competes with and impairs calcium ion signaling in nerve processes.[5,7,8] It inhibits the differentiation of neurons, suppresses long-term potentiation (LTP), alters the secretion of neurotransmitters,[9–11] and also triggers the production of β-amyloid proteins.[12] Other deleterious effects of Pb also include biochemical disruption,[13] cellular alterations,[7,14] metabolic,[15] and subclinical aberrations which ultimately lead to death in most cases.[16] An example of this is the considerable number of children that died in the Zamfara Pb poisoning in Nigeria.

According to the descriptions of Liu et al.[17] and Liu et al.,[18] tastrocytes and microglia are two of the four types of glial cells in the brain that are involved in the activation and regulation of the brain immunity in response to pathological conditions.[17] In response to excitotoxicity, astrocytes and microglia enhance the production and release of inflammatory cytokines, increase the generation of reactive oxygen species, suppress the activities of antioxidants, thereby resulting in cellular loss or injury in the central nervous system (CNS).[19–22]

Although observations suggest that Pb is capable of inducing cellular dysfunction in the cortical regions of the brain, detailed mechanisms of actions remain largely unknown. The aim of the study was to observe the effect of Pb on the cytoarchitectural profile of the medial prefrontal cortex (mPFC) following exposure to Pb-nitrate ($PbNO_3$).

Materials and Methods

All experimental procedures were in accordance with the guidelines for animal research outlined in the NIH Guidelines for the Care and Use of Laboratory Animals as approved by the Institute of Public Health, Obafemi Awolowo University, Ile-Ife, Nigeria.

The crystal salt of $PbNO_3$ (Carlo Erba, Milano, Italy) was obtained from the Department of Biochemistry, Afe Babalola University, Ado Ekiti, Nigeria. The salt was dissolved in double distilled water and administered orally using metallic oral gavage. The solution was freshly prepared before each administration.

Thirty juvenile male Wistar rats (4 weeks old) weighing between 38 and 40 g were used for this study. The rats were obtained from the Department of Pharmacy, Obafemi Awolowo University, Ile-Ife, Nigeria. The rats were allowed to acclimatize for two weeks in the Animal Holdings of the Afe Babalola University, Ado-Ekiti, Nigeriai and housed in stainless steel cages (48×28×20 cm) containing wood-shaving bedding. The beddings were changed once a week. The room was maintained on natural day/light cycle, at room temperature. The rats in all groups were allowed free access to standard laboratory rat pellet and clean drinking water was made available in polycarbonate bottles *ad libitum*.

Twenty-four hours after acclimatization, the thirty juvenile rats (now weighing about 40–44 g) were randomly assigned into three groups designated as Group A (n=10), Group B (n=10), and Group C (n=10). The rats in Group A (control group) were treated with double distilled water, the rats in Group B ($PbNO_3$-treated) with 5 mg/kg[23] $PbNO_3$ by oral gavage for 21 days, and the rats in Group C (Pb-treated) were treated with 5 mg/kg of $PbNO_3$ and left for 21 days to recover before they were sacrificed. No death of animal occurred during this study. At the end of the study, 10 rats from each group were exposed to an overdose of Nembutal (100 mg/kg, i.p.) and transcardially perfused with 4% paraformaldehyde, followed by 10% buffered formalin while the rats were in inverted position. Brain samples were excised and post-fixed in 10% formalin with 30% sucrose. The mPFC (4.70–2.70 mm ventral and 4.70–2.70 mm dorsal to the bregma) was identified using the atlas of Paxinos and Watson,[24] under dissection microscope. Subsequently, the mPFCs were paraffin-embedded and sectioned at 5 μm on a microtome.

The immunohistochemical demonstration of astrocytes was performed according to the method of Ardalan et al.[25] Briefly, floating sections were rinsed in tris buffer saline (TBS) containing 0.1% Triton X-100 for 30 min followed by blocking endogenous peroxidase using 30% H_2O_2 and methanol dissolved in TBS for a further 30 min. Antigen retrieval was done by heating the sections in the retrieval solution (Cat #S1699; Dako, Glostrup, Denmark) dissolved in distilled water in the oven for 30 min. Thereafter, the sections were rinsed three times in 1% bovine serum albumin (BSA) and 0.3% Triton-X in TBS solution for 10 min. The sections were then incubated with a polyclonal rabbit anti-GFAP (Cat #Z0334; Dako, Glostrup, Denmark) at 1:500 dilution with 1% BSA in TB buffer 50 mM overnight at 4ºC, rinsed in TBS with 0.1% BSA and Triton X- 100 for 10 min, and then incubated with polyclonal secondary goat anti-rabbit IgG antibody/HRP (Cat #P0448; Dako, Glostrup, Denmark) at 1:200 dilution for 2 hours. Subsequently, the sections were washed three times in TBS for 10 minutes. The immunolabelling was performed using 3.3'-diaminobenzidine (DAB) solution for 1 minute. Lastly, the sections were mounted on the gelatin-coated slides and counterstained with 0.25% thionin solution (T3387; Sigma-Aldrich, St. Louis, MO, USA).

Images of the histological and immunohistochemical sections were captured using Leica DM 3000 (Leica, Wetzlar, Germany) with a cameroscope connected to a computer interface. The resolution of the cameroscope

was 14 mega pixels. Histological and immunohistochemical images were photomicrographed at different magnifications and were examined using the Image Analysis and Processing for Java (Image J) program, public domain software sponsored by the National Institute of Health (USA). Normal neurons, degenerating neurons and astrocytes were counted in ten different non-overlapping sections from ten different rats in each group using high power field objective microscope lens of 40x using Apache OpenOffice Draw 3.4.1 (Apache Software Foundation, Forrest Hill, MD, USA) and Image J (NIH, USA) software. The statistical package GraphPad Prism Software (version 5.01; La Jolla, CA, USA) was used for data analysis. Cell count data were presented as mean±SD. Non-parametric data were used directly in analysis using the Mann-Whitney U and Kruskal-Wallis tests. Both Tukey's test and one-way analyses of variance (ANOVA) were used to compare the numbers of neurons, number of degenerating neurons, and number of astrocytic counts across the study groups.

Results

The number of normal neurons significantly decreased in the $PbNO_3$-treated rats (Group B) when compared with the control group (p=0.0002) (**Figure 1**). After 21 days of recovery, the number of normal neurons in Group C showed a significant decrease compared with the control group (p=0.0002). However, there was no significant difference in the number of normal neurons between Group B and Group C, suggesting that there was no improvement with recovery.

The number of degenerating neurons significantly increased in rats in the $PbNO_3$-treated group (Group B) compared with the control group (p=0.0001) (**Figure 2**). After 21 days of recovery, Group C also showed a marked significant increase in the number of degenerating neurons when compared with the control group (p=0.0001). On the other hand, there was also a significant difference (p=0.007) in the number of degenerating neurons between Group B and Group C.

The number of astrocytes showed a significant increase in the $PbNO_3$-treated group (Group B) compared with the control group (p=0.0001) (**Figure 3**). After 21 days of recovery, Group C also showed a significant increase in the number of astrocytes compared with the control group (p=0.0001). In addition, there was a significant decrease in the number of astrocytes between Group B and Group C (p=0.0001).

We used Hematoxylin and Eosin stain to evaluate the cytoarchitecture of the mPFC after treatment with $PbNO_3$ (**Figure 4**). The control group showed neurons with normal appearance, prominent basophilic cytoplasm, and small-sized neuroglia cells interspersed within the neuropil

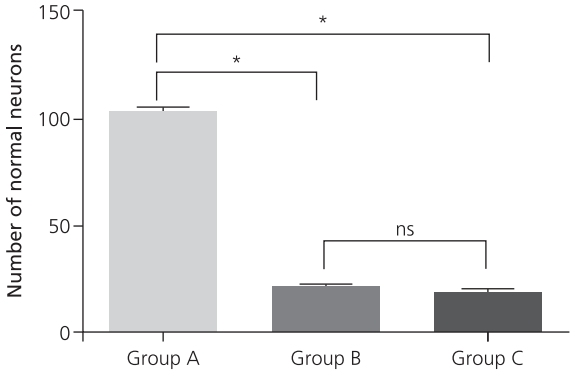

Figure 1. The number of normal neurons in the mPFC of the rats in in Groups A, B and C. *p<0.001; **ns:** non-significant.

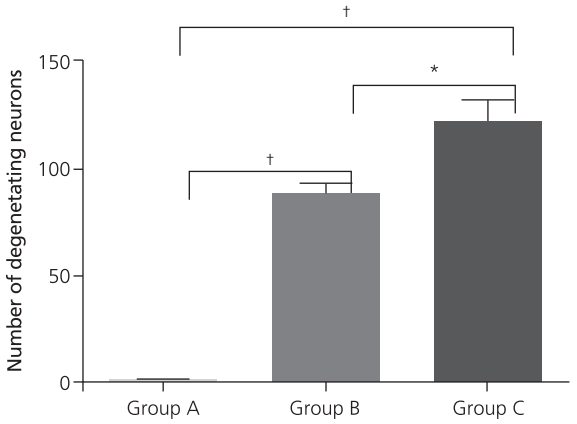

Figure 2. The number of degenerating neurons in the mPFC of the rats in Groups A, B and C. *p<0.01; †p<0.001.

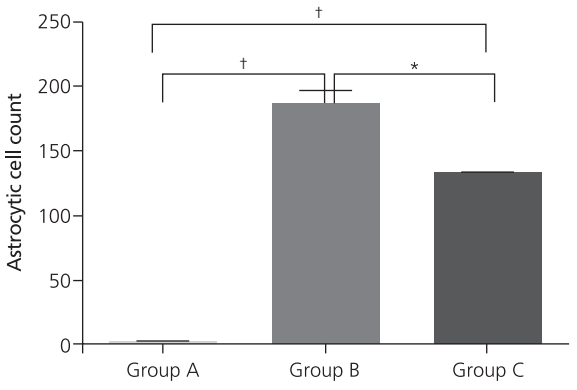

Figure 3. Astrocytic cell count in the mPFC of the rats in Groups A, B and C. *p<0.01; †p<0.001.

(**Figure 4a**). $PbNO_3$-treated group showed neurons with distorted morphology, swollen and vacuolized cytoplasm, and features of either pyknotic or karyorrhectic nuclei. Few of the neurons appeared with faintly stained cytoplasm

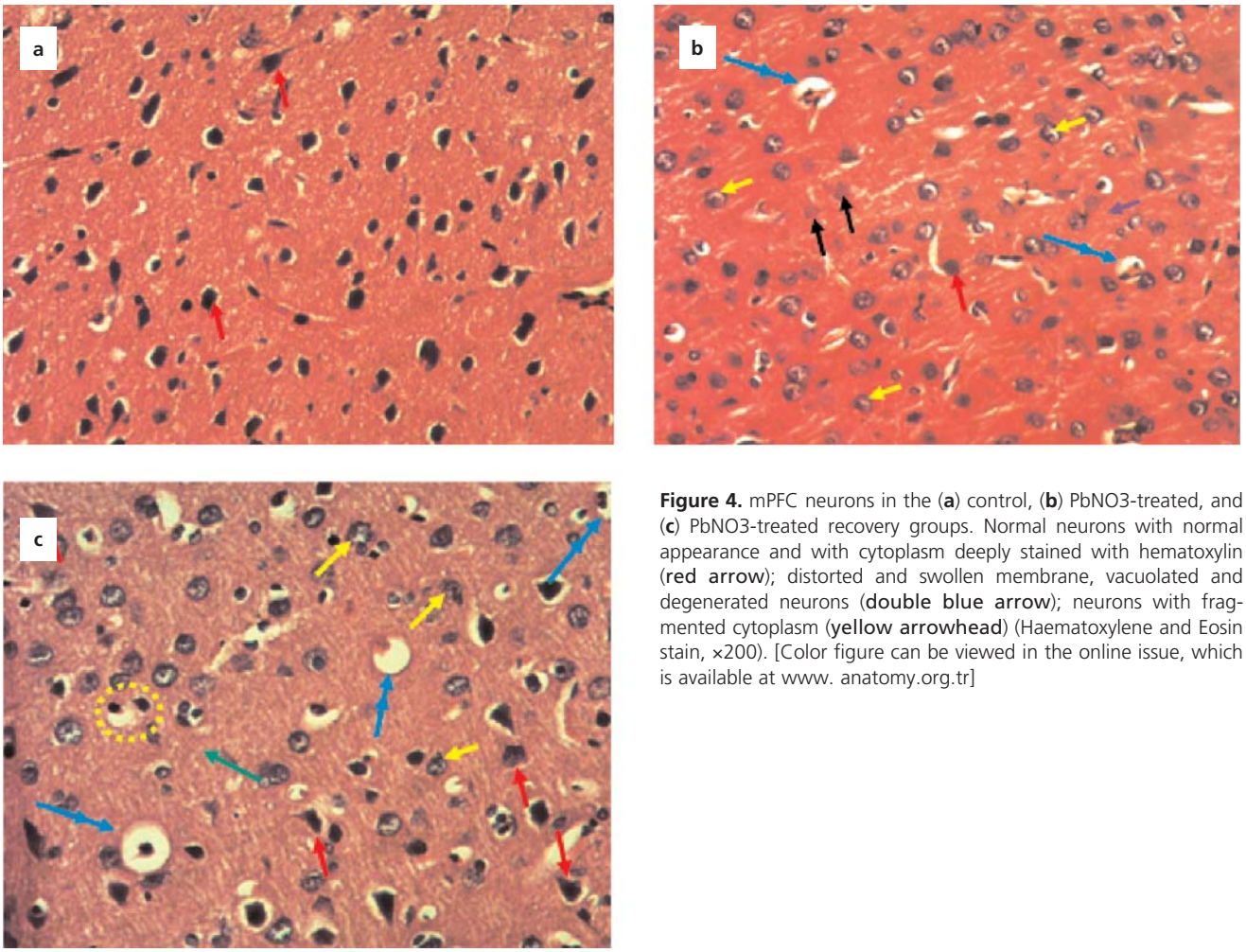

Figure 4. mPFC neurons in the (**a**) control, (**b**) PbNO3-treated, and (**c**) PbNO3-treated recovery groups. Normal neurons with normal appearance and with cytoplasm deeply stained with hematoxylin (**red arrow**); distorted and swollen membrane, vacuolated and degenerated neurons (**double blue arrow**); neurons with fragmented cytoplasm (**yellow arrowhead**) (Haematoxylene and Eosin stain, ×200). [Color figure can be viewed in the online issue, which is available at www. anatomy.org.tr]

(**Figure 4b**). The recovery group showed similar cytoarchitectural outline to the $PbNO_3$-treated; many neuronal cells with prominent cytoplasmic vacuolation and fragmented cytoplasm, with active-appearing microglial cell were observed (**Figure 4c**).

In the cresyl fast violet stained sections, distribution of Nissl bodies in mPFC neurons was investigated (**Figure 5**). The neurons in the control group were with no perineuronal cavitation or vacuolation, the neuronal cells were with darkly stained cytoplasm containing Nissl's substances (**Figure 5a**). In the $PbNO_3$-treated group, mPFC neurons showed features of chromatolysis, fragmented cytoplasm and dispersed peri-nuclear Nissl deposits (**Figure 5b**). The $PbNO_3$-treated group and the recovery group showed similar cytoarchitectural features (**Figure 5c**).

GFAP immunohistochemistry was used in this study to demonstrate astrocytic reaction as immunologic response to Pb exposure (**Figure 6**). A few GFAP immunoreactive astrocytes along with a large number of neurons were observed in the mPFCs of the control group (**Figure 6a**). In the mPFCs of the $PbNO_3$-treated group, a significant increase was observed in the reactive astrocyte count compared with the control. The astrocytes were reactive, hypertrophied with their thick cytoskeletal processes (**Figure 6b**). In the recovery group (Group C), there was also a marked increase in the number of GFAP immunoreactive astrocytes compared with the control group, though the number of the astrocytes was not significantly different from the $PbNO_3$-treated group (**Figure 6c**). The cytoplasmic processes of the astrocytes were seen with their complex cytoplasmic dendritic patterns, as a feature suggestive of inflammatory foci.

Discussion

In this present study, evidence from the histological, histochemical and immunohistochemical data showed that 21 days after exposure to $PbNO_3$, the cellular profile of the mPFC did not show any significant improvement.

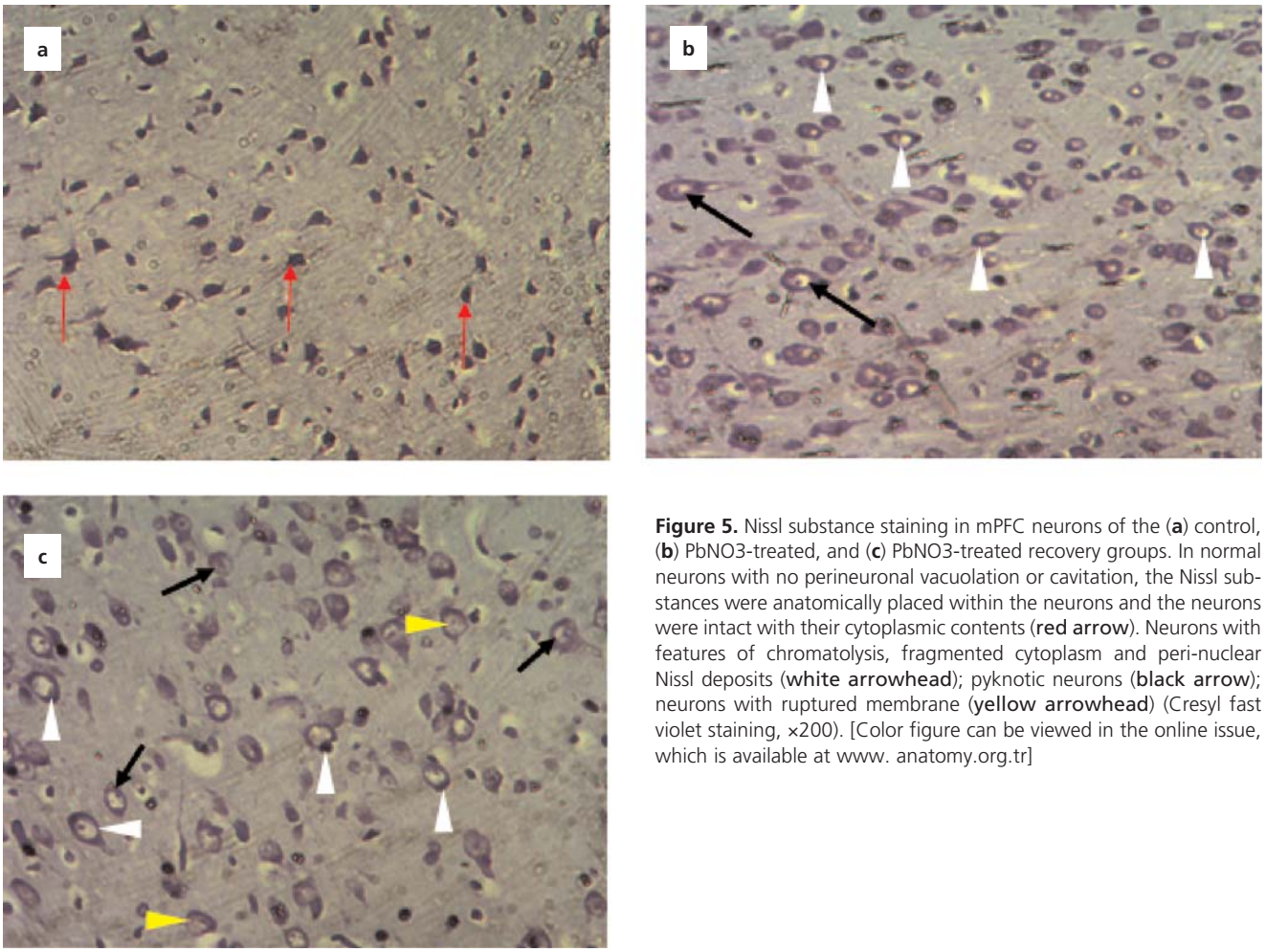

Figure 5. Nissl substance staining in mPFC neurons of the (**a**) control, (**b**) PbNO3-treated, and (**c**) PbNO3-treated recovery groups. In normal neurons with no perineuronal vacuolation or cavitation, the Nissl substances were anatomically placed within the neurons and the neurons were intact with their cytoplasmic contents (**red arrow**). Neurons with features of chromatolysis, fragmented cytoplasm and peri-nuclear Nissl deposits (**white arrowhead**); pyknotic neurons (**black arrow**); neurons with ruptured membrane (**yellow arrowhead**) (Cresyl fast violet staining, ×200). [Color figure can be viewed in the online issue, which is available at www. anatomy.org.tr]

Undoubtedly, Pb continues to affect humanity because of its ubiquitous existence, extensive and wide industrial use, as well as anthropogenic activities.[26] Pb has been reported to cause significant neuronal damage in the CNS.[27–29] Although the use of Pb has been significantly reduced, Pb exposure continues to be a risk, because level of Pb is constantly stable in the environment and no unhazardous threshold for Pb exposure has been established.[3,30] The effects of Pb are particularly damaging to the developing nervous system, causing potentially irreversible learning and behavior deficits.

Since astrocytes modulate the activities of neural circuit in the healthy and diseased brain, examining astrocytic role is key to the understanding the effect of neurotoxin in the CNS.[31] In the brain and spinal cord, the normal anatomy of astrocytes regulates important physiological functions which include heterogeneous distribution of neurotransmitters, maintenance of the extracellular balance of ions, provision of energy metabolites to neurons, participation in synaptic function and plasticity, and regulation of blood flow.[32] On the other hand, as a result of the $PbNO_3$-induced neurotoxicity in this study, astrogliosis associated with degenerative neurons and inflammatory processes occurred in the mPFC of the rats. The biological process that lead to astrogliosis are not fully known. However, degenerating neurons have been suggested to be capable of inducing astrogliosis, and astrogliosis has been used as an indicating scale for evaluating neuronal damage.[33–36]

The present model of Pb-induced inflammation in the cytoarchitectural profile of the mPFC in juvenile rats exposed to $PbNO_3$ might explain the irreversible neuropathological and neurobehavioral anomalies associated with Pb exposure.[3,37] The functional and structural integrity of the CNS is prone to various forms of insults and toxins that are capable of initiating cascades of deleterious responses.[34] In this study, Pb exposure induced upregulation of GFAP expression and also modified the structural integrity of the neurons in the cytoarchitectural profile of

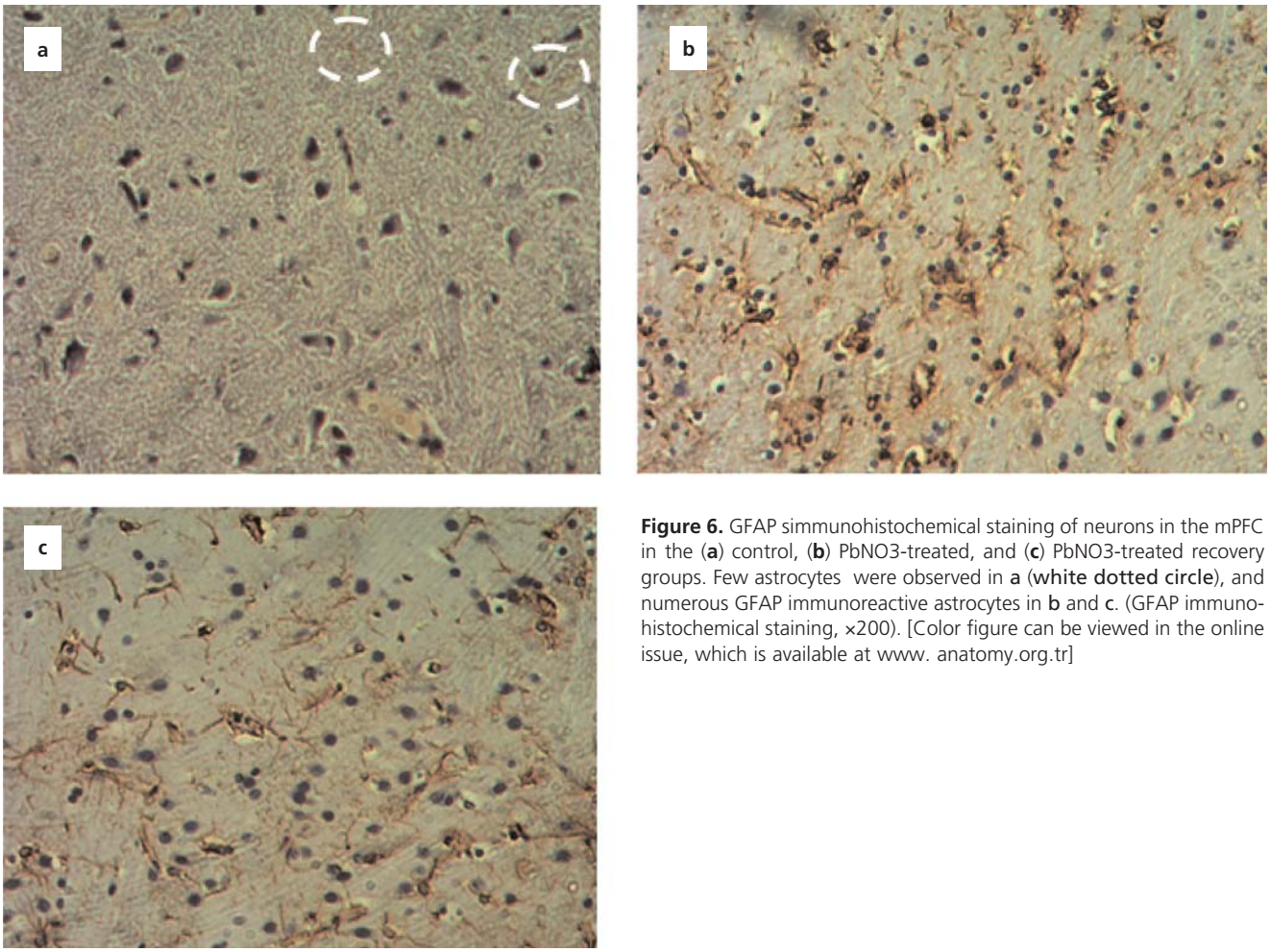

Figure 6. GFAP simmunohistochemical staining of neurons in the mPFC in the (**a**) control, (**b**) PbNO3-treated, and (**c**) PbNO3-treated recovery groups. Few astrocytes were observed in **a** (**white dotted circle**), and numerous GFAP immunoreactive astrocytes in **b** and **c**. (GFAP immunohistochemical staining, ×200). [Color figure can be viewed in the online issue, which is available at www. anatomy.org.tr]

the mPFC of juvenile rats. In a previous study, increase in the expression level of GFAP in brain regions following $PbNO_3$ treatment was documented.[38] The astrocytic cell count was augmented following $PbNO_3$ treatment suggesting that increased GFAP immunoreactivity can be an indication of the formation of gliosis as one of the mechanisms by which Pb induces its adverse effects on the CNS. In the CNS, astrocytes are abundant cells that provide support for neurons, contribute to the formation and function of synapses, thin-out synapses by phagocytosis, and participate in a wide range of homeostatic functions.[39–42]

One of the pivotal role of astrocytes is to respond to injury via an intricate process known as reactive gliosis, which causes cellular damage or loss of normal neuroprotective functions in the CNS following injury, trauma, or disease.[43]

In this study, marked damage was be observed in the cytoarchitecture of the mPFC dissected in the rats treated with $PbNO_3$ (**Figures 4b** and **5b**). Similar neurodegenerative features were also present in mPFCs of the recovery group (**Figures 4c** and **5c**). These outcomes are similar to the neuropathological observations documented in previous studies.[44,45]

In a healthy CNS, calcium ions regulate a large number of cellular processes such as cell growth, differentiation, and synaptic activity. Although physiological increase in the levels of intracellular Ca^{2+} are typically crucial to cellular processes, excessive and irregular influx of Ca^{2+}, and any other Ca^{2+} release from intracellular compartments, can impair Ca^{2+}-regulatory mechanisms and result in cell death.[27] Considering the significantly increased number of astrocytes in the mPFCs of the $PbNO_3$-treated and the recovery groups (**Figures 6b** and **6c**), another possible justification is that, exposure to $PbNO_3$ might have impaired the regulatory function of calcium on neuronal cell integrity and inhibited several intracellular biological activities.[46]

Neuronal cell death contributes to the basic neuropathology of various degenerative disorders of the

CNS.[47,48] In this study, Pb increased cell death in the PFC of the $PbNO_3$-treated rats compared with the control. This partly shows the response adopted by the neurons of the PFC in the Pb-treated rats, thus implying a definite response based on the extent of the insult which entirely relies on the cellular and genetic composition. On the other hand, it is possible that this might have occurred as a result of neuronal plasticity often seen in the different regions of the CNS due to the alteration in the ratio of DNA to RNA.[49]

Nissl staining is a quick and easy screen for neurodegeneration and the morphology of the dying neurons can be suggestive of apoptosis. Consistent with the integrity of cresyl fast violet as a marker of apoptosis, we observed in degenerating neurons peripheral deposits of Nissl substances with features of chromatolysis, suggesting that the neurons are undergoing apoptotic process. This result corroborates with the study of Dribben et al.[50]

Withdrawing the rats from further exposure to Pb did not bring any form of significant improvement in the cytoarchitectural profile of the mPFC of the rats compared with the control (**Figures 4a**, **4c**, **5a**, **5c**, **6a** and **6c**). This effect in Group C may be due to the fact that Pb might not be completely metabolized and eliminated off by the excretory system of the rats in this group, as this could further generate excitotoxic characteristics in the neurons.[51] It may as well be suggested that these observed alterations in the cellular integrity are due to excess Pb stored in the interneuronal spaces that inhibits oxygen utilization, thus reducing the production of the required level of ATP through the electron transport chain and modifying the morphology of the neuron to compensate for the available amount of energy present.[52,53]

Withdrawing the rats from further exposure to Pb did not bring any form of significant improvement in the cytoarchitecture of the mPFC compared with the control group (**Figures 4a** *versus* **4c**; **5a** *versus* **5c**; **6a** *versus* **6c**). This is in agreement with earlier studies that suggested that cellular improvement from Pb exposure was never complete.[37,50]

Conclusion

Exposure to Pb confers deleterious and toxic effects on the cellular profile of the mPFC in juvenile male rats. Furthermore, 21 days withdrawal from further exposure to Pb does not restore the cytoarchitecture of the mPFC.

References

1. Jaishankar M, Tseten T, Anbalagan N, Mathew BB, Beeregowda KN. Toxicity, mechanism and health effects of some heavy metals. Interdiscip Toxicol 2014;7:60–72.
2. Kratzer J, Lettl C, Franke N, Gloor PA. The social network position of lead users. Journal of Productive Innovation Management 2016;3:201–16.
3. Ahmed MB, Ahmed MI, Meki AR, Abdraboh N. Neurotoxic effect of lead on rats: relationship to apoptosis. Int J Health Sci (Qassim) 2013;7:192–9.
4. Thürmer K, Williams E, Reutt-Robey J. Autocatalytic oxidation of lead crystallite surfaces. Science 2002;297:2033–5.
5. Nakata H, Nakayama SM, Oroszlany B, Ikenaka Y, Mizukawa H, Tanaka K, Harunari T, Tanikawa T, Darwish WS, Yohannes YB, Saengtienchai A, Ishizuka M. Monitoring lead (Pb) pollution and identifying Pb pollution sources in Japan using stable Pb isotope analysis with kidneys of wild rats. Int J Environ Res Public Health 2017;14:pii.E56.
6. Naicker N, Mathee A, Barnes B. A follow-up cross-sectional study of environmental lead exposure in early childhood in urban South Africa. S Afr Med J 2013;103:935–8.
7. Lidsky TI, Schneider JS. Lead neurotoxicity in children: basic mechanisms and clinical correlates. Brain 2003;126:5–19.
8. Liu MC, Liu XQ, Wang W, Shen XF, Che HL, Guo YY, Zhao MG, Chen JY, Luo WJ. Involvement of microglia activation in the lead induced long-term potentiation impairment. PLoS One 2012;7:e43924.
9. Goldstein GW. Lead poisoning and brain cell function. Environ Health Perspect 1990;89:91–4.
10. Lasley SM, Gilbert ME. Rat hippocampal glutamate and GABA release exhibit biphasic effects as a function of chronic lead exposure level. Toxicol Sci 2002;66:139–47.
11. Gilbert ME, Kelly ME, Samsam TE, Goodman JH. Chronic developmental lead exposure reduces neurogenesis in adult rat hippocampus but does not impair spatial learning. Toxicol Sci 2005;86:365–74.
12. Monnet-Tschudi F, Zurich MG, Boschat C, Corbaz A, Honegger P. Involvement of environ-mental mercury and lead in the etiology of neurodegenerative diseases. Rev Environ Health 2006;21:105–17.
13. Godwin HA. The biological chemistry of lead. Curr Opin Chem Biol 2001;5:223–7.
14. Bazrgar M, Goudarzi I, Lashkarbolouki T, Elahdadi Salmani M. Melatonin ameliorates oxidative damage induced by maternal lead exposure in rat pups. Physiol Behav 2015;151:178–88.
15. Morris S, van Aardt WJ, Ahern MD. The effect of lead on the metabolic and energetic status of the Yabby, Cherax destructor, during environmental hypoxia. Aquat Toxicol 2005;75:16–31.
16. Duruibe JO, Ogwuegbu MOC, Egwurugwu JN. Heavy metal pollution and human biotoxic effects. International Journal of Physical Science 2007;2:112–8.
17. Liu W, Tang Y, Feng J. Cross talk between activation of microglia and astrocytes in pathological conditions in the central nervous system. Life Sci 2011;89:141–6.
18. Liu MC, Liu XQ, Wang W, Shen XF, Che HL, Guo YY, Zhao MG, Chen JY, Luo WJ. Involvement of microglia activation in the lead induced long-term potentiation impairment. PLoS One 2012;7:e43924.
19. Verstraeten SV, Aimo L, Oteiza PI. Aluminium and lead: molecular mechanisms of brain toxicity. Arch Toxicol 2008;82:789–802.
20. Kasten-Jolly J, Heo Y, Lawrence DA. Central nervous system cytokine gene expression: modulation by lead. J Biochem Mol Toxicol 2011;25:41–54.
21. Kasten-Jolly J, Pabello N, Bolivar VJ, Lawrence DA. Developmental lead effects on behavior and brain gene expression in male and female BALB/cAnNTac mice. Neurotoxicology 2012;33:1005–20.

22. Kumawat KL, Kaushik DK, Goswami P, Basu A. Acute exposure to lead acetate activates microglia and induces subsequent bystander neuronal death via caspase-3 activation. Neurotoxicology 2014;41: 143–53.
23. Adhikari N, Sinha N, Narayan R, Saxena DK. Lead-induced cell death in testes of young rats. J Appl Toxicol 2001;21:275–7.
24. Paxinos G, Watson C. The rat brain in stereotaxic coordinates. San Diego: Academic Press Elsevier; 2007. p. 340.
25. Ardalan M, Rafati AH, Nyengaard JR, Wegener G. Rapid antidepressant effect of ketamine correlates with astroglial plasticity in the hippocampus. Br J Pharmacol 2017;174:483–92.
26. Tchounwou PB, Yedjou CG, Patlolla AK, Sutton DJ. Heavy metals toxicity and the environment. EXS 2012;101:133–64.
27. Sanders T, Liu Y, Buchner V, Tchounwou PB. Neurotoxic effects and biomarkers of lead exposure: a review. Rev Environ Health 2009;24:15–45.
28. Flora G, Gupta D, Tiwari A. Toxicity of lead: a review with recent updates. Interdiscip Toxicol 2012;5:47–58.
29. Mason LH, Harp JP, Han DY. Pb Neurotoxicity: neuropsychological effects of lead toxicity. Biomed Res Int 2014:840547.
30. Hsiang J, Díaz E. Lead and developmental neurotoxicity of the central nervous system. Curr Neurobiol 2011;2:35–42.
31. Clarke LE, Barres BA. Emerging roles of astrocytes in neural circuit development. Nat Rev Neurosci 2013;14:311–21.
32. Sofroniew MV. Molecular dissection of reactive astrogliosis and glial scar formation. Trends Neurosci 2009;32:638–47.
33. Zhang R, Lu H, Tian S, Yin J, Chen Q, Ma L, Cui S, Niu Y. Protective effects of pre-germinated brown rice diet on low levels of Pb-induced learning and memory deficits in developing rat. Chem Biol Interact 2010;184:484–91.
34. Burda JE, Sofroniew MV. Reactive gliosis and the multicellular response to CNS damage and disease. Neuron 2014;81:229–48.
35. Zuchero JB, Barres BA. Glia in mammalian development and disease. Development 2015;142;3805–9.
36. Olajide OJ, Akinola BO, Ajao MS, Enaibe BU. Sodium azide-induced degenerative changes in the dorsolateral prefrontal cortex of rats: attenuating mechanisms of kolaviron. Eur J Anat 2016;20:47–64.
37. Eltony SA, Othman MA, Mohamed AA. Histological study on the effect of low level perinatal lead exposure on the cerebellar cortex of adult male albino rat. Egyptian Journal of Histology 2010;33:781– 97.
38. Kumar P, Singh R, Nazmi A, Lakhanpal D, Kataria H, Kaur G. Glioprotective effects of Ashwagandha leaf extract against lead induced toxicity. BioMed Res Int 2014;2014:182029.
39. Sofroniew MV, Vinters HV. Astrocytes: biology and pathology. Acta Neuropathol 2010;119:7–35.
40. Chung WS, Allen NJ, Eroglu C. Astrocytes control synapse formation, function, and elimination. Cold Spring Harb Perspect Biol 2015;7:a020370.
41. Liddelow S, Barres B. Snapshot: astrocytes in health and disease. Cell 2015;162:1170–1170.e.1.
42. Liddelow SA, Guttenplan KA, Clarke LE, Bennett FC, Bohlen CJ, Schirmer L, Bennett ML, Münch AE, Chung WS, Peterson TC, Wilton DK, Frouin A, Napier BA, Panicker N, Kumar M, Buckwalter MS, Rowitch DH, Dawson VL, Dawson TM, Stevens B, Barres BA. Neurotoxic reactive astrocytes are induced by activated microglia. Nature 2017;541:481–7.
43. Aguzzi A, Barres BA, Bennett ML. Microglia: scapegoat, saboteur, or something else? Science 2013;339:156–61.
44. Struzyñska L, Bubko I, Walski M, Rafa6owska U. Astroglial reaction during the early phase of acute lead toxicity in the adult rat brain. Toxicol 2001;165:121–31.
45. Khanam S, Devi K. Effect of *Withania somnifera* root extract on lead-induced DNA damage. Journal of Food, Agriculture & Environment 2005;3:31–3.
46. White LD, Cory-Slechta DA, Gilbert ME, Tiffany-Castiglioni E, Zawia NH, Virgolini M, Rossi-George A, Lasley SM, Qian YC, Basha MR. New and evolving concepts in the neurotoxicology of lead. Toxicol Appl Pharmacol 2007;225:1–27.
47. Cordeiro MF, Guo L, Coxon KM, Duggan J, Nizari S, Normando EM, Sensi SL, Sillito AM, Fitzke FW, Salt TE, Moss SE. Imaging multiple phases of neurodegeneration: a novel approach to assessing cell death in vivo. Cell Death Dis 2010;1:e3.
48. Lanni C, Racchi M, Memo M, Govoni S, Uberti D. p53 at the crossroads between cancer and neurodegeneration. Free Radic Biol Med 2012;52:1727–33.
49. Lee HS, Park JH, Kim SJ, Kwon SJ, Kwon J. A cooperative activation loop among SWI/SNF, gamma-H2AX and H3 acetylation for DNA double-strand break repair. EMBO J 2010;29:1434–45.
50. Dribben WH, Creeley CE, Farber N. Low-level lead exposure triggers neuronal apoptosis in the developing mouse brain. Neurotoxicol Teratol 2011;33:473–80.
51. Villeda-Hernández J, Méndez Armenta M, Barroso-Moguel R, Trejo-Solis MC, Guevara J, Rios C. Morphometric analysis of brain lesions in rat fetuses prenatally exposed to low-level lead acetate: correlation with lipid peroxidation. Histol Histopathol 2006;21:609–17.
52. Baranowska-Bosiacka I, Hlynczak AJ. The effect of lead ions on the energy metabolism of human erythrocytes in vitro. Comp Biochem Physiol C Toxicol Pharmacol 2003;134:403–16.
53. Maiti AK, Saha NC, Paul G. Effect of lead on oxidative stress, Na+K+ATPase activity and mitochondrial electron transport chain activity of the brain of *Clarias batrachus* L. Bull Environ Contam Toxicol 2010:84:672–6.

Online available at:
www.anatomy.org.tr
doi:10.2399/ana.17.015
QR code:

Correspondence to: Adekomi Damilare Adedayo, PhD
Department of Anatomy, Faculty of Basic Medical Sciences,
College of Health Sciences, Osun State University, Osogbo, Osun State, Nigeria
Phone: +234 803 844 16 71
e-mail: adedayo.adekomi@uniosun.edu.ng

Conflict of interest statement: No conflicts declared.

Original Article

www.anatomy.org.tr
Received: July 16, 2017; Accepted: July 29, 2017
doi:10.2399/ana.17.023

anatomy
An International Journal of Experimental and Clinical Anatomy

Correlation between the femoral trochlear line – epicondylar line angle and intercondylar notch width index in an Iranian population

Sasan Shahsavaripour, Mohammad Barbarestani, Gholamreza Hassanzadeh, Tayebeh Rastegar

Department of Anatomy, School of Medicine, Tehran University of Medical Sciences, Tehran, Iran

Abstract

Objectives: Distal femur anthropometric indices are the main parameters for the design of knee implants. However, there are several variations concerning the anatomy and congruence of the distal femur in different populations. The purpose of this study was to identify anthropometric data on the distal femur and investigate the correlation between the trochlear line – epicondylar line angle and intercondylar notch width index in an Iranian population.

Methods: Distal femur measurements were performed in 158 knees on bony specimens and 187 MRIs from an Iranian population. Intercondylar width, intercondylar notch width, and trochlear line – epicondylar line angle were measured and intercondylar notch width index was calculated.

Results: In bony specimens, the trochlear line – epicondylar line angle was measured as 7.38° and intercondylar notch width as 19.36 mm. In MRI images, the trochlear line – epicondylar line angle was measured as 6.07° and notch width index as 0.276 mm. Linear regression analysis showed a significant relationship between the trochlear line – epicondylar line angle and notch width index ($p<0.05$).

Conclusion: The results of this study provide fundamental data for the design of knee prostheses suitable for the Iranian population.

Keywords: anthropology; notch width index; total knee arthroplasty; trochlea epicondylar angle

Anatomy 2017;11(2):87–92

Introduction

In total knee arthroplasty (TKA), maximum implant covering on the bone surface minimizes the stress applied to the bone-implant interface.[1] A good shape match between the prosthesis and the resected surface of the knee is reported as an important factor for long term survival of TKA. Most of the available TKA prostheses are designed according to the anthropometric data from American or European populations, which is suspected to be the cause of mismatch of these prostheses in Asian people.[2]

Distal femur anthropometric indices are the main parameters in the design of knee implants, and are important determinants for achieving a well-balanced flexion-extension gap in a TKA. Several studies studied the distal femur and reported knee morphometric indices for sizing the femoral component of knee prostehesis.[3–9] The notch width index (NWI) and other morphologic parameters of the knee joint are importantin designing knee prostheses.[4] However, most of the studies are reports from North America,[4,5] Europe[6] and Asia.[7–9]

Iranic people are an ethnical group among the Asian population.[10] However, the number of previous studies on knee morphometry is limited, there is only one study on CT scans of 150 patients on some measurements from distal femur, namely width of the medial and lateral condyles, anteroposterior length of the lateral condyles, and intercondylar width.[11] Also, there were no studies in the literature investigating anthropological parameters of the bony specimens in the Iranian population. The aim of this study was to to evaluate whether current total knee prostheses are proportionally matching to anatomical pro-

files of the Iranian knees by measurements from bones and MRI images of the femur.

Materials and Methods

This cross sectional study was performed on 158 cadaveric knees from the Department of Anatomy, School of Medicine, Tehran University of Medical Sciences, Tehran, Iran, and on 187 patients that underwent MRI on one or both knees between October 2015 and April 2016 in Shariati Hospital, Tehran, Iran with institutional ethic approval. Pertinent demographic and clinical history was obtained from the existing medical charts. Patients with knee deformities or dysplasia, connective tissue or hematologic disorders, fractures involving articular surfaces, prior knee arthroscopy/surgery or osteoarthritis were excluded from the study.[12] The measurements were performed in the frontal plane in MR images, and in the horizontal plane in bone specimens. Therefore, we did not make a comparison between the bone and MRI samples.

According to earlier reports, a measurement of femoral head diameter less than 42.5 mm indicates a female and a measurement greater than 47.5 mm indicates a male. A midshaft femoral head circumference measurement less than 81 mm indicates a female, while measurements above 81 mm indicates a male.[13,14] Identification of the left and right femur was based on the anatomical position and landmarks.[15] Based on these parameters, bones studied were from 121 males and 37 females. From these, 88 bones were from the right side and 70 frpm the left side. Knee MRIs were from 187 patients (91 males, 96 females) from the Radiology Department of Shariati Hospital, Tehran, Iran. Of these, 99 MRIs were from the right and 88 from the left knee.

MRI was performed using a 1.5 Tesla whole body MRI system (Siemens 1.5 Tesla, Avanto, Germany) with an extremity coil. Pulse sequences were T1-weighted images. The direction of axial slice imaging placed the slice perpendicular to the femoral mechanical axis in the coronal plane and perpendicular to the long axis of the femur in the sagittal plane. Before performing the study, the MRI was precalibrated to provide a 0% of magnification. All 187 MRI files were reconstructed at 3 mm intervals.[16]

The following knee joint structures were measured: intercondylar width (ICW), intercondylar notch width, trochlear line - epicondylar line angle (TEA) and intercondylar notch width index (NWI). NWI was calculated as a ratio of maximum notch width to the ICW.[13] For bony specimens, angle measurements were made on photographic images using Digimizer free image analysis software (Version 4.0.0; MedCalc Software, Mariakerke, Belgium) and a digital caliper was used to measure the remaining parameters. In MRI images, all measurements were performed using the MRI device software.

In bony specimens, the ICW was measured as the maximum distance between the internal and external condyles (**Figure 1a**). In MRI images, the distal femoral popliteal groove was observed and the maximum distance between the internal and external condyles was measured.[17,18] (**Figure 1b**).

Intercondylar notch width was measured on the bones using a caliper and using the software of the MRI machine in MRI images (**Figure 2**).

According to the method reported by Souryal et al.,[17] femoral NWI was calculated by dividing the ICW by the intercondylar notch width (NW). The NW was meas-

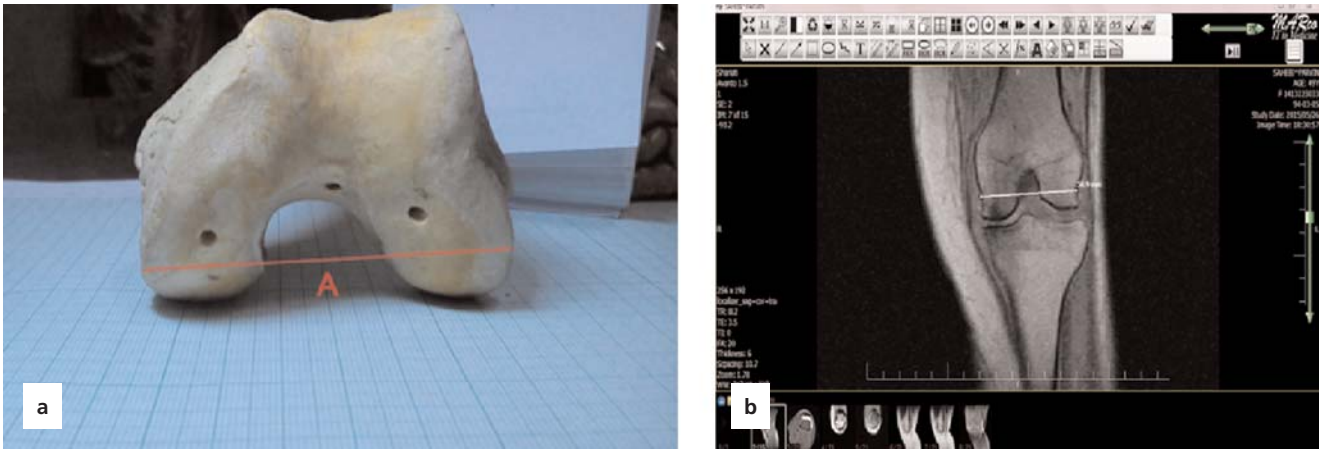

Figure 1. (**a**) Bicondylar line in distal femur and (**b**) intercondylar width on MRI image. [Color figure can be viewed in the online issue, which is available at www.anatomy.org.tr]

ured as the length between the medial projection of the lateral condyle and the lateral projection of the medial condyle of the femur. The ICW was determined by measuring the line passing through the popliteal groove and running parallel to the line drawn between the condylar ends across the most distal aspect of femur. Both measurements were performed on axial images (**Figure 3**). Employing the criteria of Domzalski et al.[18] a value of 0.27 or more for the NWI was considered as normal, whereas values equal to or below 0.269 were considered as low.

The TEA is between two lines: trochlear line as the line passing through the most anterior points of the trochlea and the epicondylar line as the maximum distance between the internal and external epicondyles.[5,19] The angle between the two lines was measured (**Figure 4**).

All comparisons between categories were made using the v2 test. p≤0.05 was considered to be statistically significant.

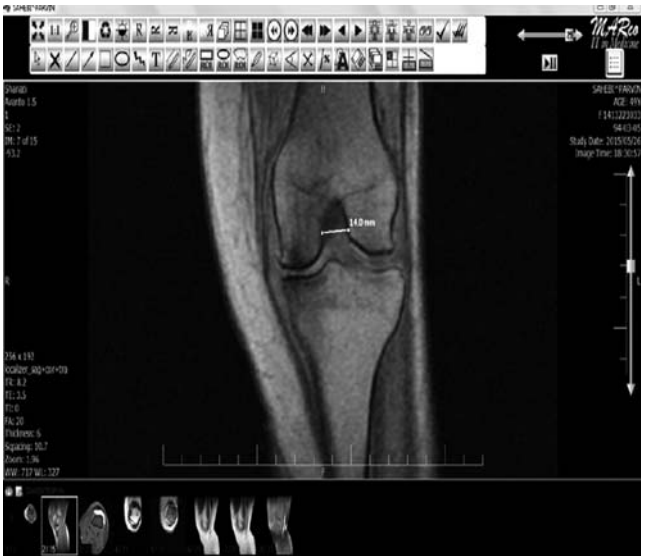

Figure 2. Measurement of notch width (NW) on MRI.

Results

In bony specimens, the mean ICW was measured as 65.98 mm, 61.33 mm in females and 67.46 mm in males and females. The NW was 17.9 mm in females and 19.8 mm in males, and 19.36 mm in males and females. The NWI was 0.292 mm in females, and 0.291 mm in males, and 0.291 mm in males and females. The mean TEA line angle was in 7.17° in females, 7.48° in males, and 7.38° in males and females.

In MRI images, the ICW was 63.92 mm in females, 74.58 mm in males, and 69.11 mm in males and females. NWI was 17.93 mm in females, 19.98 mm in males, and 18.92 mm in males and females. In bony specimens, NWI was 0.28 mm in females, 0.268 mm in males, and 0.276 mm in males and females. TEA was 5.76° in females, 6.48° in males and 6.07°, in males and females (**Table 1**).

Linear regression results showed that one degree rise of TEA decreased the NWI 0.002 units. This relationship was statistically significant (p<0.05). Linear regression analysis for MRI images showed that for one degree rise in TEA, NWI decreased by 0.006, and this correlation was also statistically significant (p<0.05) (**Figure 5**).

Discussion

Measurements of knee morphometric parameters are important in the construction, design and selection knee prosthesis. The aim of this study was to identify clearly discernible, reliable anthropometric indices of knee that could be used in construction of prosthesis commonly used in TKA. To our knowledge, this is the first study to

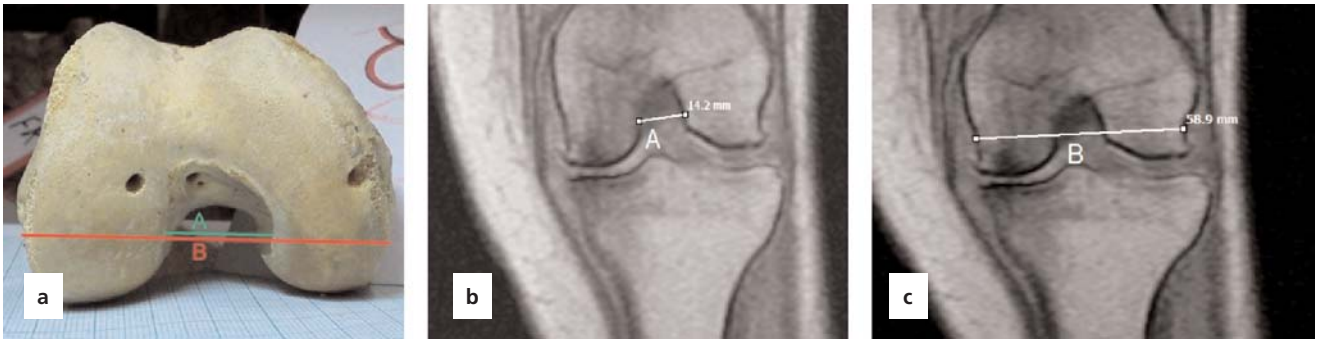

Figure 3. (**a**–**c**) Intercondylar notch width (**A**) and intercondylar width (**B**) in bony and MRI specimens. [Color figure can be viewed in the online issue, which is available at www.anatomy.org.tr]

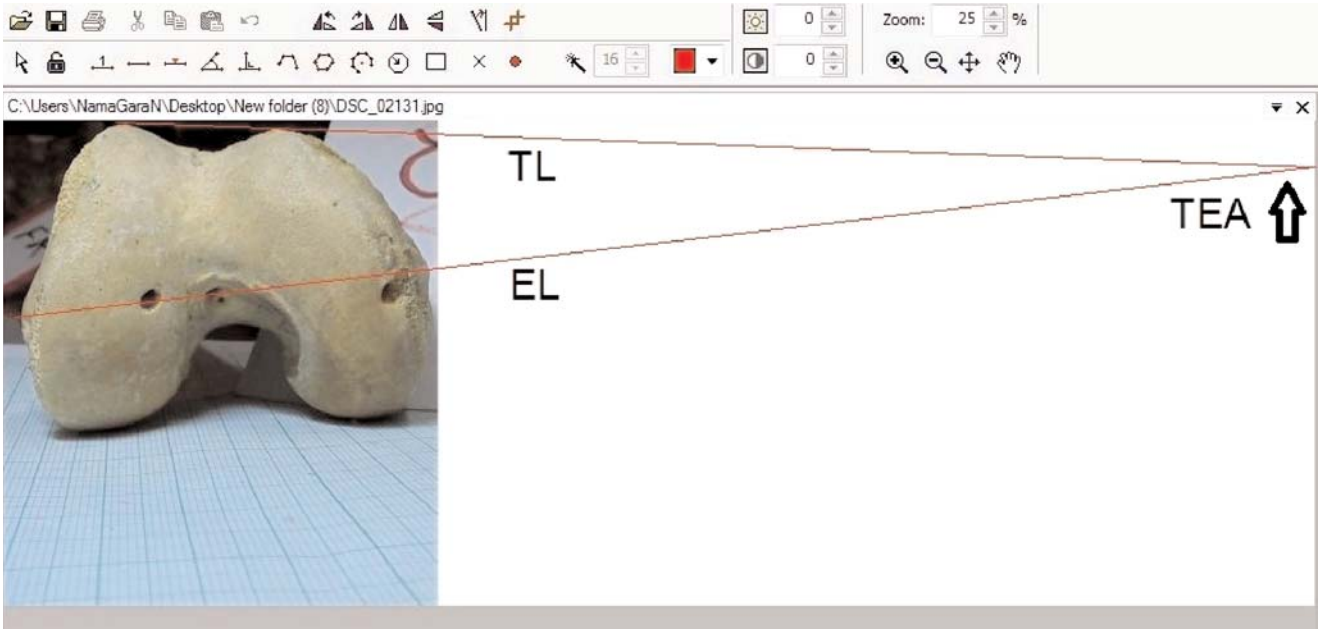

Figure 4. Measurement of **TEA** using Digimizer free image analysis software (Version 4.0.0; MedCalc Software, Mariakerke, Belgium). Trochlear line (**TL**) is the line passing from the most anterior point of the trochlea and the epicondylar line (**EL**) is the maximum distance beween the medial and lateral epicondyles. [Color figure can be viewed in the online issue, which is available at www.anatomy.org.tr]

Table 1

Intercondylar width (ICW), intercondylar notch width (NW), notch width index (NWI) and trochlear line – epicondylar line angle (TEA) in bones and MRI images (mm, Mean ± SD).

Method	Variable	ICW	NW	NWI	TEA
MRI images	Right (n=99)	69.21±6.87	19.06±2.83	0.276±0.036	6.10±1.23
	Left (n=88)	69±6.91	18.73±3.09	0.272±0.041	6.20±1.14
	Male (n=91)	74.58±4.8	19.98±3.07	0.268±0.028	6.48±1.08
	Female (n=96)	63.92±3.85	17.93±2.46	0.280±0.035	5.76±1.05
Dry bones	Right (n=88)	65.98±5.35	19.3±2.76	0.291±0.028	7.61±2.22
	Left (n=70)	66±5.98	19.44±2.56	0.292±0.028	7.07±1.8
	Male (n=121)	67.44±5.14	19.80±2.66	0.291±0.029	7.48±2.12
	Female (n=37)	61.33±4.13	17.99± 2.24	0.292±0.025	7.17±1.93

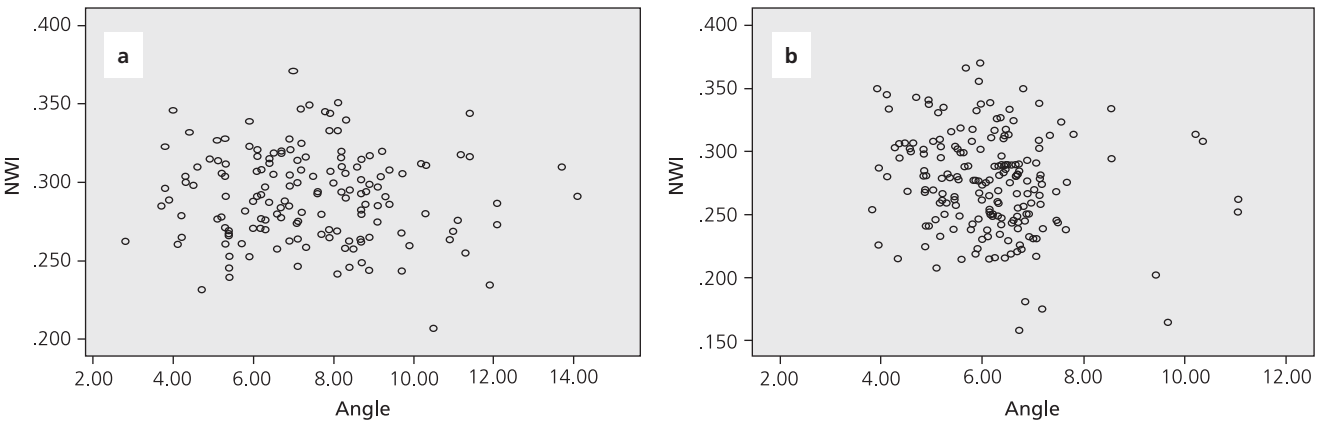

Figure 5. Linear regression of NWI and TEA in (**a**) bones and (**b**) MRI images.

investigate the relationship between NWI and TEA in normal knees using MRI and dissected bones in an Iranian population.

ICW is important in anatomical, clinical, anthropometric and orthopedic parameter, particularly for TKA. According to our results, ICW was 65.9 mm (61.3 mm in females and 67.4 mm in males) in bony specimens, and 69.1 mm (63.9 mm in females and 74.5 mm in males) in MRI images. This variable was 70.6 mm in Japanese, 71.2 mm in Chinese,[20] 70.2 mm in Koreans,[9] and 71.5 mm Germans.[21] This shows a significant difference between measurements of these studies and the current study in an Iranian population; however, it can be noted that distal femur parameters in Iranian population were closer to German and Chinese populations.

Intercondylar notch is an anatomic site of interest as it lodges the anterior cruciate ligament. The morphology of the intercondylar notch may be clinically relevant to anterior cruciate ligament pathologies. NWI is also an important parameter to estimate knee prosthesis measurements.[22] It is associated with damage to knee ligaments and is a useful parameter in knee arthroplasty and prostheses. So measurements of this variable is very important.[5,11,23,24] In a recent CT study on an Iranian population, intercondylar notch width was measured as 20.39±3.4 mm, 21.76 in males and 17.96 mm in females.[11] These results are similar to our findings of NW in bony and MRI specimens.

The average NWI in this study was 0.29 mm. This is slightly higher than the average NWI in previously published papers. Souryal et al.[17] calculated NWI as 0.23, Anderson et al.[25] 0.26, and results of the study by Chandrashekar et al.[26] was the closest to the current study as 0.29. This shows that there is a wide range in both intercondylar notch width and bicondylar width measurements, possibly due to the different age, gender or population of the study groups.

Poilvache et al.[19] measured TEA in 111 knees and found as 5.38° in females and 4.41° in males. In this study, in bony specimens, TEA was 7.38° (7.4° in males and 7.1° in females) and in MRI images 6° (6.4° in males and 5.7° in females). This value is higher than reported in the previous studies.

Conclusion

The findings of this study on distal femur morphometry will be useful for the design and construction of knee prostheses for the Iranian population, and also be useful for clinicians involved in the TKA.

References

1. Chaichankul CA, Tanavalee M, Itiravivong P. Anthropometric measurements of knee joints in Thai population: correlation to the sizing of current knee prostheses. Knee 2011;18:5–10.
2. Yue B, Varadarajan KM, Ai S, Tang T, Rubash HE, Li G. Differences of knee anthropometry between Chinese and white men and women. J Arthroplasty 2011;26:124–30.
3. Vaidya SV, Ranawat CS, Aroojis MA, Laud NS. Anthropometric measurements to design total knee prostheses for the Indian population. J Arthroplasty 2000;15:79–85.
4. Dienst M, Schneider G, Altmeyer K, Voelkering K, Georg T, Kramann B, Kohn D. Correlation of intercondylar notch cross sections to the ACL size: a high resolution MR tomographic in vivo analysis. Arch Orthop Trauma Surg 2007;127:253–60.
5. Ireland ML, Ballantyne BT, LittlE K, MCClay IS. A radiographic analysis of the relationship between the size and shape of the intercondylar notch and anterior cruciate ligament injury. Knee Surg Sports Traumatol Arthrosc 2001;9:200–5.
6. Singh JA, Inacio MC, Namba RS, Paxton EW. Rheumatoid arthritis is associated with higher ninety-day hospital readmission rates compared to osteoarthritis after hip or knee arthroplasty: a cohort study. Arthritis Care Res 2015;67:718–24.
7. Uehara K, Kadoya Y, Kabayashi A, Ohashi H, Yamano Y. Anthropometry of the proximal tibia to design a total knee prosthesis for the Japanese population. J Arthroplasty 2002;17:1028–32.
8. Kwak DS, Surendran S, Pengatteeri YH, Park SE, Choi KN, Gopinattan P, Han SH, Han CW. Morphometry of the proximal tibia to design the tibial component of total knee arthroplasty for the Korean population. Knee 2007;14:295–300.
9. Kwak DS, Han S, Han CW, Han SH. Resected femoral anthropometry for design of the femoral component of the total knee prosthesis in a Korean population. Anat Cell Biol 2010;43:252–9.
10. Rashidvash V. Anthropological and genetic characteristics of Atropatene population. Int J Humanit Soc Sci 2012;2:139–47.
11. Moghtadaei M, Moghimi J, Shahhoseini G. Distal femur morphology of iranian population and correlation with current prostheses. Iran Red Crescent Med J 2016;18(2):e21818.
12. Khodair SA, Ghieda UE, Elsayed AS. Relationship of distal femoral morphometrics with anterior cruciate ligament injury using MRI. Tanta Medical Journal 2014;42:64–68.
13. Reinhard KJ, Welner M, Okoye MI, Marotta M, Plank G, Anderson B, Mastellon T. Applying forensic anthropological data in homicide investigation to the depravity standard. J Forensic Leg Med 2013;20:27–39.
14. Scott JB, Gill GW, Kieffer DA. Race and sex determination from the intercodular notch of the distal femur. In: Gill GW, Rhine S, editors. Skeletal attribution of race. Albuquerque (NM): Maxwell Museum of Anthropology, University of New Mexico; 1990. pp. 83–90.
15. Johnston TB, Whillis J. Gray's anatomy. Descriptive and applied. 31st ed. London: Longmans Green and Co; 1954.
16. Al-Saeed O, Brown M, Athyal R, Sheikh M. Association of femoral intercondylar notch morphology, width index and the risk of anterior cruciate ligament injury. Knee Surg Sports Traumatol Arthrosc 2013;21:678–82.

17. Souryal TO, Freeman TR. Intercondylar notch size and anterior cruciate ligament injuries in athletes. A prospective study. Am J Sports Med 1993;21:535–9.
18. Domzalski M, Grzelak P, Gabos P. Risk factors for anterior cruciate ligament injury in skeletally immature patients: analysis of intercondylar notch width using magnetic resonance imaging. Int Orthop 2010;34:703–7.
19. Poilvache PL, Insall JN, Scuderi GR, Font-Rodriguez DE. Rotational landmarks and sizing of the distal femur in total knee arthroplasty. Clin Orthop Relat Res 1996;(331):35–46.
20. Cheng FB, Ji XF, Lai Y, Feng JC, Zheng WX, Sun YF, Fu YW, Li YQ. Three dimensional morphometry of the knee to design the total knee arthroplasty for Chinese population. Knee 2009;16:341–7.
21. Dargel J, Micheal JW, Feiser J, Ivo R, Koebke J. Human knee joint anatomy revisited: morphometry in the light of sex-specific total knee arthroplasty. J Arthroplasty 2011;26:346–53.
22. Ameet KJ, Murlimanju BV. A morphometric analysis of intercondylar notch of femur with emphasis on its clinical implications. Medicine and Health 2014;9:103–8.
23. Yue B, Varadarajan KM, Ai S, Tang T, Rubash HE, Li G. Gender differences in the knees of Chinese population. Knee Surg Sports Traumatol Arthrosc 2011;19:80–8.
24. Tillman MD, Smith KR, Bauer JA, Cauraugh JH, Falsettl AB, Pattishall JL. Differences in three intercondylar notch geometry indices between males and females: a cadaver study. Knee 2002;9:41–6.
25. Anderson AF, Anderson CN, Gorman TM, Cross MB, Spindler KP. Radiographic measurements of the intercondylar notch: are they accurate? Arthroscopy 2007;23:261–8.
26. Chandrashekar N, Slauterbeck J, Hashemi J. Sex-based differences in the anthropometric characteristics of the anterior cruciate ligament and its relation to intercondylar notch geometry a cadaveric study. Am J Sports Med 2005;33:1492–8.

Online available at:
www.anatomy.org.tr
doi:10.2399/ana.17.023
QR code:

Correspondence to: Tayebeh Rastegar, PhD
Department of Anatomy, School of Medicine,
Tehran University of Medical Sciences, Tehran, Iran
Phone: +98 21 64053404
e-mail: trastegar@sina.tums.ac.ir

Conflict of interest statement: No conflicts declared.

Original Article

www.anatomy.org.tr
Received: May 17, 2017; Accepted: July 28, 2017
doi:10.2399/ana.17.016

anatomy
www.anatomy.org.tr
An International Journal of Experimental and Clinical Anatomy

Effect of zinc sulphate and Essentiale® Forte in managing carbon tetrachloride-induced hepatotoxicity in adult Wistar rats

Babatunde E. Arayombo, Olarinde S. Adewole, David A. Ofusori, Taiwo S. Adelodun, Stephen S. Olusola, Ronald Bejide

Department of Anatomy and Cell Biology, Faculty of Basic Medical Sciences, Obafemi Awolowo University, Ile-Ife, Nigeria

Abstract

Objectives: The aim of this study was to assess and compare the ameliorative effect of zinc sulphate and Essentiale® Forte on the histomorphology and lipid histochemistry of carbon tetrachloride (CCl_4)-induced hepatic injury in adult Wistar rats.

Methods: Twenty-five adult Wistar rats, weighing between 150 g and 170 g, were used for the study. The animals were divided into five groups A, B, C, D and E (n=5). Group A received 0.7 ml/kg of olive oil orally. Groups B, C, D and E were administered CCl_4 (0.7 ml/kg, orally) for 1 week in 1:1 dilution with olive oil. After CCl_4 administration, Group C was treated with Essentiale® Forte (4.5 mg/kg/bw, orally) for four weeks. Group D was treated with zinc sulphate (7 mg/kg/bw, orally) daily for four weeks. Group E received zinc sulphate (7 mg/kg/bw, orally) and Essentiale® Forte (4.5 mg/kg/bw, orally) for a period of 4 weeks, while Group B was left untreated. Animals were left for another one week and subsequently sacrificed under ether anaesthesia. The liver was harvested, weighed and divided into two parts for histological and histochemical studies.

Results: Histological analysis showed that treatment of liver with CCl_4 caused hepatotoxicity as marked by presence of inflammatory cells and distortion in the connective tissue fibers, as compared to the ones treated with zinc sulphate and or Essentiale® Forte which restored the hepatic histoarchitecture and protected the liver tissue from fatty and degenerative changes.

Conclusion: This study showed that combination of Essentiale® Forte and zinc supplement offered better ameliorative effects on the liver of Wistar rats following CCl_4-induced hepatotoxicity compared with separate administration of either Essentiale® Forte or zinc sulphate.

Keywords: carbon tetrachloride; Essentiale® Forte; hepatotoxicity; liver; zinc sulphate

Anatomy 2017;11(2):93–98

Introduction

Liver is highly vulnerable to a wide variety of metabolic, toxic, microbial, circulatory and neoplastic insults. Liver diseases may be primary, but more often hepatic involvement is secondary. The liver has enormous functional reserves, such that early liver impairment is clinically masked and the progression of the deranged liver function makes the condition life threatening.[1] Morphologically, liver responds to injurious events in five different ways, irrespective of the cause, degeneration and intracellular accumulation, necrosis and apoptosis, inflammation, regeneration, fibrosis.[1]

Liver injury may follow the inhalation, ingestion or parenteral administration of a number of pharmacologic and chemical agents. These include industrial toxins *e.g.* carbon tetrachloride (CCl_4), trichloroethylene and yellow phosphorus, heat-stable toxic bi-cyclic octapeptides of certain species of *Amanitia* and *Galerina* (hepatotoxic mushroom poisoning), and more commonly, phamarcologic agents used in medical therapy. Hepatotoxic drugs can injure the hepatocyte directly, *e.g. via* a free radical or

metabolic intermediate that causes peroxidation of membrane lipids and that results in liver cell injury.[2]

CCl_4 is a colourless liquid, ether-like in odour with a density of l6 gcm-3 melting point is 22.9°C, boiling point is 76.7°C and soluble in water at 0.08 g/100 ml (25°C). It is also soluble in alcohol, ether, chloroform, benzene, naptha and carbon sulfide. The vapour pressure is 11.9 4kPa at 20°C and refractive index is 1.5. CCl_4 has a crystal structure with tetrahedral shape. It is not flammable, its auto-ignition tempt is 982°C and LD_{50} is 2350 mg/kg.[3] It has been reported to produce free radicals which affect the cellular permeability of the liver cells, leading to altered level of serum biochemistry and liver enzymes.[4] In time series, CCl_4 was found to have an atmospheric life time of 85 years and liver damage inflicted by it has lethal consequences.[4]

Over the years, chronic liver disease (CLD) is one of the major health challenges, and despite research and development of various new drugs, morbidity and mortality accompanying hepatic pathology still remained high.[5] Prolonged exposure of liver to CCl_4 has been researched with consequent spectrum of chronic liver disease, such as fatty liver, hepatitis, liver cirrhosis, hepatoma.[5] Liver damage can occur after 24 hours of exposure to CCl_4, and in serious cases this can result in painful swollen liver, ascites, hemorrhages, hepatic coma and death.[3]

Essentiale® Forte has been for a long time indicated and used in the cases and management of CLD. It is a 300 mg hard gel capsule that contains de-oiled enriched phospholipids from neutral soya beans. It works by replacing and regenerating the phospholipids in the liver cell membranes that have been damaged by various means especially through hepatotoxin. It is mainly made up of polyenylphosphatidylcholine from natural soya beans with vitamins B1, B2, B3, B6, and B12. The pharmaceutical excipients are chiefly ethanol (96%), hard fat, hydrogenated castor oil, ethyl vanillin, 4-methoxyl phenyl ethanone, alpha tocopherol, gelatin, colouring agents, sodium lauryl sulfate, and purified water.

Zinc is known as an essential trace element necessary for protein metabolism, as well as membrane integrity and also involved in the structure and function of over 300 metalloenzymes. It has important functions in skin and connective tissue, metabolism as well as in wound healing.[6] It exerts its antioxidant effects indirectly by maintaining membrane structures, involving in the structure of SOD, increasing the metallothionein concentrations and, competing with redox reactive metals, iron and cuprous for critical binding sites.[7] It is shown that hepatic and serum zinc levels of patients in liver disease decreased depending on the degree of liver damage.[8]

This study was thus designed to investigate the effect of zinc in form of zinc sulphate ($ZnSO_4$) when used separately or in combination with the long standing known drug Essentiale® Forte on CCl_4-induced hepatotoxicity in adult Wistar rats.

Materials and Methods

Twenty-five adult Wistar rats, weighing between 150 g and 170 g (6–10 weeks old) obtained from Animal Holding of International Institute of Tropical Agriculture Ibadan, Oyo State, Nigeria were used in this study. The animals were housed in plastic cages in a clean environment under standard laboratory conditions of light, temperature and humidity, in the animal holding of the Department of Anatomy and Cell Biology, Faculty of Basic Medical Sciences, Obafemi Awolowo University, Ile-Ife, Nigeria. They were fed on standard laboratory rat pellets and given water *ad libitum*. Ethical clearance for the study was obtained from the Health Research Ethical Committee, Institute of Public Health, Obafemi Awolowo University, Ile-Ife, Nigeria (Approval number: IPHOAU/12/416). The animals were given humane care according to the guidelines of HREC and IPHOAU.

2.5 liters of CCl_4 was obtained from the central research laboratory of Obafemi Awolowo University. 60 ml of CCl_4 was diluted with 60 ml of olive oil in 1:1 equivalent, and this was administered orally at a dose of 0.7 ml/kg. Three tablets of $ZnSO_4$ (20 mg each, Chi Pharmaceuticals Ltd, Lagos, Nigeria) were dissolved in 60 ml of water and this was administered at a dose of 7 ml/kg. 300 mg Essentiale® Forte capsule (Sanofi Aventis, manufactured by Nattermann & Cie GmbH, Cologne, Germany) was prepared by dissolving a capsule in 60 ml of water, and was administered at a dose of 4.5 mg/kg all being freshly prepared on each day of administration.

The rats were randomly divided into five groups: A, B, C, D and E (n=5, each). Group A: negative control, received oral administration of olive oil only; Group B: positive control, received daily administration of CCl_4 (0.7 ml/kg p.o) for 1 week in 1:1 dilution with olive oil without treatment; Group C received Essentiale® Forte 4.5 mg/kg/day for four weeks after the administration of CCl_4; Group D received $ZnSO_4$ (7 mg/kg/day, orally) daily for four weeks after the administration of CCl4; Group E received $ZnSO_4$ 7 mg/kg/day for four weeks and Essentiale® Forte (4.5 mg/kg/day p.o) concurrently for four weeks, after CCl_4 administration. All administrations were via oral route and the animals were then monitored for another one week for possible recovery.

At the end of the experimental procedures, all animals were sacrificed by cervical dislocation. A midline

incision was made along the anterior abdominal wall blood were taken by cardiac puncture, the liver specimens were perfused with isotonic saline, excised, blotted dry and weighed. Liver tissues were fixed in 10% formol saline processed for routine paraffin embedding a semi-quantitative method described by Pilette et al.[9]

Sectioned tissues were stained with Haematoxylin and Eosin for demonstration of the liver architecture, Masson's trichrome stain for demonstration of collagen fibers, Gordon and Sweet's silver impregnation method for demonstration of reticular fibers, and Sudan black B for the demonstration of lipid histochemistry. Conventional morphological evaluation of the liver tissue was made. Stained sections were viewed under a Leica DM 750 microscope (Leica Microsystems, Wetzlar Germany) and digital photomicrographs were taken using an attached Leica ICC50 camera. The degree of hepatic necrosis and fibrosis were determined by a semi-quantitative method.[9]

One-way ANOVA was used to analyze the data, followed by Student Newman-Keuls test for multiple comparisons. Graph Pad Prism 5 (Version 5.03; Graph Pad Inc., San Diego, CA, USA) was the statistical package used for data analysis. Significant difference was set at $p<0.05$.

Results

There was no significant weight gain in Group B, but a relative increase in organ weight compared to Group A. Significant weight gain was observed in all groups except Group B (**Table 1**).

The histological layout of the liver in the control group stained with Hematoxylin and Eosin, with the cytoplasm stained in pink and the nucleus stained in purple, showed parenchymal cells arranged in lobules with the characteristic central vein at the center and portal canals located peripherally (**Figure 1a**). The liver cells were arranged in a branching pattern within which were the sinusoidal plates. The portal triads contained the bile duct, hepatic vein and hepatic artery. In the untreated CCl_4 group, the hepatocytes showed features of inflammation with the presence of inflamed and inflammatory liver cells as seen in **Figures 1b–d**; there was also disruption of the normal histoarchitecture of the of the liver lobules. There were vacuolations, sinusoidal congestion, inflammatory cell infiltration within the sinusoids and aggregating around the central vein in the group treated with CCl_4 and Essentiale® Forte (**Figure 1c**). However, in the group treated with CCl_4 and $ZnSO_4$, there were areas of sinusoidal congestion which were not as congested as Group B, the inflammatory cells were less numerous, there was gradual restoration of the hepatic histoarchiture, though the cytoplasmic boundaries were not distinctly demarcated (**Figure 1d**). In the group treated with CCl_4, Essentiale® Forte and $ZnSO_4$, there were prominent nucleoli within the hepatocyte nucleus surrounding the central vein, and the inflammatory liver cells were reduced (**Figure 1e**).

In Masson's trichrome stainings, the negative control group presented normal hepatic histoarchitecture as maintained with radially arranged sinusoids. In addition, there was scanty distribution of the collagen fibers around the central vein as shown in **Figure 2a**. Collagen fibers were found aggregated around the sinusoids, close to the central vein of the untreated group (**Figure 2b**). There were also collagen fibers around the central vein and within the sinusoids of animals in Group C (**Figure 2c**). Collagen fibers in the hepatic tissues of animals in Group D revealed increased density within the liver sinusoids around the inflammatory cells (**Figure 2d**). In Group E, deposition of collagen fibers around the hepatic vessel and sinusoids were minimally evident (**Figure 2e**).

In Gordon and Sweet's silver impregnation stainings, regular distribution of the reticular fibers around the central vein and within the sinusoids of the hepatic tissue were observed (**Figure 3a**). The reticular fibers were observed to be scanty in the untreated group as indicated by the arrowed area (**Figure 3b**). In Group C, the reticular fibers were sparsely distributed as represented by the arrowed area in **Figure 3c** compared to the nor-

Table 1

Absolute organ weight and difference in body weight (bw) in control and treatment groups (mean±SEM; n=5 for each group).

Groups	Initial bw (g)	Final bw (g)	Change in bw (g)	Absolute liver weight (g)	Relative liver weight (%)
Group A (Olive oil)	161.2±3.14	165.6±2.42	4.4±2.29	3.35±0.16†	2.10±0.09
Group B (CCl_4)	160.4±1.97	160.8±3.06	0.6±1.36*‡	4.68±0.17*‡	2.92±0.12*
Group C (CCl_4+EPL)	162.2±3.15	170.6±3.63	8.4±1.29†	3.93±0.1	2.42± 0.1
Group D (CCl_4+$ZnSO_4$)	162±2.49	166.2±2.4	4.2±0.80†	4.16±0.09*	2.56±0.17*
Group E (CCl_4+$ZnSO_4$+EPL)	161.8±1.99	167.4±1.72	5.6±0.81†	4.04± 0.10*	2.50±0.16*

*Significantly different from normal control at $p<0.05$, †Significantly different from toxic control at $p<0.05$, ‡Significantly different from C, D and E at $p<0.05$. **EPL:** Essentiale® Forte

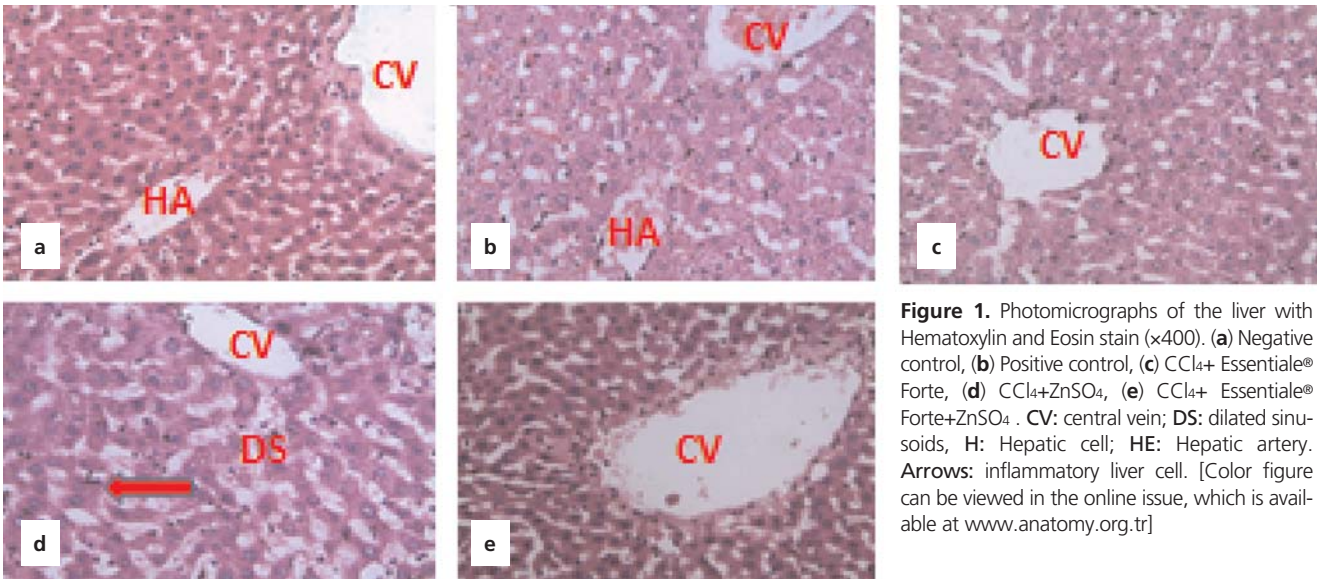

Figure 1. Photomicrographs of the liver with Hematoxylin and Eosin stain (×400). (**a**) Negative control, (**b**) Positive control, (**c**) CCl_4+ Essentiale® Forte, (**d**) CCl_4+$ZnSO_4$, (**e**) CCl_4+ Essentiale® Forte+$ZnSO_4$. **CV:** central vein; **DS:** dilated sinusoids, **H:** Hepatic cell; **HE:** Hepatic artery. **Arrows:** inflammatory liver cell. [Color figure can be viewed in the online issue, which is available at www.anatomy.org.tr]

mal control Group A. Also, there was very scanty distribution of reticular fibers along the central vein and lining of the sinusoids (**Figure 3d**). The reticular fibers of the liver tissue in Group E were completely effaced compared to that in the normal control group (**Figure 3e**).

In Sudan black B staining (**Figure 4a**), liver histoarchitecture revealed varying degrees of darkly stained blue-black areas where the cells appeared to have clumped together. These are lipid globule depositions in the CCl_4 treated Group B as can be seen in the area marked with arrow and area labeled F in **Figure 4b**. In contrast, in the CCl_4+$ZnSO_4$ group, the lipid granules were not evident as shown in **Figure 4c**. Also, in the other tissue sections (**Figures 4d** and **e**), the lipid granules were not evident either when compared to the untreated group (**Figure 4b**).

Discussion

In this study, data showed that CCl_4 toxicity led to a minimum increase in organ weight in Group B, while there was significant weight gain observed in all other groups similar to the findings of Raza et al.[10] and Teo et al.[11] Body weight change is one of the parameters used as indicator of adverse effects of drugs and chemicals.[12] When animals are anorexic, weight loss is bound to ensue due to disturbances in carbohydrate, protein or fat metabolism.[13]

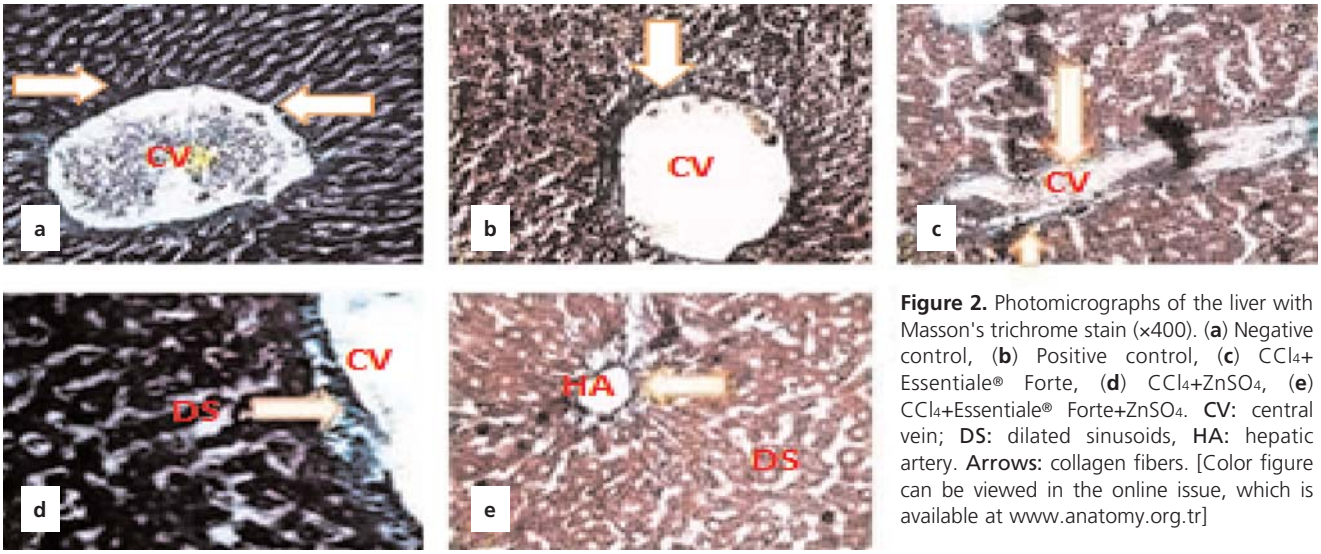

Figure 2. Photomicrographs of the liver with Masson's trichrome stain (×400). (**a**) Negative control, (**b**) Positive control, (**c**) CCl_4+ Essentiale® Forte, (**d**) CCl_4+$ZnSO_4$, (**e**) CCl_4+Essentiale® Forte+$ZnSO_4$. **CV:** central vein; **DS:** dilated sinusoids, **HA:** hepatic artery. **Arrows:** collagen fibers. [Color figure can be viewed in the online issue, which is available at www.anatomy.org.tr]

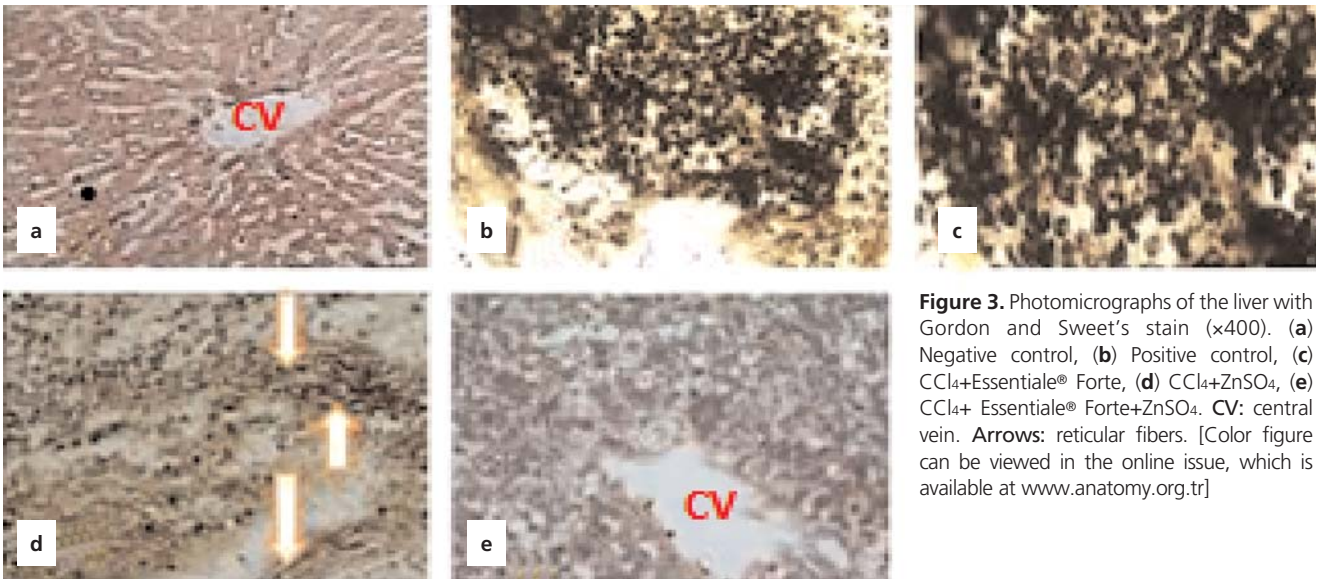

Figure 3. Photomicrographs of the liver with Gordon and Sweet's stain (×400). (**a**) Negative control, (**b**) Positive control, (**c**) CCl_4+Essentiale® Forte, (**d**) CCl_4+$ZnSO_4$, (**e**) CCl_4+ Essentiale® Forte+$ZnSO_4$. **CV:** central vein. **Arrows:** reticular fibers. [Color figure can be viewed in the online issue, which is available at www.anatomy.org.tr]

There was also a significant increase in relative liver weight in group B and this is in agreement with previous study where there was mild to moderate liver effects where there was increased liver weight and fatty degeneration following intermittent exposure of mice to CCl_4.[14]

Treatment with $ZnSO_4$ and Essentiale® Forte produced regenerative changes and absence of centrilobular necrosis, indicating that these agents possess hepatoprotective property by restoring the hepatic architecture and protecting the liver tissue from fatty and degenerative changes. These changes are achievable by prevention of toxic chemical reaction, lipid peroxidation, micro and macro vesicular fatty changes, ultimately preventing necrosis. Hence, the hepatoregenerative effect of $ZnSO_4$ and Essentiale® Forte may have a role in the process of regeneration and prevention of fibrosis in the long-term use of Essentiale® Forte. In the CCl_4+Essentiale® Forte group, although the histoarchitecture of liver seemed to be normal, minimal dilatation in sinusoids were observed. Changes in the CCl_4+Essentiale® Forte+$ZnSO_4$ group were minimal, almost close to the structures in the normal control group. This effect may be due to membrane stabiliza-

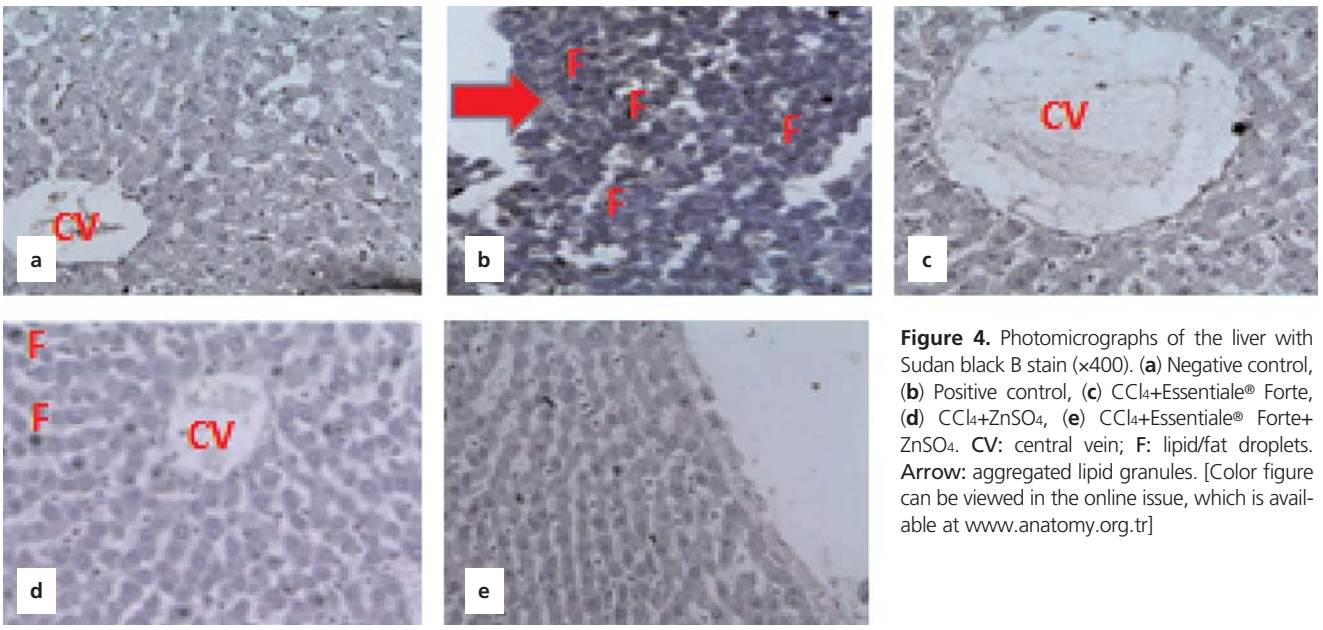

Figure 4. Photomicrographs of the liver with Sudan black B stain (×400). (**a**) Negative control, (**b**) Positive control, (**c**) CCl_4+Essentiale® Forte, (**d**) CCl_4+$ZnSO_4$, (**e**) CCl_4+Essentiale® Forte+$ZnSO_4$. **CV:** central vein; **F:** lipid/fat droplets. **Arrow:** aggregated lipid granules. [Color figure can be viewed in the online issue, which is available at www.anatomy.org.tr]

tion activity of $ZnSO_4$ in combination with Essentiale® Forte. Results obtained in this study are in agreement with earlier finding of Yadrick et al.[7] who reported that zinc exerts its antioxidant effects indirectly by maintaining membrane structures, involving in the structure of SOD, increasing the metallothionein concentrations and, competing with redox reactive metals for critical binding sites.

Histological observations depict that $ZnSO_4$ along with Essentiale® Forte showed significant recovery over either $ZnSO_4$ or Essentiale® Forte alone treated groups. In this study, combined supplementation of $ZnSO_4$ and Essentiale® Forte to CCl_4-treated rats was found to ameliorate hepatic toxicity when compared with the group treated with either $ZnSO_4$ alone or Essentiale® Forte only. Essentiale® Forte pretreatment in rats protects hepatocytes against lipid peroxidation.[15] Similar results were found by Guiliano et al.[16] with even a positive influence on the survival rate. It was also shown that hepatic and serum zinc levels of patients in liver disease decreased depending on the degree of liver damage.[8]

Therefore, it is assumed that administration of both $ZnSO_4$ and Essentiale® Forte synergistically act on injury induced by CCl_4. Essentiale® Forte alone also shows a positive effect, however it is less efficacious compared with $ZnSO_4$ and Essentiale® Forte combination.

Conclusion

Combined administration of $ZnSO_4$ and Essentiale® Forte may be considered more potentially and synergistically therapeutic through preclusion of cellular leakage mechanism and thereby inhibiting liver toxicity induced by CCl_4. $ZnSO_4$ and Essentiale® Forte have hepatoprotective activity against CCl_4 induced liver damage, this activity could be due to the presence of flavonoids in Essentiale® Forte and membrane stabilization ability in both, thereby preventing cellular leakage.

References

1. Cotran RS, Vinay K, Tucker C, Robbins SL. Robbins pathologic basis of disease. 6th ed. Philadelphia: Saunders; 1999.
2. Adaramoye OA, Akinloye O. Possible protective effect of kolaviron on CCl4-induced erythrocyte damage in rats. Biosci Rep 2000;259–64.
3. World Health Organization. International Programme on Chemical Safety (IPCS). Health and safety guide no. 107. Geneva: WHO; 1998.
4. Walker BL, Cooper CD. Air pollution emission factors for medical waste incenerators. J Air Waste Manag Assoc 1992;42:784–91.
5. Bojuwoye BU. The burden of viral hepatitis in Africa. West Afr J Med 1997;16:198–203.
6. Berger A. What does zinc do? BMJ 2002;325:1062.
7. Yadrick MK, Kenney MA, Winterfeldt EA. Iron, copper and zinc status: response to supplementation with zinc or zinc and iron in adult females. Am J Clin Nutr 1989;49:145–50.
8. Zhou Z, Sun X, Lambert JC, Saari JT, Kang YJ. Metallothionein-independent zinc protection from alcoholic liver injury. Am J Pathol 2002;160:2267–74.
9. Pilette C, Rousselet MC, Bedossa P, Chappard D, Oberti F, Rifflet H, Maïga MY, Gallois Y, Calès P. Histopathological evaluation of liver fibrosis: quantitative image analysis vs semi-quantitative scores. Comparison with serum markers. J Hepatol 1998;28:439–46.
10. Raza M, Al-Shabanah OA, El-Hadiyah TM, Al-Majed AA. Effect of prolonged vigabatrin treatment on haematological and biochemical parameters in plasma, liver, and kidney of Swiss albino mice. Sci Pharm 2002;70:127–37.
11. Teo S, Stirling D, Thomas S, Hoberman A, Kiorpes A, Khetani V. A 90-day oral gavage toxicity study of D-methylphenidate and D,L-methylphenidate in Sprague-Dawley rats. Toxicology 2002;179:183–96.
12. Tofovic SP, Jackson EK. Effect of long-term caffeine consumption on renal function in spontaneously hypertensive heart failure prone rats. J Cardiovasc Pharmacol 1999;33:360–6.
13. Klaassen CD, editor. Casarett and Doull's toxicology: the basic science of poisons. 6th ed. NewYork: McGraw-Hill; 2001.
14. Smyth HF, Smyth HF Jr, Carpenter CP. The chronic toxicity of carbon tetrachloride; animalexposure and field studies. J Ind Hyg Toxicol 1936;18:277–97.
15. Martelli A, Mereto E, Ghia M. Protective effect of phosphatidylcholine on hepatic lipid peroxidation in rats. Med Sci Res 1989;17:995–6.
16. Guiliano L, Loche A, Ottonello M. Evaluation of the protective activity of phosphatidylcholine in comparing lipid peroxidation processes. [Article in Italian] Boll Soc Ital Biol Sper 1987;63:481–7.

Online available at:
www.anatomy.org.tr
doi:10.2399/ana.17.016
QR code:

deomed

Correspondence to: Babatunde E. Arayombo, BMLS, MBChB, MSc
Department of Anatomy and Cell Biology, Faculty of Basic Medical Sciences, Obafemi Awolowo University, Ile-Ife, Nigeria
Phone: +8062893329
e-mail: arayombo82@gmail.com

Conflict of interest statement: No conflicts declared.

Teaching Anatomy

www.anatomy.org.tr
Received: June 1, 2017; Accepted: June 22, 2017
doi:10.2399/ana.17.021

anatomy
www.anatomy.org.tr
An International Journal of Experimental and Clinical Anatomy

Study preferences in anatomy education: a descriptive study including preliminary results*

Ekremcan Karaer[1], Çağatay Barut[2]

[1]*School of Medicine, Bahçeşehir University, Istanbul, Turkey*
[2]*Department of Anatomy, School of Medicine, Bahçeşehir University, Istanbul, Turkey*

Abstract

Objectives: In anatomical education, there is a lack of consensus about the best or most efficient method used. Additionally, the learning style of students varies, and information related with the medical students' preferences for learning anatomy is rather limited. Thus, this article aimed to identify the study preferences of medical students in Turkey.

Methods: Ninety-seven medical students aged between 19–26 years participated in the study. Participants were asked 16 questions related with the education system and study preferences of anatomy. Nine of the questions were related with the education system of their school in general and in terms of anatomy and seven of the questions were related with their way of studying anatomy, including time spent for studying, preference for a group or individual study, study materials and methods.

Results: 88.6% of the respondents indicated that integrated medical education was the education system used in their schools. Systematic anatomy was the main method (93.8%) chosen for anatomy. Plastic models were the most frequent preference for lab studies (90.7%) followed by prosections (58.8%), specimens (30.9%) and cadaver dissections (21.6%). Majority of the respondents preferred studying anatomy alone (86.6%). Furthermore, students stated their preference of study methods as one or more at the same time, and the distribution of these methods were as follows: correlation of structures with relations (53.6%), functions (52.6%), clinical situations (30.9%), memorizing with mnemonics (53.6%) or tables and lists (45.4%), flash cards (7.2%), and regular repetitions (40.2%).

Conclusion: Study preferences may lead changes in anatomy curricula in the future.

Keywords: anatomy; dissection preference; study

Anatomy 2017;11(2):99–103

Introduction

Many variations have occurred amongst the tools of anatomy education since the time Greek physician Herophilus of Chalcedon performed the first scientific dissection in the early part of the third century BC. Particularly with the influence of developing technology, dissection has had increasing alternatives in this journey. These diversified methods of teaching have been classified essentially into following categories: dissections made by students; inspection of prosected specimens; didactic teaching; use of models; use of computer-assisted learning (CAL); slides and tapes; and teaching of living and radiological anatomy.[1–4]

Different students learn anatomy in different ways.[1–17] Some students prefer learning in pairs, trios or even larger groups.[3,8,18] However, some students rarely turn to their peers for help, working happily as individuals.[3] On the other hand, selecting the method of studying is the main thing that shapes the study preferences of a student. Within

**This study was presented in the 111th Annual Meeting of the Anatomische Gesellschaft, 21–24 September 2016, Göttingen, Germany; and the National Medical Education Symposium (UTES), 15–17 March 2017, Antalya, Turkey.*

the observation of numerous students and educational sources, these diversified methods of studying have been classified essentially into following categories: correlation of adjacent structures; correlation made with clinical or functional knowledge; studying with anatomy games; studies made on cadavers; studying topics in small pieces; memorization with codes, tables, lists or flash cards; regular repetition of the studied subject.

Researchers trying to find the "ideal" method for anatomy education were mostly focused on what is the best teaching method for students, and finding the best studying method for studying anatomy has remains nearly unexplored. Thus, this study aims to evaluate the importance of study methods in student's success and determine the most preferred study method.

Materials and Methods

Ninety-seven medical students aged between 19–26 years participated in the study. A structured questionnaire was prepared using Google Forms. All of the participants were invited to complete the questionnaire via e-mail or social media (Facebook, WhatsApp *etc.*). Participants that did not respond to the required questions of the survey were excluded from the study. The Ethics Committee of Bahçeşehir University endorsed its approval for the study.

The contents of the survey were divided into three parts: (i) socio-demographic characteristics of the participants, (ii) education system of participants' medical school and structure of the anatomy education, and (iii) study preferences for anatomy. Participants were asked five questions related with socio-demographic characteristics, followed by 16 questions related with the education system and study preferences of anatomy (**Table 1**). Nine of the questions were related with the education system of their school in general or in terms of anatomy and the rest of the questions were related with their way of studying anatomy including time spent for studying, preference for group or individual study, study materials, and study methods. Descriptive statistics for categorical variables were given with frequency and percentage.

Results

Students from various medical schools of Turkey answered the survey. 68.8% of these respondents were

Table 1

Questions related with education system and structure of the anatomy education and study preferences for anatomy.

Anatomy in the medical school	Study methods
What is the educational system of your medical school?	How much time do you spend on studying anatomy?
What kind of educational methods are used in the anatomy courses of your medical school?	How do you prefer studying anatomy?
Please rank your chosen methods, starting from one, with one being the most preferred.	Please rank your chosen study preferences, starting from one, with one being the most preferred. [(Study groups: More than 2 people – 2 people) – Alone]
What is the duration of the anatomy course in your medical faculties curriculum?	What kind of study sources are you using during your anatomy studies?
Considering the the selected time period above; please distribute the anatomy topics that have been systematically separated below, according to the year they are covered/going to be covered, from the table. *[If your anatomy education is still not finished in your school; and due to this, if you have no information about someof the topics, please choose the "star (*)" option for them.]*	Please rank your chosen study sources, starting from one, with one being the most preferred. [Textbooks – Notes that have been prepared by the lecturer – Notes that have been taken during the lecture by yourself – Anatomy Channels – Websites – Atlases]
How is the distribution of theoretical lectures to practicals in the anatomy courses of your medical school?	What kind of methods do you use during your anatomy studies?
What kind of teaching method is used mainly in your theoretical lectures?	Please rank your chosen study methods, starting from one, with one being the most preferred. [Correlating with clinical knowledge] [Correlating adjacent structures] [Correlating with functional knowledge] [Studying with anatomy games] [Studying from cadavers] [Studying topics in small pieces] [Memorizing with codes] [Memorizing wit tables or lists] [Memorizing with flash cards] [Repeating the study regulary]
What kind of tools are used in your practical sessions?	
Please rank your selected tools, starting from one, with one being the most preferred. [(Cadavers: Dissection – Prosection) – Models Plastinated samples – Sections – Specimens]	

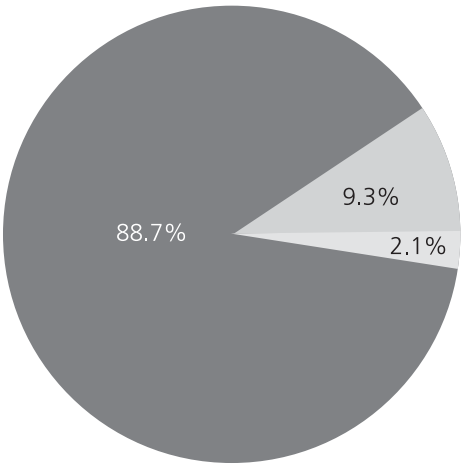

	n	%
Classical medicine education	2	2.1
Integrated medical education (Cummittee system)	86	88.6
Modern medical education (PBL system)	9	9.3
Other	0	0

Figure 1. Distribution of medical education systems of the medical schools among the participants.

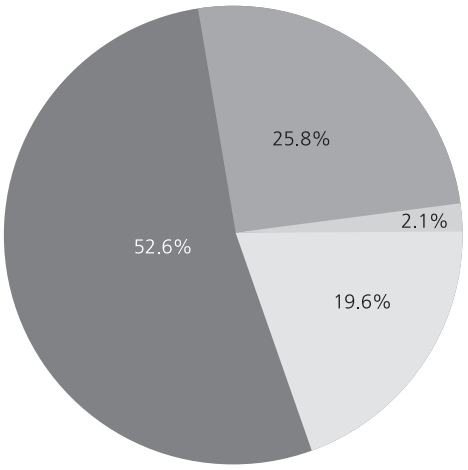

	n	%
1 year	19	19.6
2 years	51	52.6
3 years	25	25.8
More than 3 years	2	2.1

Figure 3. Distribution of anatomy classes within the whole curriculum.

first year students and 8.3% were second year. Rest of the respondents was 3rd–6th year medical students (22.9%).

88.6% of the respondents indicated that integrated medical education was the education system used in their schools (**Figure 1**). Systematic anatomy was the main method (93.8%) chosen for anatomy education. Topographic anatomy (42.3%), clinical anatomy (41.2%) and radiological anatomy (33%) were also present within the curricula of the schools (**Figure 2**).

52.6% of the respondents indicated that anatomy classes were spread through two years of the curriculum, while 25.8% stated that the anatomy classes were spread through three years of the education (**Figure 3**).

38.1% of the respondents stated that 70% of the classes were theoretical classes and 30% were lab hours. Rest of the respondents indicated that the distribution of lab hours was between 45% and 50% (**Figure 4**).

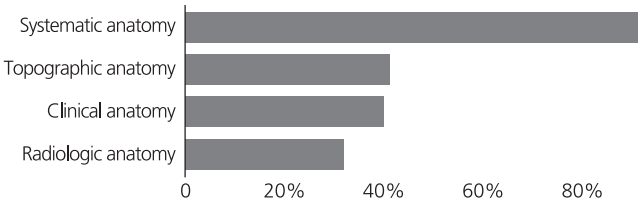

Figure 2. Distribution of anatomy methods within curricula of medical schools.

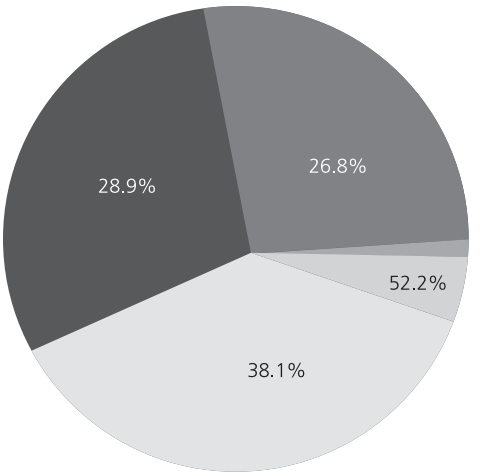

	n	%
Theoretical 100% – Practical 0%	0	0
Theoretical 85% – Practical 15%	5	5.2
Theoretical 70% – Practical 30%	37	38.1
Theoretical 55% – Practical 45%	28	28.9
Theoretical 50% – Practical 50%	26	26.8

Figure 4. Distribution of theoretical and practical hours of anatomy among different medical schools.

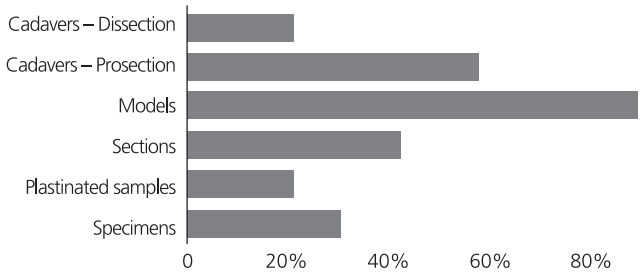

Figure 5. Preferences for lab studies.

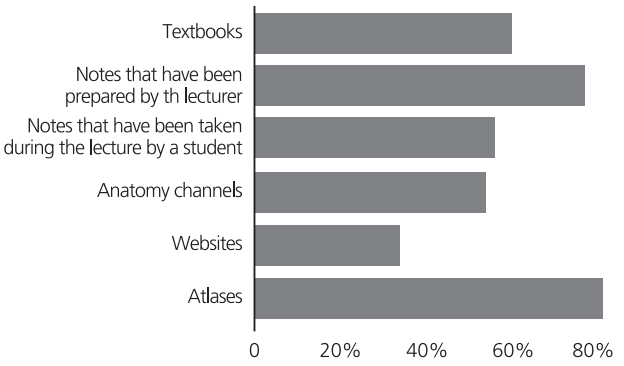

Figure 7. Distribution of sources for studying anatomy.

Plastic models were the most frequent preference for lab studies (90.7%), followed by prosections (58.8%), specimens (30.9%), and cadaver dissections (21.6%) (**Figure 5**).

41.3% of the respondents stated that time spent for anatomy studying was not less than 10–15 hours per month. Majority of the respondents preferred studying anatomy alone (86.6%). But this was not the only preference. 29.9% of the students indicated that they also preferred study groups which were composed of 2 individuals (**Figure 6**).

Slide layouts of the theoretical class presentations were the leading preference for anatomy study sources (79.9%). In addition to that, textbooks (61.9%), web based anatomy videos (55.7%) and anatomy web sites (35.1%) were also other preferred sources. Moreover, it was a common sense that is difficult to study without an anatomy atlas (83.5%) The students were able to prefer one or more of these sources at the same time (**Figure 7**).

The distribution of study methods were as follows: correlation of structures with relations (53.6%), functions (52.6%), clinical situations (30.9%), memorizing with mnemonics (53.6%), tables and lists (45.4%) and flash cards (7.2%), and regular repetitions (40.2%). The students were able to prefer one or more of these methods at the same time (**Figure 8**).

Discussion

Study preferences in anatomy is an unexplored and crucial research field that has the potential to play an important role in the future of anatomy education. By letting students prefer one or more of study methods (correlation of adjacent structures; correlation made with clinical or functional knowledge; studying with anatomy games; studies made on cadavers; studying topics in small pieces; memorization with codes, tables, lists or flash cards; regular repetition of the studied subject) at the same time and rank these methods according to their wish, this study expects to contribute to the important research field of study preferences. Due to the fact that it is still continuing, evaluation of statistical data was seen unnecessary in this article. Once the research is complete and all results are gathered, the statistical assessment shall be done.

Conclusion

Despite with only preliminary results, this descriptive study still shows a glimpse of that potential that study preferences may lead changes in anatomy curricula in the future.

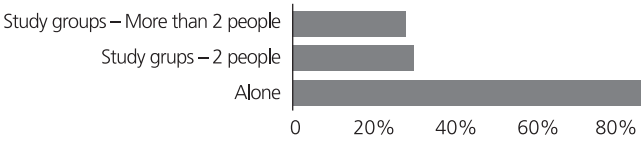

Figure 6. Distribution of the studying style among the participants.

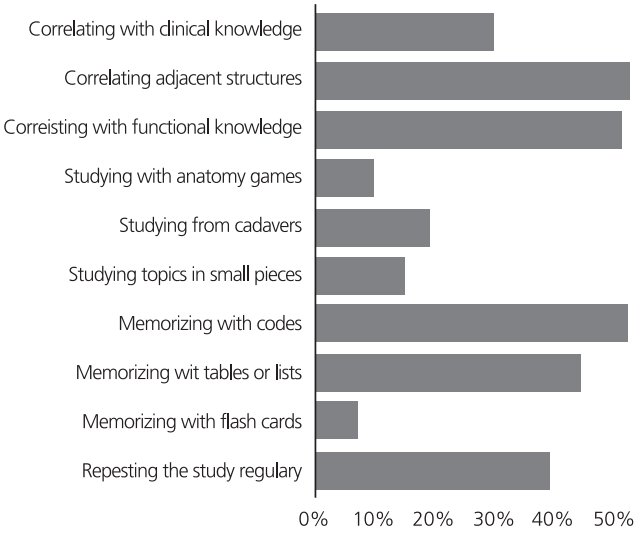

Figure 8. Distribution of the study methods of participants.

References

1. Brenner E, Maurer H, Moriggl B, Pomaroli A. General educational objectives matched by the educational method of a dissection lab. Ann Anat 2003;185:173229–30.
2. Kerby J, Shukur ZN, Shalhoub J. The relationships between learning outcomes and methods of teaching anatomy as perceived by medical students. Clin Anat 2011;24:489–97.
3. Mitchell BS. Learning styles in anatomy teaching and learning. In: Chen LK, Pawlina W, editors. Teaching anatomy: a practical guide. 1st ed. New York (NY): Springer; 2015. p. 23–30.
4. Patel KM, Moxham BJ. The relationships between learning outcomes and methods of teaching anatomy as perceived by professional anatomists. Clin Anat 2008;21:182–9.
5. Anyanwu EG. Anatomy adventure: a board game for enhancing understanding of anatomy. Anat Sci Educ 2014;7:153–60.
6. Benninger B. Google Glass, ultrasound and palpation: the anatomy teacher of the future? Clin Anat 2015;28:152–5.
7. Buenting M, Mueller T, Raupach T, Luers G, Wehrenberg U, Gehl A, Anders S. Post mortem CT scans as a supplementary teaching method in gross anatomy. Ann Anat 2016;208:165–9.
8. Burgess AW, Ramsey-Stewart G, May J, Mellis C. Team-based learning methods in teaching topographical anatomy by dissection. ANZ J Surg 2012;82:457–60.
9. Donnelly L, Patten D, White P, Finn G. Virtual human dissector as a learning tool for studying cross-sectional anatomy. Med Teach 2009;31:553–5.
10. Fitzpatrick CM, Kolesari GL, Brasel KJ. Teaching anatomy with surgeons' tools: use of the laparoscope in clinical anatomy. Clin Anat 2001;14:349–53.
11. Fruhstorfer BH, Palmer J, Brydges S, Abrahams PH. The use of plastinated prosections for teaching anatomy – the view of medical students on the value of this learning resource. Clin Anat 2011;24:246–52.
12. Granger NA, Calleson DC, Henson OW, Juliano E, Wineski L, McDaniel MD, Burgoon JM. Use of web-based materials to enhance anatomy instruction in health sciences. Anat Rec B New Anat 2006; 289:121–7.
13. Jones DG. Re-inventing anatomy: the impact of plastination on how we see the human body. Clin Anat 2002;15:436–40.
14. Op Den Akker JW, Bohnen A, Oudegeest WJ, Hillen B. Giving color to a new curriculum: bodypaint as a tool in medical education. Clin Anat 2002;15:356–62.
15. Ruthenbeck GS, Carati CJ, Gibbins IL, Reynolds KJ. A virtual reality 3D jigsaw for teaching anatomy. Stud Health Technol Inform 2008;132:436–8.
16. Solyar A, Cuellar H, Sadoughi B, Olson TR, Fried MP. Endoscopic sinus surgery simulator as a teaching tool for anatomy education. Am J Surg 2008;196:120–4.
17. Winkelmann A, Hendrix S, Kiessling C. What do students actually do during a dissection course? First steps towards understanding a complex learning experience. Acad Med 2007;82:989–95.
18. Shankar N, Roopa R. Evaluation of a modified team based learning method for teaching general embryology to 1st year medical graduate students. Indian J Med Sci 2009;63:4–12.

Online available at:
www.anatomy.org.tr
doi:10.2399/ana.17.021
QR code:

Correspondence to: Çağatay Barut, MD, PhD
Department of Anatomy, School of Medicine,
Bahçeşehir University, Istanbul, Turkey
Phone: +90 532 463 84 71
e-mail: cagbarut@yahoo.com

Conflict of interest statement: No conflicts declared.

anatomy
www.anatomy.org.tr
An International Journal of Experimental and Clinical Anatomy

Terminology Zone

www.anatomy.org.tr
Received: May 20, 2017; Accepted: June 25, 2017
doi:10.2399/ana.17.018

The erroneous eponym of the carotico-clinoid foramen of Henle: attribution is due to Alexander Monro (primus)

Matthew J. Zdilla[1,2]

[1]*Department of Natural Sciences and Mathematics, West Liberty University, West Liberty, WV, USA*
[2]*Department of Graduate Health Sciences, West Liberty University, West Liberty, WV, USA*

Abstract

The carotico-clinoid foramen is an inconsistent anatomical variation created by an osseous bridging between the anterior and middle clinoid processes that encircles the internal carotid artery. Due to its neurosurgical importance, several articles make note of the foramen. When describing the carotico-clinoid foramen, articles attribute its first description to Jakob Henle in 1855 and, likewise, use the eponym carotico-clinoid foramen of Henle. This report presents evidence that Henle was not the first to describe the carotico-clinoid foramen. Rather, the foramen was first described by Alexander Monro (primus) over a century earlier in 1726. Future studies noting the provenance of the carotico-clinoid foramen should attribute its discovery to Monro. Therefore, the eponym carotico-clinoid foramen of Henle should be named the *carotico-clinoid foramen of Monro.*

Keywords: anatomy; caroticoclinoid foramen; terminology

Anatomy 2017;11(2):104–106

The carotico-clinoid foramen (CCF) is an anatomical variation formed by an osseous bridging between the anterior clinoid and middle clinoid processes of the sphenoid.[1,2] When present, the CCF encompasses the internal carotid artery (ICA).[2] Due to this relationship, retraction of the ICA in the presence of a CCF may have life- threatening consequences.[3] Therefore, the carotico-clinoid is frequently noted in neurosurgical literature.

A literature review regarding the CCF reveals numerous manuscripts that either use the eponymous term carotico-clinoid foramen of Henle or otherwise state that the CCF was first described by Henle in 1885.[1,4–16] However, Henle was not the first to describe the CCF.

Although Henle mentions the *foramen carotico-clinoideum* in his 1885 text '*Handbuch der systematischen Anatomie des Menschen*', Alexander Monro (primus) described the CCF over a century earlier in his 1726 text '*The anatomy of the humane bones*' (**Figure 1**).[17,18] Monro notes that anterior clinoid processes are frequently joined with the posterior clinoid processes or with the "Body of the Bone itself, by a bony Cross-bridge under which the *Carotide* Arteries pass" (**Figures 2** and **3**).[17]

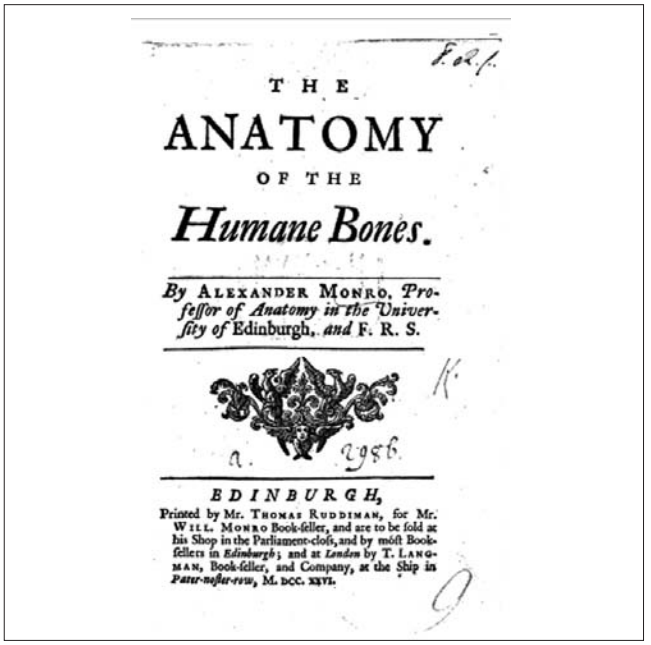
THE
ANATOMY
OF THE
Humane Bones.

By ALEXANDER MONRO, *Professor of Anatomy in the University of* Edinburgh, *and* F. R. S.

EDINBURGH,
Printed by Mr. THOMAS RUDDIMAN, for Mr. WILL. MONRO Book-seller, and are to be sold at his Shop in the Parliament-close, and by most Book-sellers in *Edinburgh*; and at *London* by T. LONGMAN, Book-seller, and Company, at the Ship in *Pater-noster-row*, M. DCC. XXVI.

Figure 1. Cover page from the first edition of Alexander Monro's *'The anatomy of the humane bones'* published in 1726.

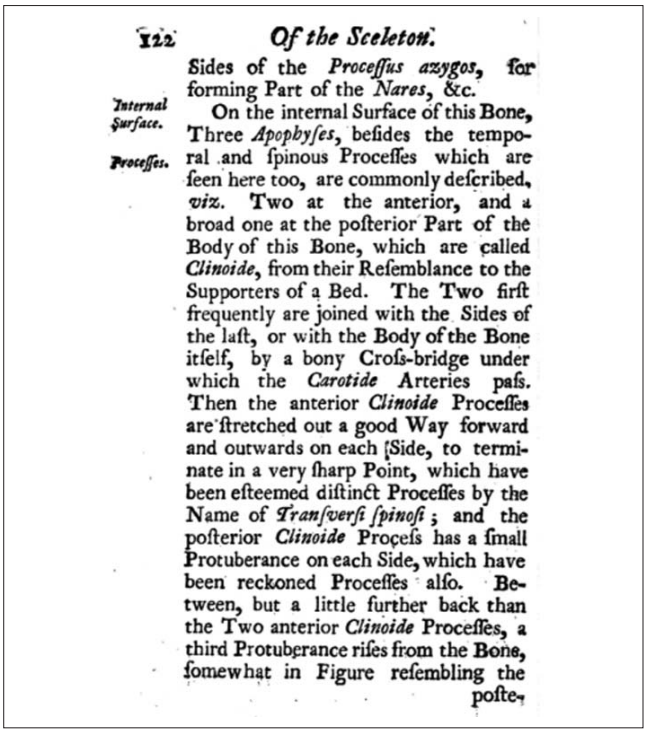

122 *Of the Sceleton.*

Sides of the *Proceſſus azygos*, for forming Part of the *Nares*, &c.

Internal Surface. On the internal Surface of this Bone, Three *Apophyſes*, beſides the temporal and ſpinous Proceſſes which are ſeen here too, are commonly deſcribed, *viz.* Two at the anterior, and a broad one at the poſterior Part of the Body of this Bone, which are called *Clinoide*, from their Reſemblance to the Supporters of a Bed. The Two firſt frequently are joined with the Sides of the laſt, or with the Body of the Bone itſelf, by a bony Croſs-bridge under which the *Carotide* Arteries paſs. Then the anterior *Clinoide* Proceſſes are ſtretched out a good Way forward and outwards on each Side, to terminate in a very ſharp Point, which have been eſteemed diſtinct Proceſſes by the Name of *Tranſverſi ſpinoſi*; and the poſterior *Clinoide* Proceſs has a ſmall Protuberance on each Side, which have been reckoned Proceſſes alſo. Between, but a little further back than the Two anterior *Clinoide* Proceſſes, a third Protuberance riſes from the Bone, ſomewhat in Figure reſembling the poſte-

Proceſſes.

Figure 2. Page 122 of Monro's 1726 text *'The anatomy of the humane bones'* which documents the carotico-clinoid foramen and its relationship to the carotid artery.

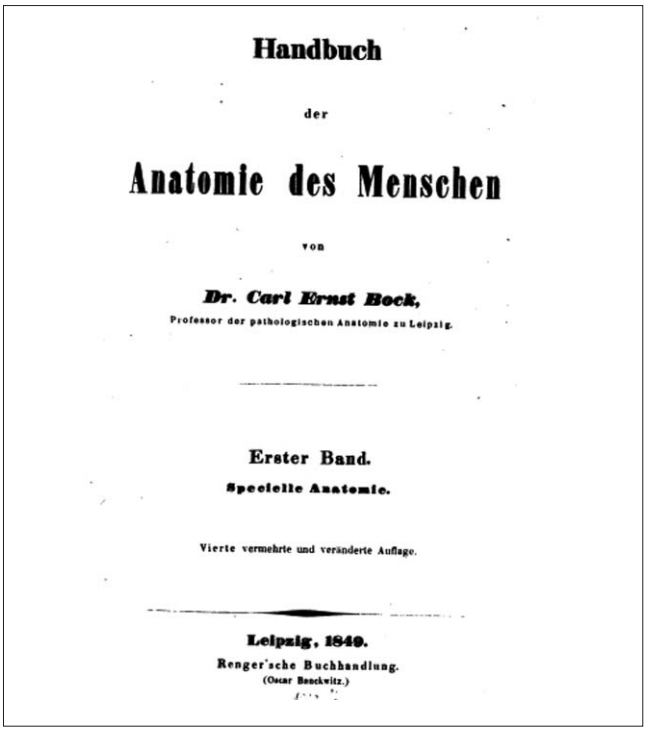

Handbuch

der

Anatomie des Menschen

von

Dr. Carl Ernst Bock,

Professor der pathologischen Anatomie zu Leipzig.

Erster Band.

Specielle Anatomie.

Vierte vermehrte und veränderte Auflage.

Leipzig, 1849.

Renger'sche Buchhandlung.

(Oscar Beschwitz.)

Figure 4. Cover page from Carl Ernst Bock's *'Handbuch der Anatomie des Menschen'* published in 1849.

Furthermore, even Henle's contemporaries described the CCF prior to 1855 in anatomical handbooks including Carl Ernst Bock's 1849 publication *'Handbuch der Anatomie des Menschen'* and Joseph Hyrtl's 1850 publication *'Lehrbuch der Anatomie des Menschen, mit Rücksicht auf physiologische Begründung und praktische Anwendung: Histologie, Knochen-, Bänder- und Muskellehre'* (**Figures 4** and **5**).[19,20] Excerpts from the aforementioned texts may be seen in **Figure 6**. Further, Hyrtl made note of morphological variation of the CCF— specifically, that the middle clinoid

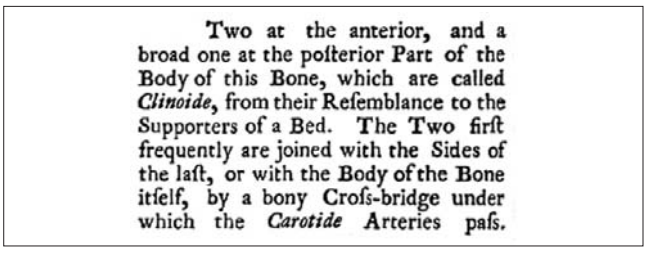

Two at the anterior, and a broad one at the poſterior Part of the Body of this Bone, which are called *Clinoide*, from their Reſemblance to the Supporters of a Bed. The Two firſt frequently are joined with the Sides of the laſt, or with the Body of the Bone itſelf, by a bony Croſs-bridge under which the *Carotide* Arteries paſs.

Figure 3. Excerpt from page 122 of Monro's 1726 text *'The anatomy of the humane bones'*, as seen in Figure 2 that has been enlarged and digitally enhanced. The excerpt notes that the two anterior clinoid processes join either the posterior clinoid processes or the body of the bone forming a bony cross-bridges under which the carotid arteries pass.

Lehrbuch

der

Anatomie des Menschen,

mit Rücksicht

auf

physiologische Begründung und praktische Anwendung.

Von

Joseph Hyrtl,

I. Abtheilung:

Histologie, Knochen-, Bänder- und Muskel-Lehre.

Zweite, sorgfältig verbesserte,

WIEN, 1850.

Wilhelm Braumüller,

Figure 5. Cover page from Joseph Hyrtl's *'Lehrbuch der Anatomie des Menschen, mit Rücksicht auf physiologische Begründung und praktische Anwendung: Histologie, Knochen-, Bänder- und Muskellehre'* published in 1850.

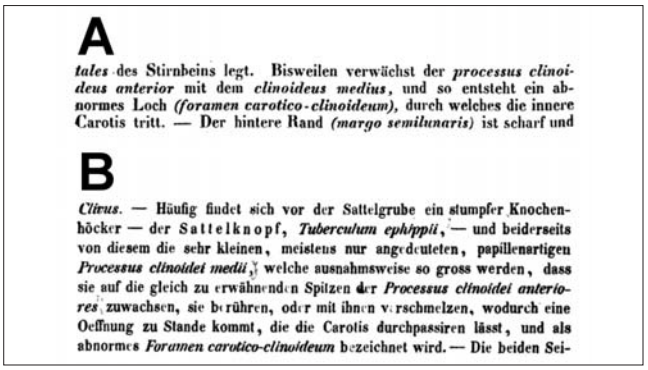
A

tales des Stirnbeins legt. Bisweilen verwächst der *processus clinoideus anterior* mit dem *clinoideus medius*, und so entsteht ein abnormes Loch *(foramen carotico-clinoideum)*, durch welches die innere Carotis tritt. — Der hintere Rand *(margo semilunaris)* ist scharf und

B

Clivus. — Häufig findet sich vor der Sattelgrube ein stumpfer Knochenhöcker — der Sattelknopf, *Tuberculum ephippii*, — und beiderseits von diesem die sehr kleinen, meistens nur angedeuteten, papillenartigen *Processus clinoidei medii*, welche ausnahmsweise so gross werden, dass sie auf die gleich zu erwähnenden Spitzen der *Processus clinoidei anteriores* zuwachsen, sie berühren, oder mit ihnen verschmelzen, wodurch eine Oeffnung zu Stande kommt, die die Carotis durchpassiren lässt, und als abnormes *Foramen carotico-clinoideum* bezeichnet wird. — Die beiden Sei-

Figure 6. Descriptions of the carotico-clinoid foramen (i.e., *foramen carotico-clinoideum*) in excerpts from the texts of Carl Ernst Bock's 1849 *'Handbuch der Anatomie des Menschen'* (**A**) and Joseph Hyrtl's 1850 *'Lehrbuch der Anatomie des Menschen, mit Rücksicht auf physiologische Begründung und praktische Anwendung: Histologie, Knochen-, Bänder- und Muskellehre'* (**B**).

process could extend toward, touch, or fuse with the anterior clinoid (**Figure 6**).[20]

In conclusion, this article provides evidence that the provenance of the carotico-clinoid foramen heretofore ascribed to Henle is ill-suited. Indeed, the CCF was described in 1726 by Alexander Monro (primus)– predating Henle's description by more than a century. Therefore, with regard to the eponym, the carotico-clinoid foramen of Henle should be renamed *the carotico-clinoid foramen of Monro*.

References

1. Lang J. Structure and postnatal organization of heretofore uninvestigated and infrequent ossifications of the sella turcica region. Acta Anat 1977;99:121–39.
2. Zdilla MJ, Cyrus LM, Lambert HW. Carotico-clinoid foramina and a double optic canal: a case report with neurosurgical implications. Surg Neurol Int 2015;6:13.
3. Lee HY, Chung IH, Choi BY, Lee KS. Anterior clinoid process and optic strut in Koreans. Yonsei Med J 1997;38:151–4.
4. Erturk M, Kayalioglu G, Govsa F. Anatomy of the clinoidal region with special emphasis on the caroticoclinoid foramen and interclinoid osseous bridge in a recent Turkish population. Neurosurg Rev 2004;27:22–6.
5. Desai SD, Sreepadma S. Study of carotico clinoid foramen in dry human skulls of north interior Karnataka. National Journal of Basic Medical Sciences 2010;1:60–4.
6. Kapur E, Mehiç A. Anatomical variations and morphometric study of the optic strut and the anterior clinoid process. Bosn J Basic Med Sci 2012;12:88–93.
7. Shaikh SI, Ukey RK, Kawale DN, Diwan CV. Study of carotico-clinoid foramen in dry human skulls of Aurangabad district. Iran J Basic Med Sci 2012;3:148–54.
8. Archana BJ , Shivaleela C, Kumar GV, Pradeep P, Lakshmiprabha S. An Osteological study of incidence, morphometry and clinical correlations of carotico-clinoid foramen in dried adult human skulls. Research Journal of Pharmaceutical, Biological and Chemical Sciences 2013;4: 347–52.
9. Hasan T. Bilateral caroticoclinoid and absent mental foramen: rare variations of cranial base and lower jaw. Ital J Anat Embryol 2013;118: 288–97.
10. Yadav Y, Nayeemuddin SM, Chakradhar V, Goswami P. Ossification of caroticoclinoid ligament and its clinical importance. Int J Biomed Res 2014;5:294–5.
11. Brahmbhatt RJ, Bansal M, Mehta C, Chauhan KB. Prevalence and dimensions of complete sella turcica bridges and Its clinical significance. Indian J Surg 2015;77:299–301.
12. Gupta N, Rai AL. Anatomical variations of anterior clinoid process with its surgical importance. Innovative Journal of Medical and Health Science 2015;5:28–30.
13. Mallik S, Sawant VG. Bilateral "Carotico-clinoid Foramen" with "Sella Turcica Bridge"-a case report. Anat Physiol 2015;5:S5.
14. Ota N, Tanikawa R, Miyazaki T, Miyata S, Oda J, Noda K, Tsuboi T, Takeda R, Kamiyama H, Tokuda S. Surgical microanatomy of the anterior clinoid process for paraclinoid aneurysm surgery and efficient modification of extradural anterior clinoidectomy. World Neurosurg 2015;83:635–43.
15. Bilodi A, Kumar S, Karthikeyan V. Study of inconsistent structure in the anterior cranial fossa of an Indian human skull. World Journal of Pharmacy and Pharmaceutical Sciences 2016;5:1671–7.
16. Jha S, Singh S, Bansal R, Chauhan P, Shah MP, Shah A. Nonmetric analysis of caroticoclinoid foramen in foothills of Himalayas: its clinicoanatomic perspective. Morphologie 2017;101:47–51.
17. Monro A. The anatomy of the human bones. Edinburgh: Thomas Ruddiman; 1726. p. 122.
18. Henle J. Handbuch der systematischen Anatomie des Menschen. Braunschweig: Druck und Verlag von Friedrich Vieweg und Sohn; 1855. p. 99.
19. Bock CE. Handbuch der Anatomie des Menschen. Vol 1. Leipzig: Oscar Banckwitz; 1849. p. 42.
20. Hyrtl J. Lehrbuch der Anatomie des Menschen, mit Rücksicht auf physiologische Begründung und praktische Anwendung: Histologie, Knochen-, Bänder- und Muskellehre. Wein: Wilhelm Braumüller; 1850. p. 180.

Online available at:
www.anatomy.org.tr
doi:10.2399/ana.17.018
QR code:

deomed

Correspondence to: Matthew J. Zdilla, D.C.
Department of Natural Sciences and Mathematics, West Liberty University, CSC 139; P.O. Box 295, 26074, West Liberty, WV, USA
Phone: +1 304 336 8631
e-mail: mzdilla@westliberty.edu

Conflict of interest statement: No conflicts declared.

ANATOMİ KIŞ GÜNLERİ 2018

Patalya Thermal Hotel-Kızılcahamam
25-26-27 Ocak 2018

BAŞKENT ÜNİVERSİTESİ
Tıp Fakültesi

TÜRK ANATOMİ VE KLİNİK ANATOMİ DERNEĞİ
•1991•

Üçlü Anatomi Seti

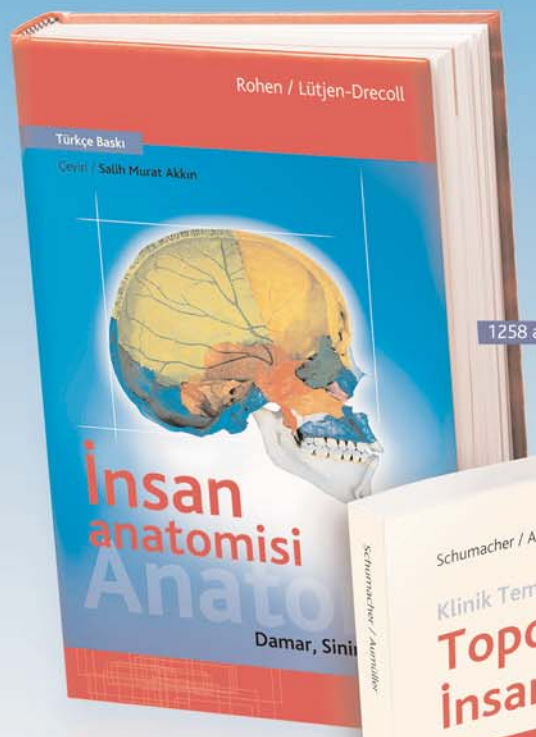

1258 anatomik görsel

Rohen / Yokochi / Lütjen-Drecoll
İnsan Anatomisi Fotoğraflı Disseksiyon Atlası
Çeviri / **Salih Murat Akkın**
21x29 cm, Renkli XII+532 Sayfa, Sert Kapak
Deomed / Türkçe 1. Baskı 2009
ISBN 978-975-8882-18-2

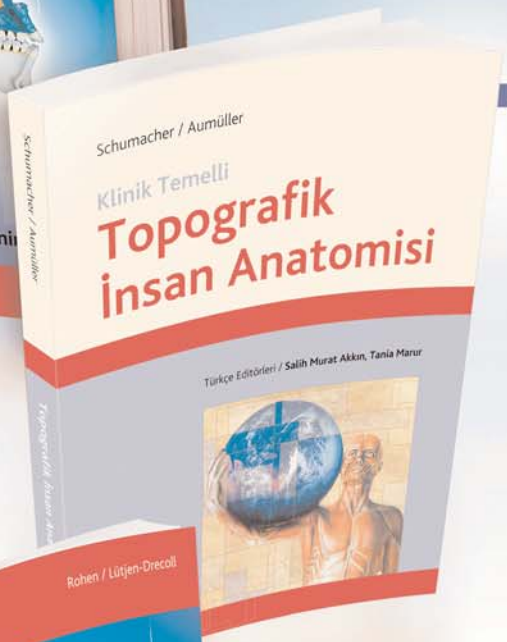

350'den fazla anatomik şekil

Schumacher / Aumüller
Klinik Temelli
Topografik İnsan Anatomisi
Türkçe Editörleri / **S. M. Akkın, T. Marur**
Çeviri /
Salih Murat Akkın
Zafer Arı
Hakan Ay
Barçın O. Barlas
Ayhan Cömert
Mehmet Çimen
Mehmet Demir
Alaittin Elhan
S. Tuna Karahan
Tania Marur
Osman Sulak
M. Yakup Tuna
16.5x24 cm, Renkli X+454 sayfa, Kuşe kapak
Deomed / Türkçe 1. Baskı 2010
978-975-8882-22-9

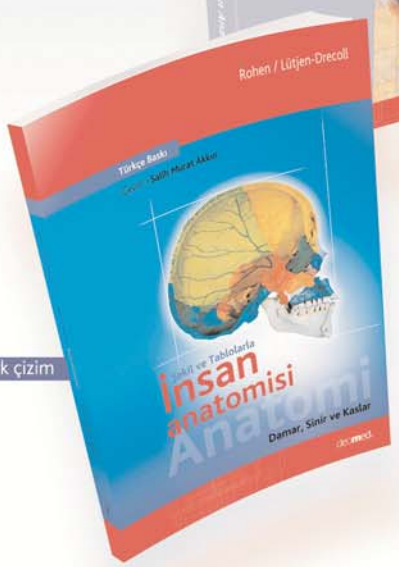

61 anatomik çizim

Rohen / Yokochi / Lütjen-Drecoll
Şekil ve Tablolarla İnsan Anatomisi: Damar, Sinir ve Kaslar
Türkçe Çeviri / **Salih Murat Akkın**
14,5x22 cm, Renkli VI+90 sayfa, Karton kapak
Deomed / Türkçe 1. Baskı 2008
ISBN 978-975-8882-28-1

deomed®

Sağlıklı Bilgi Kaynağı

Deomed Yayıncılık
T. +90 216 414 83 43 pbx F. +90 216 414 83 42

Ayrıntılı bilgi ve online alışveriş: **www.deomed.com**

Table of Contents

Volume **11** / Issue **2** / August **2017**

(Continued from back cover)

Teaching Anatomy

Terminology Zone

On the Front Cover:
Electromicrographs of placental labyrinth in control and chronic anemic rat placenta at gestational day 21. (**a**) Electromicrograph of placental labyrinth in control rats showing normal maternal blood spaces (**MBS**), fetal capillaries (**FC**) with red blood cells (**RBCs**) and a number of giant cells with clear cell margins and prominent nucleoli (**arrows**) (×1200). From Awad O, Ochieng SJ, Malek A, Ogeng'o J. Chronic anaemia causes degenerative changes in trophoblast cells of the rat placenta. *Anatomy* 2017;11(2):72–78.

Colored images of the published articles can be found in the online version of the journal which is available at www.anatomy.org.tr

www.anatomy.org.tr

anatomy

An International Journal of Experimental and Clinical Anatomy

Table of Contents

Volume **11** / Issue **2** / August **2017**

Original Articles

(Contents continued on inside back cover)

deomed®